Appendix 2.10.1

**ES-3100 CONTAINMENT VESSEL ASME CODE EVALUATION
(DAC-EA-900000-A006 and DAC-EA-900000-A007)**

2-100

GENERAL DESIGN AND COMPUTATION SHEET

JOB ASME Code Subsection NB Stress Analysis of ES-3100 Containment Vessel		DATE 14 December 2006	SHEET 1 of 26
DAC NO. DAC-EA-900000-A006	REVISION NO. 2	COMPUTED C. R. Hammond	CHECKED BY R. M. Jessee

TABLE OF CONTENTS

Y/LF-717/Rev 2/ES-3100 HEU SAR/Ch-2/rlw/3-06-08

GENERAL DESIGN AND COMPUTATION SHEET

JOB ASME Code Subsection NB Stress Analysis of ES-3100 Containment Vessel		DATE 14 December 2006	SHEET 2 of 26
DAC NO. DAC-EA-900000-A006	REVISION NO. 2	COMPUTED C. R. Hammond	CHECKED BY R. M. Jessee

OBJECTIVE

The design for the ES-3100 Containment Vessel is evaluated for compliance with ASME Code, Section III structural design rules using bounding loads taken from the U. S. Code of Federal Register and International Atomic Energy Agency Requirements.

EVALUATION INPUT (CRITERIA) AND SOURCE

REFERENCES USED

BWXT Y-12 drawings (Project: ES-3100 Shipping Package, all dated 10/29/03):

M2E801580A011, Rev. C, "Containment Vessel Assembly"

M2E801580A012, Rev. C, "Containment Vessel Body Assembly"

M2E801580A013, Rev. B, "Containment Vessel O-ring Details"

M2E801580A014, Rev. B, "Containment Vessel Lid Assembly"

M2E801580A015, Rev. C, "Containment Vessel Sealing Lid"

M2E801580A016, Rev. B, "Containment Vessel Closure Nut"

Texts

(B1.1) *Unified Inch Screw Threads*, ASME B1.1-1989, The American Society of Mechanical Engineers, 1989.

(B1.9) *Buttress Inch Screw Threads*, ANSI B1.9 – 1973, The American Society of Mechanical Engineers, 1973.

(CFR) *Packaging and Transportation of Radioactive Material*, 10CFR71, Code of Federal Regulations, the Nuclear Regulatory Commission, 2004.

(Code) *Class 1 Components, Section III, Rules for Construction of Nuclear Power Plant Components*, Division 1, 2001 Edition with 2003 Addenda, The American Society of Mechanical Engineers, 2003.

(IAEA) *Regulations for the Safe Transport of Radioactive Material, Requirements*, 1996 Edition (Revised), No. TS-R-1 (ST-1, Revised), International Atomic Energy Agency, 2000.

(Parker) *Parker O-Ring Handbook*, 2001 Edition, Catalog ORD 5700A/US, Parker Seals, 2001.

(Roark) R. J. Roark and W. C. Young, *Formulas for Stress and Strain*, 5th Ed., McGraw-Hill Book Company, 1975, p. 363.

(Section II) *Section II, Materials*, Part D – Properties, 2001 Edition with 2003 Addenda, The American Society of Mechanical Engineers, 2003.

2-102

GENERAL DESIGN AND COMPUTATION SHEET

ASSUMPTIONS MADE

Calculations are based on geometry and specifications from referenced drawings.

Results are rounded to significant figures although more digits may be retained in intermediate calculations.

IDENTIFICATION OF COMPUTER CALCULATION

Computer Type: Dell PC x86 Family processor Family 6 Model 8 Stepping 1 using the Microsoft Windows 2000 operating system level 5.00.2195 with Service Pack 4.

Computer Program Name, Revision, Verification, Applicability: Programs used were Algor (R) Linear Static Stress Version 12.26-WIN 28-OCT-2002, ALG.DLL VERSION:13180000 and FEMPRO Version 13.26-WIN 22-NOV-2002. Verification was by running example programs with known solutions on the same computer used for final calculations. The expected results were produced exactly. Hand calculations are used here to confirm results. The program is applicable to linear elastic solutions for bodies of revolution as needed here.

METHODS TO BE USED

The Finite Element Method is used to determine the response of the CV components to internal pressure and gasket seating loads. External pressure resistance of the cylindrical shell is evaluated following Code rules. The finite element results also serve to demonstrate the external pressure resistance of the lid and bottom of the CV. Buttress threads used to restrain the lid are evaluated by a method derived from an accepted way of determining the strength of standard threads.

ANALYSES AND/OR CALCULATIONS

DESIGN CONDITIONS

Internal Pressure: 101.5 psig at 300 F. per IAEA.

External Pressure: 21.7 psig at 300 F. per 10CFR71.73.

2-103

GENERAL DESIGN AND COMPUTATION SHEET

JOB ASME Code Subsection NB Stress Analysis of ES-3100 Containment Vessel	DATE 14 December 2006	SHEET 4 of 26

DAC NO. DAC-EA-900000-A006	REVISION NO. 2	COMPUTED C. R. Hammond	CHECKED BY R. M. Jessee

ALLOWABLE STRESS INTENSITIES

From Section II.

PART	SPECIFICATION	ALLOWABLE STRESS INTENSITY, PSI
Containment vessel	ASME SA-182, Type F304L forging or bar (<5 in. thick)	12,800 @ 300 F.*
Containment lid	ASME SA-479, 304 bar	12,800 @ 300 F.*
Closure nut	ASME SA-479, UNS-S21800 bar	22,100 @ 300 F.

* The lower of two allowable values was chosen to limit deflection of the flange.

NB-3133 COMPONENTS UNDER EXTERNAL PRESSURE

The design internal pressure is higher than the external pressure across the bottom of the vessel and the lid. Since stability or buckling was not an issue, these flat heads were evaluated for resistance to internal pressure only. They can resist the external pressure by linearity.

NB-3133.3 Cylindrical Shells and Tubular Products

Data: Outside diameter of cylindrical shell, $D_o = 5.04" + 2(0.100") = 5.24"$

Shell thickness, $T = 0.100"$

Total length, $L = 32.40" - (0.25")/2 - 1.10" = 31.18"$

$D_o/T = 52.4$

$L/D_o = 5.95$

From ASME Section II, Fig. G, $A = 0.00053$

From ASME Section II, Fig. HA-3, conservatively using the 400 F. curve, B(400 F.) = 4900.

The maximum acceptable external pressure in this case is $P_a = 4B/3(D_o/T) = 125$ psig.

This allowable value exceeds the design external pressure and the shell is acceptable.

NB-3133.6 Cylinders Under Axial Compression

Data: Inside radius, $R = 5.04"/2 = 2.52"$

$A = 0.125/(R/T) = 0.0050$

From ASME Section II, Fig. HA-3, conservatively using the 400 F. curve, B(400 F.) = 7100.

2-104

GENERAL DESIGN AND COMPUTATION SHEET

This is the maximum acceptable compressive stress limited by axial buckling. The maximum external pressure applied to the axial cross section of the cylinder at 400 F. can be derived using nominal values from:

$$7100\,psi = \frac{p_e \frac{\pi}{4}(5.24\,in.)^2}{\frac{\pi}{4}\left[(5.24\,in.)^2 - (5.04\,in.)^2\right]}$$

p_e = 532 psi. This is less than the design external pressure and the shell is still acceptable.

NB-3200 DESIGN BY ANALYSIS

Individual axisymmetric finite element models were constructed of the CV body, the lid, and the closure nut and identified es5100, es3100lid, and es3100nut, respectively. Two loading conditions were applied to each model per Section III requirements: internal pressure and gasket seating. Load Case 1 is internal pressure including gasket load and Load Case 2 is gasket load alone.

The material properties at 300 F. obtained from Section II are as follows:

MATERIAL	MODULUS OF ELASTICITY	POISSON'S RATIO*
304 or 304L stainless steel	27,000,000 psi	0.3
UNS-S21800 stainless steel	27,000,000 psi**	0.3

* Typical values. Stress distributions are not sensitive to Poisson's ratios near 0.3 .

** Not in Tables. Based on principal constituents same as 304 stainless (18% Cr, 8% Ni).

Gasket load

Two concentric O-rings are specified to provide a redundant and testable seal. Per normal ASME practice, the O-ring grooves were not included in the finite element model. Elements reasonably close to the actual O-ring locations were chosen and elements representing the O-rings were added to the model of the CV. The gasket force was applied by displacing the top surface by 0.139 in. − 0.114 in. = 0.025 in. This way a reduction in gasket load will be caused by deformation of the CV from application of pressure.

Each O-ring has a 0.139 inch cross section diameter and is specified to have a 70 +/- 5 Shore A durometer reading. The O-ring manufacturer's catalog (Parker, P. 2-15) gives ranges of distributed force required to compress O-rings. The O-ring grooves cut into the flange surface are specified to be 0.114 inch deep. The lid is expected to be pressed down so contact is metal-to-metal. Then the O-rings will be compressed

$$\frac{0.025\,in.}{0.139\,in.} \times 100\,^{\circ}/_{\circ} = 18.0\,^{\circ}/_{\circ}$$

This is equivalent to a strain of 0.18 in./in.

Y/LF-717/Rev 2/ES-3100 HEU SAR/Ch-2/rlw/3-06-08

GENERAL DESIGN AND COMPUTATION SHEET

Attachment A shows the effective distributed compression force for different amounts of compression based on values of distributed force averaged between high and low values for the highest allowed durometer reading, 75. The distributed force for 18% compression was about 20 lb/in. The stress-strain relationship for a thin annular shell t thick of average radius r loaded axially by the force F=20 lb/in(2πr) and an elastic modulus E is approximately

$$\frac{20\,lb/in(2\pi r)}{2\pi r t} = E\varepsilon = E(0.18\,in/in). \text{ So}$$

$$E = \frac{20\,lb/in}{0.18t}.$$

For the outer O-ring, the thickness is 3.04584 in. − 2.96172 in. and E_o = 1321 psi. For the inner O-ring, the thickness is 2.817 in. − 2.718 in. and E_i = 1122 psi.

These moduli were applied to the respective O-ring elements in the CV model.

Pressure was applied over the inner surface of the CV model up to the outer edge of the inner O-ring groove per Code rules. Two nodal forces had to be applied at the inner corner of the flange area since the program could not apply pressure to two faces of one element. The pressure and gasket seating forces were resisted by stiff elastic boundary elements canted 7 degrees out from the axis of symmetry to simulate the effect of the 7 degree surface on the threads to meet Code rules to consider radial forces and resulting hoop stress at the threads.

Results from the O-ring elements and the boundary element restraint are collected in Attachment B. The local 2-axes of the O-ring elements are parallel to the CV axis of symmetry, the global Z-axis. The values from load case 2 are -237.1 psi for the first set of elements representing the outer O-ring and -201.3 psi for the inner O-ring. These stresses were achieved by applying a displacement of 0.025 inches. The equivalent distributed loads in the O-ring elements are -237.1 psi (3.04584 in. − 2.96172 in.) = -19.94 lb/in. and -201.3 psi (2.817 in. − 2.718 in.) = -19.93 lb/in. which are within 1% of the target, 20 lb/in.

The gasket reaction forces and internal pressure were applied to a model of the lid. The nodal forces are shown in Attachment C. The lid was restrained by a portion of the surface under the nut. The contact area was moved radially inward until there was no tension developed during Load Case 1. The dimensions of the contact area may not be exact but the Code requirement to maintain equilibrium of forces and moments is met. One of the contact nodes for Load Case 2 was in tension but equilibrium of force and moment were still maintained by the force distribution applied to the model of the nut. Also Load Case 2 produces such low stresses that optimizing the model for it is unnecessary.

The interface forces were applied to a model of the nut. The force magnitude and moment of the distributed forces was maintained using small added nodal forces as shown in Attachment D.

The distribution of stress intensity is shown on Figs. 1 − 10. Stress intensities are very low relative to the basic allowable stress for the material. Code compliance is trivial since the Code tests subdivide the computer results but the sum is less than the allowable for any of the subsets. By the numbers.

GENERAL DESIGN AND COMPUTATION SHEET

NB-3221.1 General Primary Membrane Stress Intensity

General primary membrane stress intensity is limited to the basic allowable stress intensity at temperature. That is 12,800 psi in the CV. The general primary membrane stress intensity is based on stresses averaged across the thickness of a section. The highest calculated stress intensities (called 2 times Tresca Stress by the program) were 7436 psi for Load Case 1 and 1203 psi for Load Case 2. Average stress is always less than peak stress so the CV is acceptable.

Fig. 4 is a close look at the cylindrical section. The stress intensity away from thickened sections appears to be less than 3000 psi. As a check the average elastic stresses in the middle of the cylindrical side of the vessel are easily calculated from equilibrium. Section III of the ASME Code provides values in Nonmandatory Appendix A. The tolerance on critical dimensions is ±0.01 in. and is taken into consideration to calculate maximum values of stress intensity.

A-2221 General Primary Membrane Stress Intensity

$$S = (pR/t) + (p/2) = 101.5\,psig\left(\frac{5.04\,in. + 0.01\,in.}{2(0.10\,in. - 0.01\,in.)}\right) + \frac{101.5\,psig}{2} = 2898\,psi.$$

A-2222 Maximum Value of Primary Plus Secondary Stress Intensity

$$S = 2pY^2/(Y^2 - 1) = \frac{2(101.5\,psig)\left(\dfrac{5.04\,in. + 0.01\,in.}{5.04\,in. + 0.01\,in. - 2(0.10\,in. - 0.01\,in.)}\right)^2}{\left(\dfrac{5.04\,in. + 0.01\,in.}{5.04\,in. + 0.01\,in. - 2(0.10\,in. - 0.01\,in.)}\right)^2 - 1} = 2899\,psi.$$

This confirms the computer solution for the cylindrical section.

There is a small radial membrane stress in the CV bottom but there is no need to calculate it since the sum of all order stresses is less than the allowable for the membrane stress.

The highest calculated stress intensity in the lid was 2398 psi for Load Case 1 and 872 psi for Load Case 2. The general primary membrane radial stress in the lid is zero from equilibrium so the highest average membrane stress is p/2 = 200 psi/2 = 100 psi. The allowable stress intensity is also 12,800 psi so the lid is acceptable.

NB-3221.2 Local Membrane Stress Intensity

Local membrane stress intensity is the average stress across the thickness of a cross section at the junction between the side and bottom of the CV. The allowable value of this stress component is 1.5 times the basic allowable stress. Figs. 4 and 5 show that the peak values of stress at this junction are below the basic allowable so the average must also be below the allowable and the CV is acceptable.

NB-3221.3 Primary Membrane plus Primary Bending Stress Intensity

Primary membrane plus primary bending stress intensity in the CV bottom and the lid.

JOB ASME Code Subsection NB Stress Analysis of ES-3100 Containment Vessel		DATE 14 December 2006	SHEET 8 of 26
DAC NO. DAC-EA-900000-A006	REVISION NO. 2	COMPUTED C. R. Hammond	CHECKED BY R. M. Jessee

Fig. 3 shows the stress intensity at the center of the CV bottom. The distribution is primarily due to bending and the peak value is less than 1.5 times the basic allowable stress intensity.

The stress in the bottom cover is complicated by attachment to the side but bending stress at the center can be checked by bounding stress by assuming both simple support and fixed support around the outside edge. From the Code Appendix:

A-5212 Radial bending stress at center (r = 0) and outside surface (x = t/2)

$$\sigma_r = p \frac{3(x)}{4t^3}\left[(3+v)(R^2 - r^2)\right] = 101.5\,psig\,\frac{3(t/2)}{4t^3}\left[(3+0.3)\left(\frac{5.04\,in.}{2}\right)^2\right]$$

$$= 101.5\,psig\,\frac{3}{8(0.25\,in.)^2}\left[3.3(2.52\,in.)^2\right] = 12{,}762\,psi.$$

This equation is based on a simply supported outer edge. For a fixed edge, the stress at the same point using Roark (Table 24, Case 10b) is:

$$\sigma_r = p \frac{6}{16(0.25\,in.)^2}\left[(1+v)R^2\right] = 101.5\,psig\,\frac{3}{8(0.25\,in.)^2}\left[1.3(2.52\,in.)^2\right] = 5{,}028\,psi.$$

From Fig. 3 it is seen that the peak stress intensity at the center of the CV bottom is about 7,000 psi. This value is between the bending stresses for the simply supported and fixed edge cases as expected.

The pattern of stress intensity in the lid is also primarily bending of the relatively thin outboard edge with bearing under the restraining nut and some intensification at a fillet. The bending stress appears to be less than 300 psi which is far below the allowable.

NB-3222.3 Expansion Stress Intensity

Expansion stress intensity is undefined but can be bounded. The largest temperature range possible for the CV is between -40 F. which is the minimum temperature specified in 10CFR71 and 300 F. defined here. Suppose a tendril maintains a temperature of -14 F. while the surrounding material is heated to 300 F. The result is a 340 F. temperature difference across a sharp boundary – an infinite gradient. The stress in the tendril would be $\sigma = E\alpha_{(-40)-300}\,340°$. E is the cold modulus of elasticity – 28,800,000 psi by interpolation from Table TM-1 in Section II. The temperature at the midpoint of the range is 170 F. and the instantaneous α at that temperature is 9.1×10^{-6} in/in/° F. from Table TE-1 in Section II. The bounding expansion stress is 89,000 psi. This is a fictitious elastic stress per the Code. Add to this the highest stress from the CV and lid models multiplied by an intensification factor of 2 since the finite element program may extrapolate to the surface too simplistically. That is 89,000 psi + 2 (7436 psi) = 100,000 psi. The alternating stress is half this value or 50,000 psi. The allowable number of cycles for this stress per Fig. I-9.2.1 in Code Mandatory Appendix I is 30,000. The vessel should acceptable for a few hundred years although a severe transportation accident should be counted as two cycles, one for impact and one for fire.

GENERAL DESIGN AND COMPUTATION SHEET

NB-3230 STRESS LIMITS FOR BOLTS

NB-3232.1 Average Stress

Average stress across a bolt cross section has a different allowable value. Since the CV is threaded to retain the lid special consideration is given to the neck above the lid. Allowable stress on bolts per Appendix III, Article III-2000, of Section III is one-third of the minimum specified yield strength of the material. This is half of the basic allowable but the service stress may be twice the allowable so we are back to an allowable service stress of 12,800 psi. Fig. 5 shows that the peak stress intensity in the neck region is under 6000 psi and the average service stress is much less so the CV is acceptable.

NB-3232.2 Maximum Stress

Maximum service stress in a bolt including bending stress may be three times the basic allowable bolt stress and since the bending component is included in the calculated stress the CV is clearly acceptable.

NB-3227.2 Pure Shear

Pure shear across threads on CV and Closure Nut. These threads are 7.0 inch 8 threads per inch push buttress threads Class 2A fit per ANSI B1.9-1973. The 7 degree slope of the mating surface was accounted for in the finite element models. The threads were not modeled in detail and they are evaluated using a traditional method (B1.1). Internal threads are limiting because the allowable stress for the CV material is about half the allowable stress for the nut material. The appropriate shear area on internal threads is the cylindrical area at the tip of the external thread with minimum height. That is the area at the minimum major diameter of the external thread called $MIN\,D_s$ in B1.9. $MIN\,D_s$ is the nominal D_s, $D - G$, where D is the nominal diameter and G is the allowance for easy assembly minus the tolerance on D. The minimum width of the internal thread at this radius, say t_e, is a function of the theoretical sharp thread form, H, defined as $0.89064p$ where p is the thread pitch, the crest truncation, f (=$0.14532p$), and the sum of radial allowance and tolerances (the gap). The gap based on thread tolerances is half the tolerance on the pitch diameter and half the tolerance on the major diameter of the thread. The gap should also include any outward radial deformation of the threads. Fig. 11 shows that due to rotation of the flange, the threads in the CV actually move inward and do not increase the gap. In any case the calculated displacements are smaller than the thread tolerances. So, limited to thread properties

$$gap = \frac{PDtol}{2} + \frac{G}{2} + \frac{Dtol}{2} = \frac{0.0101\,in.}{2} + \frac{0.0067}{2} + \frac{0.0101\,in.}{2} = 0.0134\,in.$$

$$t_e = (0.89064\,p - 0.14532\,p - gap)(\tan(7°) + \tan(45°))$$
$$= ((0.89064 - 0.14532)(0.125\,in.) - 0.0134\,in.)(1.1228)$$
$$= 0.08956\,in.$$

$$MIN\,D_s = 7\,in. - 0.0067 - 0.0101\,in. = 6.9832\,in.$$

2-109

GENERAL DESIGN AND COMPUTATION SHEET

JOB ASME Code Subsection NB Stress Analysis of ES-3100 Containment Vessel		DATE 14 December 2006	SHEET 10 of 26
DAC NO. DAC-EA-900000-A006	REVISION NO. 2	COMPUTED C. R. Hammond	CHECKED BY R. M. Jessee

Three threads are fully engaged so the shear area is at least

$$A_{s,i} = 3(0.08956\,in.)\pi(6.9832\,in.) = 5.894\,in^2.$$

The shear capacity given the Code limit on shear stress of 0.6 S_m is 0.6 (12,800 psi)(5.894 in.^{2})

= 45,300 lb.

The load due to pressure to the outer edge of the inner O-ring groove is

$$W_{m1} = \pi\frac{101.5\,psi\,(5.624\,in.)^2}{4} = 2521\;lb.$$

The force due to gasket seating is

$$W_{m2} = 20\,lb./in.\pi\left[(5.359\,in. + 0.139\,in.) + (5.859\,in. + 0.139\,in.)\right] = 722.3\,lb.$$

The combined force is 3244 lb. This is much less than the shear capacity so the threads are acceptable for shear.

NB-3232.3 Fatigue Analysis of Bolts

Fatigue analysis of bolts is contained in Section 2 of the Safety Analysis Report for Packaging

CONCLUSIONS

The ES-3100 Containment Vessel meets ASME Code, Section III, requirements for structural design except for fatigue analysis of the threaded closure which was not evaluated. Fatigue analysis of the threaded closure is contained in Section 2 of the Safety Analysis Report for Packaging.

GENERAL DESIGN AND COMPUTATION SHEET

JOB ASME Code Subsection NB Stress Analysis of ES-3100 Containment Vessel		DATE 14 December 2006	SHEET 11 of 26
DAC NO. DAC-EA-900000-A006	REVISION NO. 2	COMPUTED C. R. Hammond	CHECKED BY R. M. Jessee

Stress
Tresca * 2
lbf/(in^2)

7436.433
5956.012
4475.592
2995.171
1514.751
34.33044

Load Case: 1 of 2

Maximum Value: 7436.43 lbf/(in^2)

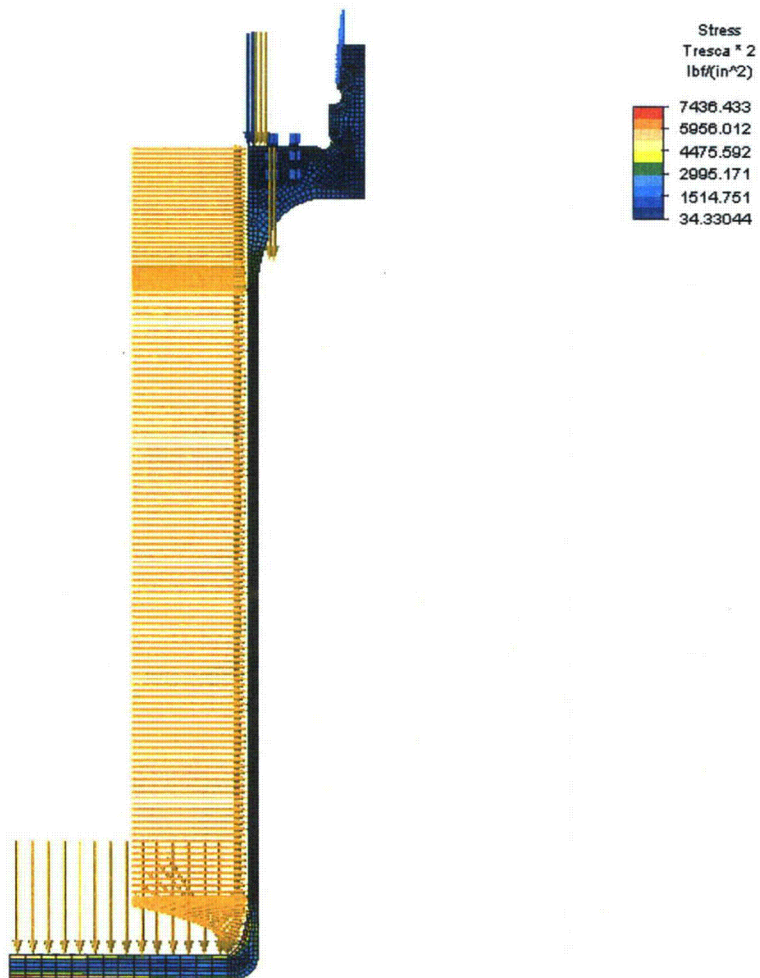Minimum Value: 34.3304 lbf/(in^2)

Fig. 1 – Stress Intensity in Containment Vessel due to Load Case 1

GENERAL DESIGN AND COMPUTATION SHEET

JOB ASME Code Subsection NB Stress Analysis of ES-3100 Containment Vessel		DATE 14 December 2006	SHEET 12 of 26
DAC NO. DAC-EA-900000-A006	REVISION NO. 2	COMPUTED C. R. Hammond	CHECKED BY R. M. Jessee

Stress
Tresca * 2
lbf/(in^2)

1202.601
962.0807
721.5605
481.0404
240.5202
4.685358e-009

Load Case: 2 of 2

Maximum Value: 1202.6 lbf/(in^2)
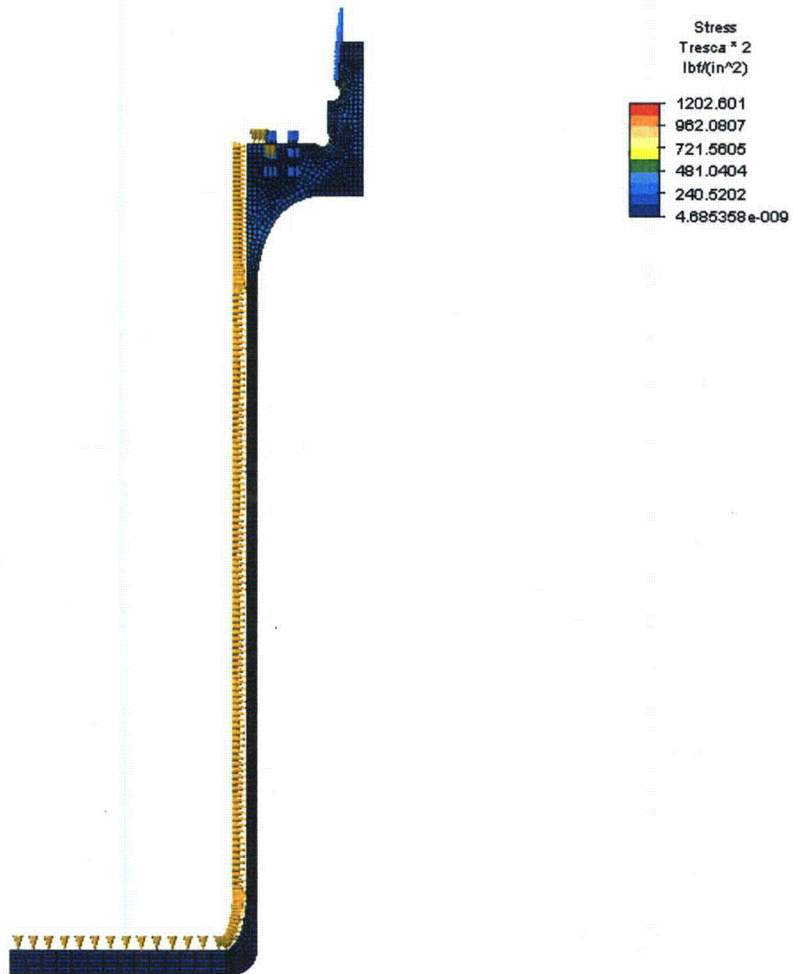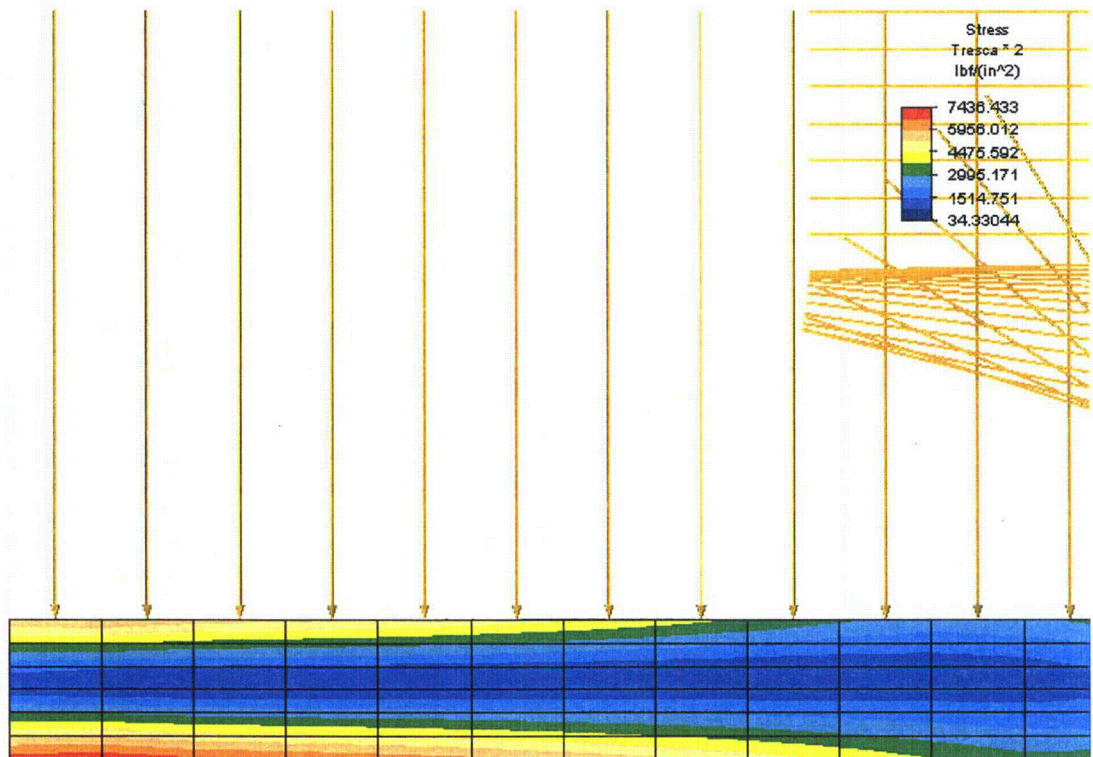
Minimum Value: 4.68536e-009 lbf/(in^2)

Fig. 2 – Stress Intensity in Containment Vessel due to Load Case 2

2-112

GENERAL DESIGN AND COMPUTATION SHEET

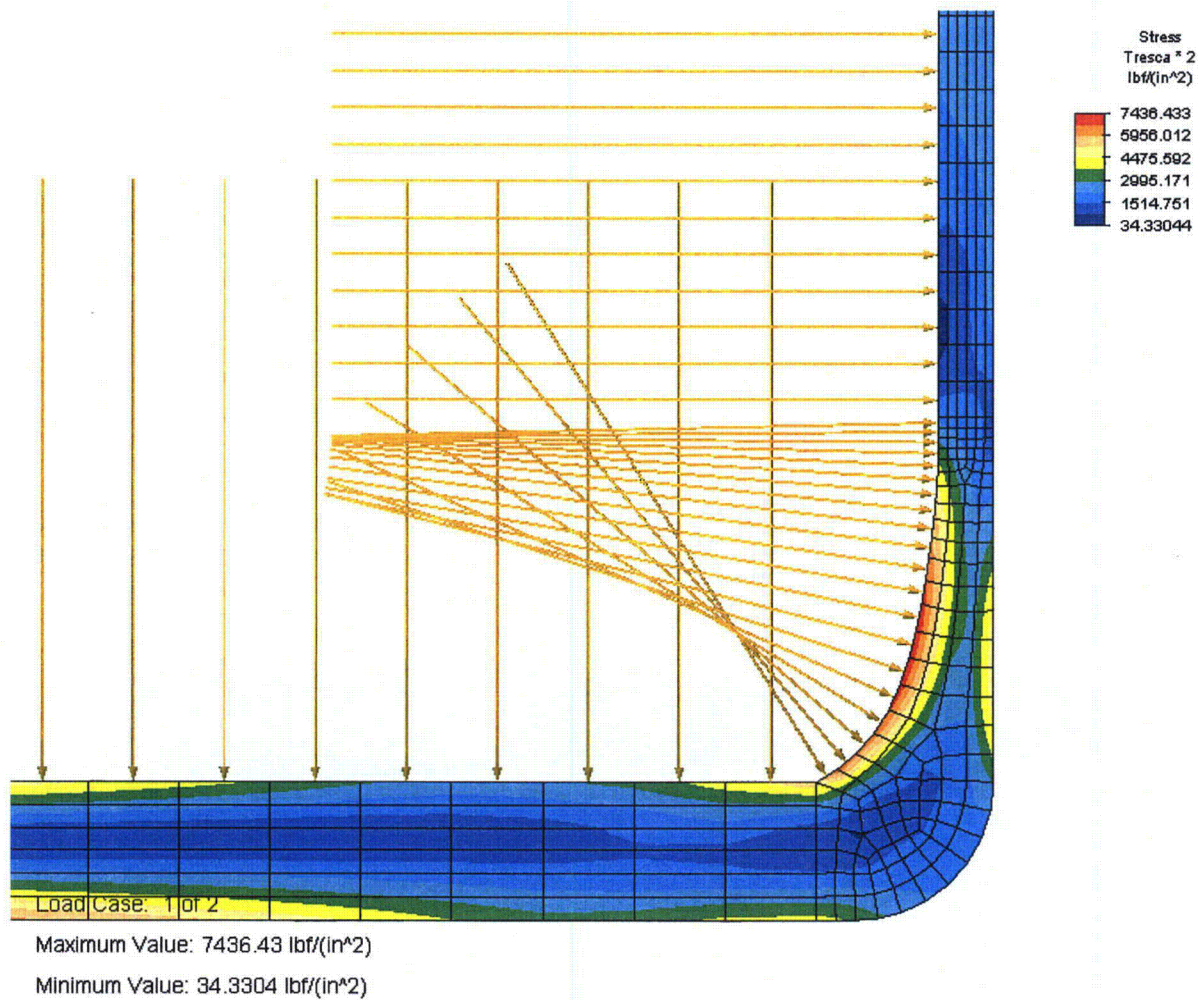| JOB ASME Code Subsection NB Stress Analysis of ES-3100 Containment Vessel		DATE 14 December 2006	SHEET 13 of 26
DAC NO. DAC-EA-900000-A006	REVISION NO. 2	COMPUTED C. R. Hammond	CHECKED BY R. M. Jessee

Load Case: 1 of 2

Maximum Value: 7436.43 lbf/(in^2)

Minimum Value: 34.3304 lbf/(in^2)

Fig. 3 – Stress Intensity in the Bottom of the Containment Vessel due to Load Case 1

GENERAL DESIGN AND COMPUTATION SHEET

JOB ASME Code Subsection NB Stress Analysis of ES-3100 Containment Vessel		DATE 14 December 2006	SHEET 14 of 26
DAC NO. DAC-EA-900000-A006	REVISION NO. 2	COMPUTED C. R. Hammond	CHECKED BY R. M. Jessee

Stress
Tresca * 2
lbf/(in^2)

7436.433
5956.012
4475.592
2995.171
1514.751
34.33044

Load Case: 1 of 2

Maximum Value: 7436.43 lbf/(in^2)

Minimum Value: 34.3304 lbf/(in^2)

. Fig. 4 – Stress Intensity at Junction of Bottom and Side of Containment Vessel due to Load Case 1

2-114

GENERAL DESIGN AND COMPUTATION SHEET

JOB ASME Code Subsection NB Stress Analysis of ES-3100 Containment Vessel		DATE 14 December 2006	SHEET 15 of 26
DAC NO. DAC-EA-900000-A006	REVISION NO. 2	COMPUTED C. R. Hammond	CHECKED BY R. M. Jessee

Fig. 5 – Stress Intensity in Flange Region of Containment Vessel due to Load Case 1

GENERAL DESIGN AND COMPUTATION SHEET

JOB ASME Code Subsection NB Stress Analysis of ES-3100 Containment Vessel		DATE 14 December 2006	SHEET 16 of 26
DAC NO. DAC-EA-900000-A006	REVISION NO. 2	COMPUTED C. R. Hammond	CHECKED BY R. M. Jessee

Load Case: 2 of 2

Maximum Value: 1202.6 lbf/(in^2)

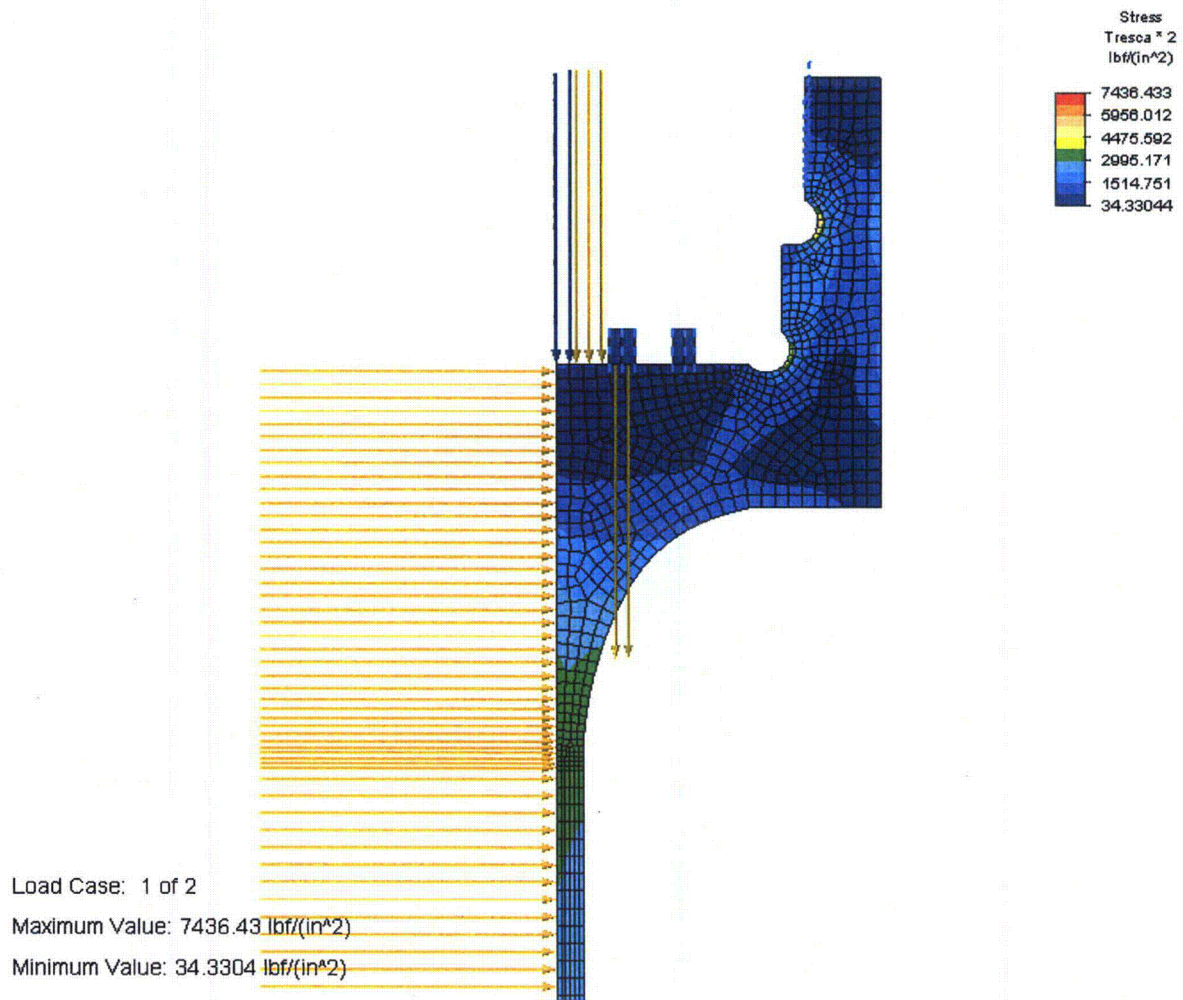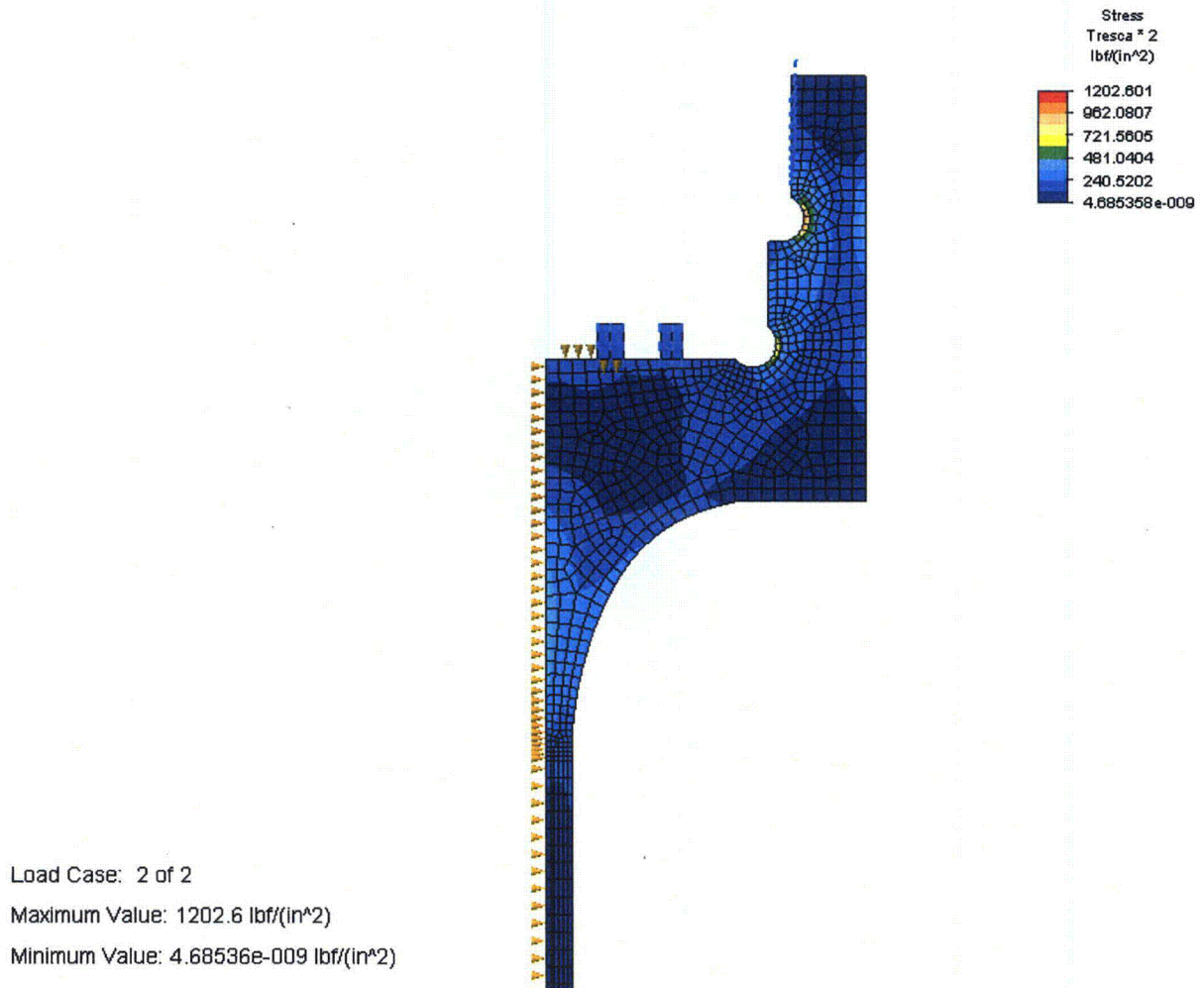Minimum Value: 4.68536e-009 lbf/(in^2)

Fig. 6 – Stress Intensity in Flange Region of Containment Vessel due to Load Case 2

2-116

GENERAL DESIGN AND COMPUTATION SHEET

JOB ASME Code Subsection NB Stress Analysis of ES-3100 Containment Vessel		DATE 14 December 2006	SHEET 17 of 26
DAC NO. DAC-EA-900000-A006	REVISION NO. 2	COMPUTED C. R. Hammond	CHECKED BY R. M. Jessee
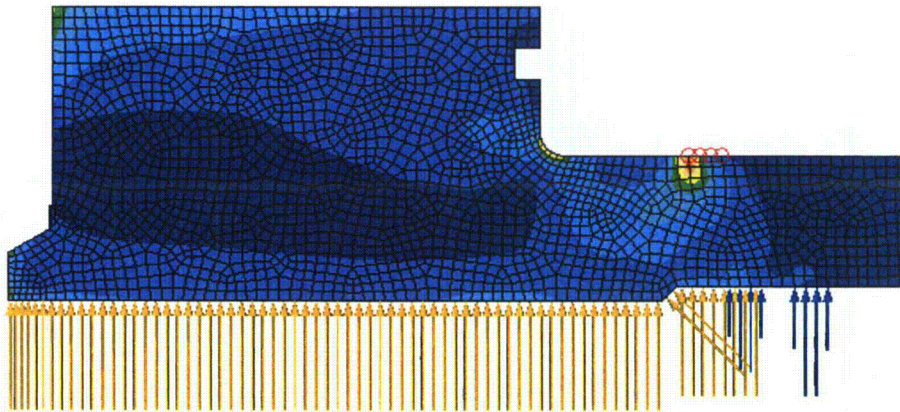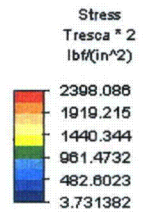
Load Case: 1 of 2

Maximum Value: 2398.09 lbf/(in^2)

Minimum Value: 3.73138 lbf/(in^2)

Fig. 7 – Stress Intensity in CV Lid due to Load Case 1

GENERAL DESIGN AND COMPUTATION SHEET

JOB ASME Code Subsection NB Stress Analysis of ES-3100 Containment Vessel		DATE 14 December 2006	SHEET 18 of 26
DAC NO. DAC-EA-900000-A006	REVISION NO. 2	COMPUTED C. R. Hammond	CHECKED BY R. M. Jessee

Stress
Tresca * 2
lbf/(in^2)

871.9193
697.7833
523.6473
349.5113
175.3754
1.23938
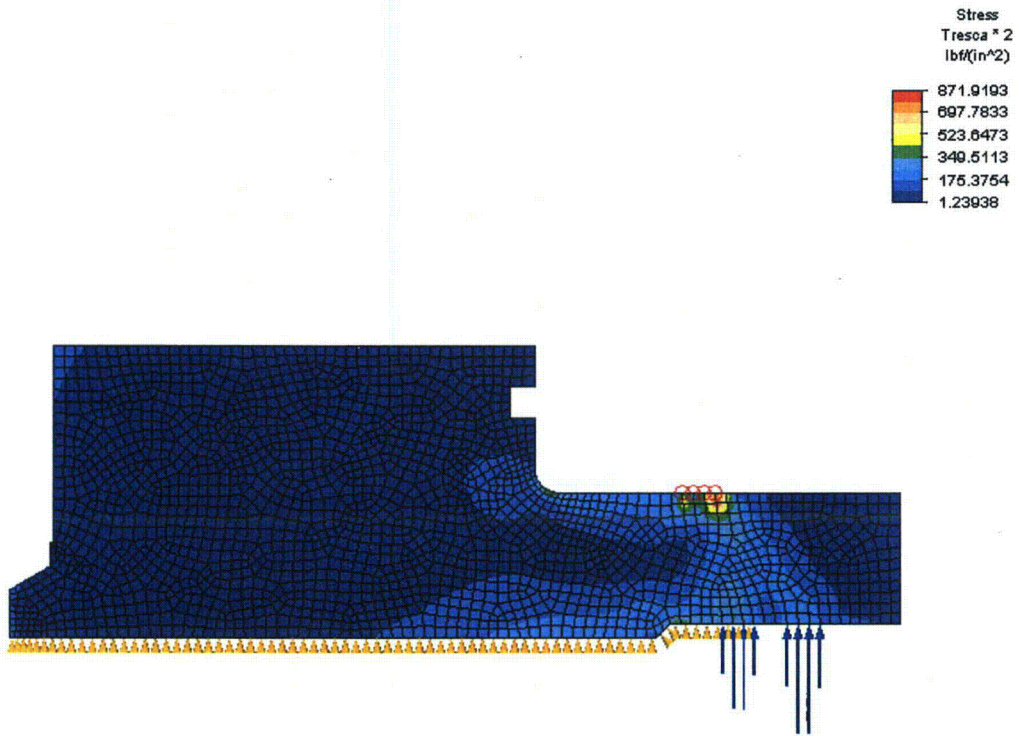
Load Case: 2 of 2

Maximum Value: 871.919 lbf/(in^2)

Minimum Value: 1.23938 lbf/(in^2)

Fig. 8 – Stress Intensity in CV Lid due to Load Case 2

GENERAL DESIGN AND COMPUTATION SHEET

JOB ASME Code Subsection NB Stress Analysis of ES-3100 Containment Vessel		DATE 14 December 2006	SHEET 19 of 26
DAC NO. DAC-EA-900000-A006	REVISION NO. 2	COMPUTED C. R. Hammond	CHECKED BY R. M. Jessee

Stress
Tresca * 2
lbf/(in^2)

8569.746
6869.954
5170.162
3470.37
1770.578
70.78623
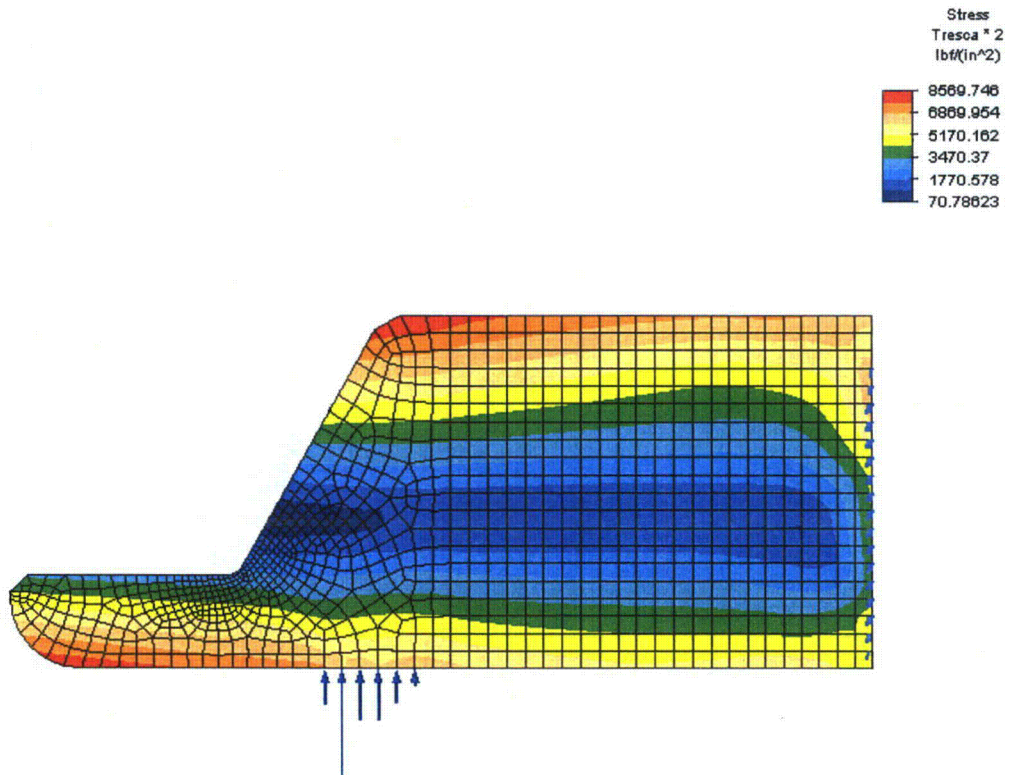
Load Case: 1 of 2

Maximum Value: 8569.75 lbf/(in^2)

Minimum Value: 70.7862 lbf/(in^2)

Fig. 9 – Stress Intensity in Nut due to Load Case 1

GENERAL DESIGN AND COMPUTATION SHEET

JOB ASME Code Subsection NB Stress Analysis of ES-3100 Containment Vessel		DATE 14 December 2006	SHEET 20 of 26
DAC NO. DAC-EA-900000-A006	REVISION NO. 2	COMPUTED C. R. Hammond	CHECKED BY R. M. Jessee

Stress
Tresoa * 2
lbf/(in^2)

- 2223.51
- 1786.188
- 1348.867
- 911.5452
- 474.2237
- 36.9021
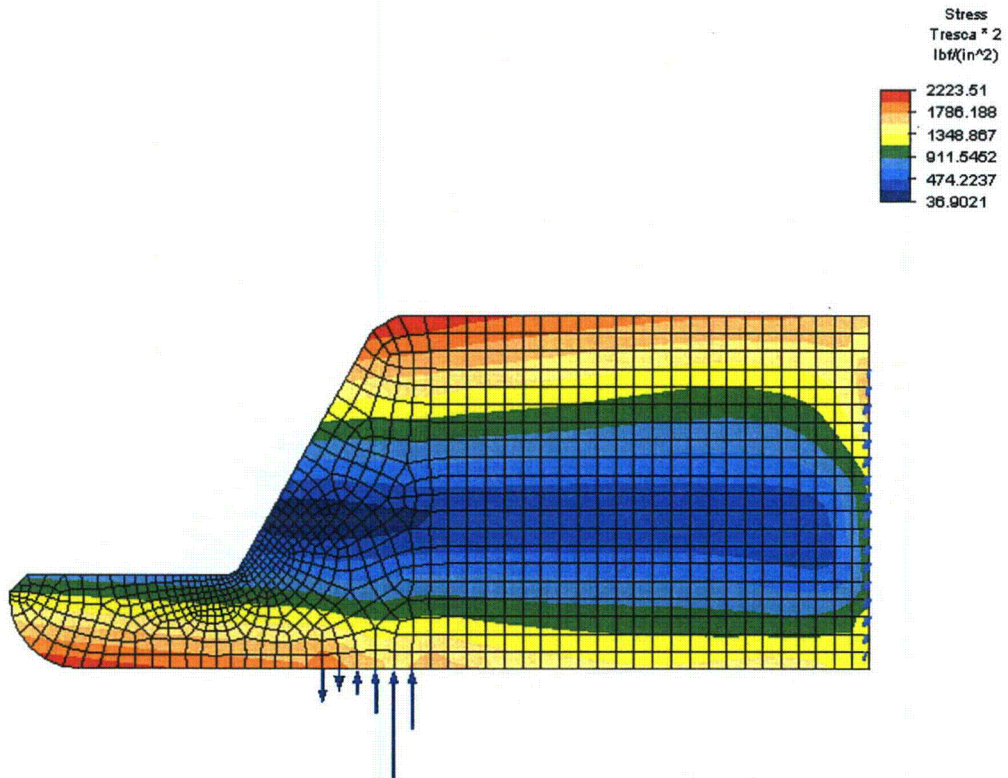
Load Case: 2 of 2

Maximum Value: 2223.51 lbf/(in^2)

Minimum Value: 36.9021 lbf/(in^2)

Fig. 10 – Stress Intensity in Nut due to Load Case 2

GENERAL DESIGN AND COMPUTATION SHEET

JOB ASME Code Subsection NB Stress Analysis of ES-3100 Containment Vessel		DATE 14 December 2006	SHEET 21 of 26
DAC NO. DAC-EA-900000-A006	REVISION NO. 2	COMPUTED C. R. Hammond	CHECKED BY R. M. Jessee

Strain
Tensor Y-Y
lbf/(in^2)

0.0001772113
0.0001126586
4.810583e-005
-1.644692e-005
-8.099967e-005
-0.0001455524

Load Case: 1 of 2

Maximum Value: 0.000177211 lbf/(in^2)

Minimum Value: -0.000145552 lbf/(in^2)
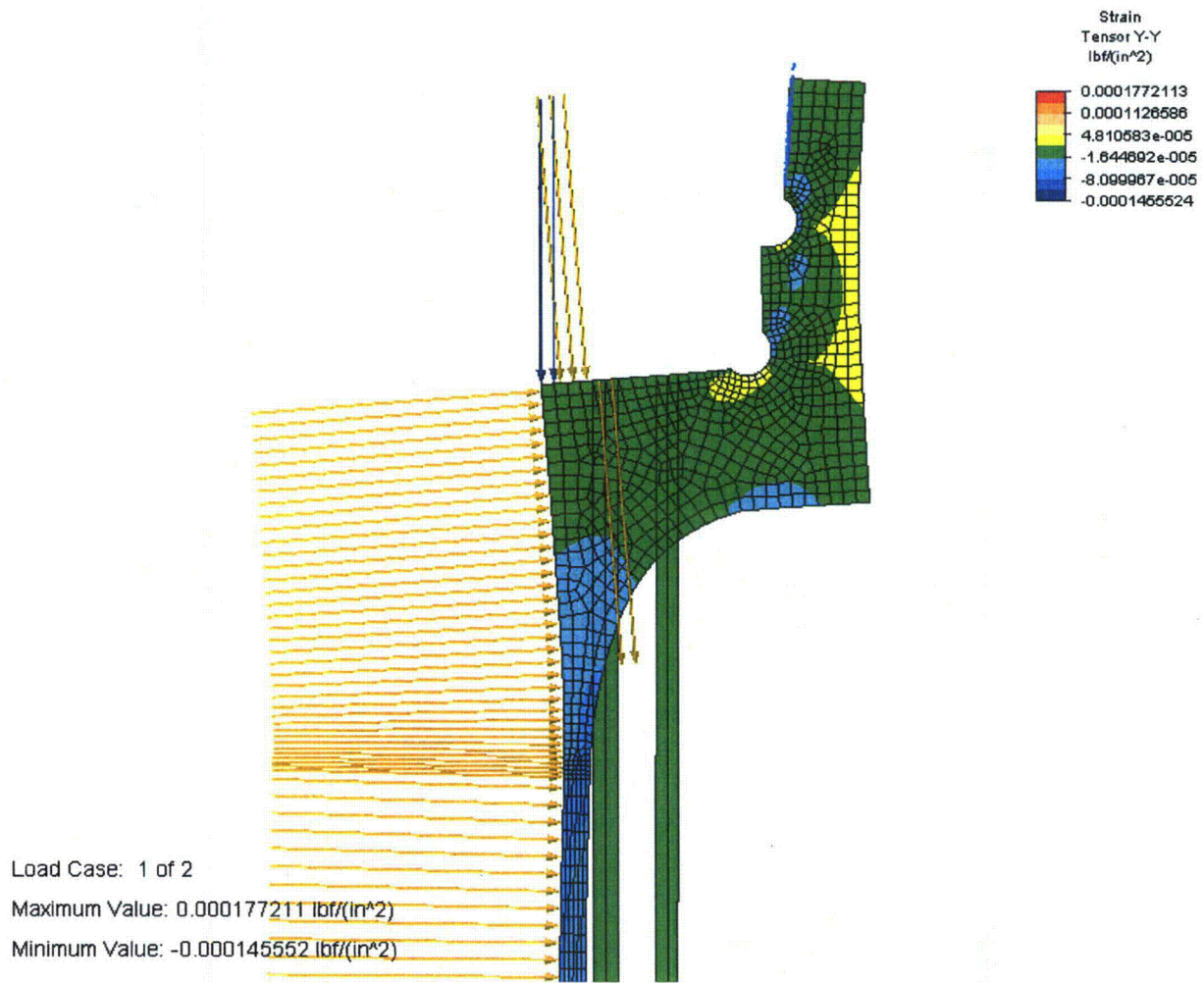
Fig. 11 – Radial Strain in the Flange Region of the Containment Vessel due to Load Case 1

(Distortion is Exaggerated)

GENERAL DESIGN AND COMPUTATION SHEET

DAC NO. DAC-EA-900000-A006	REVISION NO. 2	COMPUTED C. R. Hammond	CHECKED BY R. M. Jessee

ATTACHMENT A – O-RING SPRING CONSTANT

Compression of 0.139 in. dia. O-ring (Parker Seals, "O-Ring Handbook," ORD-5700A/US, 2001) [a]

Diameter = 0.139 D = 70 D = 80

% compression	Min (Force)	Max				Ave	Del	K
5	0.00695	0.93	6.1	2.5	10	4.8825	0.00695	702.518
10	0.0139	2	14	4.5	20	10.125	0.0139	728.4173
20	0.0278	4.5	30	9	45	22.125	0.0278	795.8633
30	0.0417	11	72	20	90	48.25	0.0417	1157.074
40	0.0556	19	160	40	180	99.75	0.0556	1794.065

K
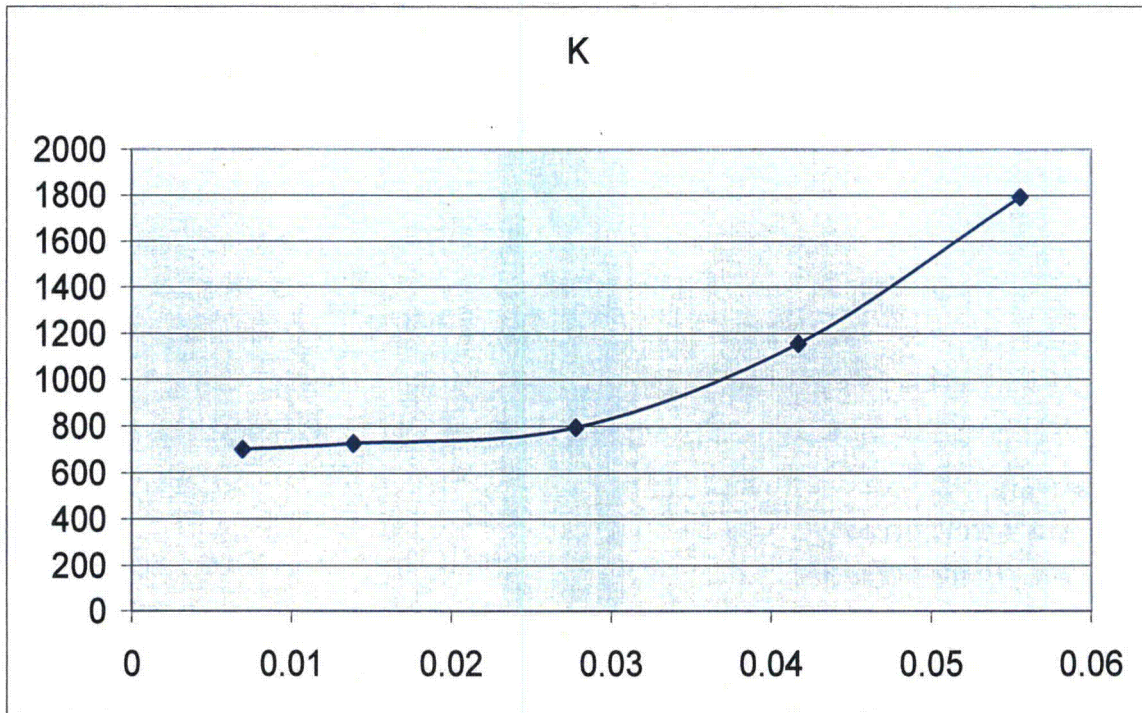
a. Page 2-15 in the O-ring Handbook.

2-122

GENERAL DESIGN AND COMPUTATION SHEET

JOB ASME Code Subsection NB Stress Analysis of ES-3100 Containment Vessel		DATE 14 December 2006	SHEET 23 of 26
DAC NO. DAC-EA-900000-A006	REVISION NO. 2	COMPUTED C. R. Hammond	CHECKED BY R. M. Jessee

ATTACHMENT B –RESULTS FOR O-RING ELEMENTS FROM FINITE ELEMENT ANALYSIS OF CONTAINMENT VESSEL

```
**** Nodal stresses for 2-D elasticity elements:

El. #  LC ND  Sigma-11    Sigma-22    Sigma-33    Tau-12      Sigma-Max   Sigma-Min
              Sigma-Int
-----  --- --  ----------  ----------  ----------  ----------  ----------  ----------
    1   1  I   7.151E-03   -2.347E+02  -3.629E-02  1.115E-02   7.152E-03   -2.347E+02
              -3.629E-02
    1   1  J   6.460E-03   -2.348E+02  -3.564E-02  1.099E-02   6.460E-03   -2.348E+02
              -3.564E-02
    1   1  K   7.565E-04   -2.348E+02  -4.589E-02  9.078E-03   7.568E-04   -2.348E+02
              -4.589E-02
    1   1  L   1.448E-03   -2.347E+02  -4.662E-02  9.233E-03   1.448E-03   -2.347E+02
              -4.662E-02
    1   2  I  -3.586E-03   -2.371E+02  -6.498E-03  8.397E-03  -3.586E-03   -2.371E+02
              -6.498E-03
    1   2  J  -3.713E-03   -2.371E+02  -6.454E-03  8.271E-03  -3.713E-03   -2.371E+02
              -6.454E-03
    1   2  K   5.712E-03   -2.371E+02  -7.804E-03  7.936E-03   5.712E-03   -2.371E+02
              -7.804E-03
    1   2  L   5.839E-03   -2.371E+02  -8.014E-03  8.062E-03   5.839E-03   -2.371E+02
              -8.014E-03

    2   1  I   8.755E-03   -2.348E+02  -3.608E-02  -8.886E-03  8.756E-03   -2.348E+02
              -3.608E-02
    2   1  J   8.182E-03   -2.350E+02  -3.552E-02  -8.763E-03  8.183E-03   -2.350E+02
              -3.552E-02
    2   1  K  -7.855E-05   -2.350E+02  -4.575E-02  -1.064E-02  -7.807E-05  -2.350E+02
              -4.575E-02
    2   1  L   4.944E-04   -2.348E+02  -4.633E-02  -1.077E-02  4.949E-04   -2.348E+02
              -4.633E-02
    2   2  I  -3.637E-03   -2.371E+02  -6.900E-03  -9.129E-03  -3.636E-03  -2.371E+02
              -6.900E-03
    2   2  J  -3.745E-03   -2.371E+02  -6.860E-03  -9.012E-03  -3.745E-03  -2.371E+02
              -6.860E-03
    2   2  K   5.687E-03   -2.371E+02  -8.074E-03  -9.358E-03  5.687E-03   -2.371E+02
              -8.074E-03
    2   2  L   5.795E-03   -2.371E+02  -8.250E-03  -9.475E-03  5.796E-03   -2.371E+02
              -8.250E-03


**** 2-D Elasticity elements:

        Number of elements       =     2
        Number of materials      =     5
        Maximum temperature pts  =     1
        Analysis code            =     0
          0 : axisymmetric
          1 : plane strain
          2 : plane stress
        Incompatible modes       =     0
          0 : included
          1 : not included

**** Nodal stresses for 2-D elasticity elements:

El. #  LC ND  Sigma-11    Sigma-22    Sigma-33    Tau-12      Sigma-Max   Sigma-Min
              Sigma-Int
-----  --- --  ----------  ----------  ----------  ----------  ----------  ----------
    1   1  I   1.838E-03   -1.987E+02  -3.397E-02  7.582E-03   1.838E-03   -1.987E+02
              -3.397E-02
    1   1  J   1.110E-03   -1.988E+02  -3.334E-02  7.464E-03   1.111E-03   -1.988E+02
              -3.334E-02
```

2-123

JOB ASME Code Subsection NB Stress Analysis of ES-3100 Containment Vessel		DATE 14 December 2006	SHEET 24 of 26
DAC NO. DAC-EA-900000-A006	REVISION NO. 2	COMPUTED C. R. Hammond	CHECKED BY R. M. Jessee

```
1    1    K    1.855E-03   -1.988E+02  -4.282E-02   5.515E-03   1.856E-03   -1.988E+02
                -4.282E-02
1    1    L    2.583E-03   -1.987E+02  -4.364E-02   5.634E-03   2.583E-03   -1.987E+02
                -4.364E-02
1    2    I   -1.419E-03   -2.013E+02  -5.945E-03   6.027E-03  -1.419E-03   -2.013E+02
                -5.945E-03
1    2    J   -1.558E-03   -2.013E+02  -5.865E-03   5.923E-03  -1.558E-03   -2.013E+02
                -5.865E-03
1    2    K    3.687E-03   -2.013E+02  -7.071E-03   5.591E-03   3.687E-03   -2.013E+02
                -7.071E-03
1    2    L    3.825E-03   -2.013E+02  -7.268E-03   5.696E-03   3.825E-03   -2.013E+02
                -7.268E-03

2    1    I    1.931E-03   -1.988E+02  -3.367E-02  -3.542E-03   1.931E-03   -1.988E+02
                -3.367E-02
2    1    J    1.223E-03   -1.990E+02  -3.305E-02  -3.463E-03   1.223E-03   -1.990E+02
                -3.305E-02
2    1    K    1.761E-03   -1.990E+02  -4.236E-02  -5.358E-03   1.762E-03   -1.990E+02
                -4.236E-02
2    1    L    2.469E-03   -1.988E+02  -4.316E-02  -5.436E-03   2.469E-03   -1.988E+02
                -4.316E-02
2    2    I   -1.833E-03   -2.013E+02  -6.185E-03  -5.247E-03  -1.833E-03   -2.013E+02
                -6.185E-03
2    2    J   -1.970E-03   -2.013E+02  -6.110E-03  -5.152E-03  -1.969E-03   -2.013E+02
                -6.110E-03
2    2    K    3.840E-03   -2.013E+02  -7.192E-03  -5.486E-03   3.841E-03   -2.013E+02
                -7.192E-03
2    2    L    3.977E-03   -2.013E+02  -7.391E-03  -5.581E-03   3.978E-03   -2.013E+02
                -7.391E-03
```

GENERAL DESIGN AND COMPUTATION SHEET

JOB ASME Code Subsection NB Stress Analysis of ES-3100 Containment Vessel	DATE 14 December 2006	SHEET 25 of 26
DAC NO. DAC-EA-900000-A006	REVISION NO. 2	COMPUTED C. R. Hammond	CHECKED BY R. M. Jessee

ATTACHMENT C – O-RING INTERFACE LOADS

Axisymmetric nodal forces on lid from O-ring pressure

Inner O-ring

Node number	Node radius	Mean radius	Force/pressure factor	Load case 1 Pressure	Load case 1 Force	Load case 2 Pressure	Load case 2 Force
143	2.69812		0.053659565	198.825	10.66886299	201.3	10.80167042
		2.717935					
144	2.73775		0.108483245	198.825	21.56918112	201.3	21.83767716
		2.75756					
145	2.77737		0.110053385	198.825	21.88136433	201.3	22.15374646
		2.797185					
146	2.817		0.055622538	198.825	11.0591511	201.3	11.19681688

Outer O-ring

149	2.942		0.061513619	234.825	14.44493549	237.1	14.58487897
		2.962835					
150	2.98367		0.124314506	234.825	29.19215396	237.1	29.47496946
		3.0045					
151	3.02533		0.126050479	234.825	29.59980364	237.1	29.88656848
		3.046165					
152	3.067		0.063683896	234.825	14.95457097	237.1	15.09945183

2-125

GENERAL DESIGN AND COMPUTATION SHEET

ATTACHMENT D – INTERFACE LOADS ON NUT

Matching interface pressure loads
Load Case 1

		Side 1					Side 2		
Index	Radius	Szz	FORCEz	Force/Rad	Index	Radius	Szz	FORCEz	Force/Rad
0	2.50507	0				2.50964	0		
1	2.54629	-3300.16	-136.0161	-346.3364		2.53798	-800	-22.668	-57.53093
2	2.5875	-1230.75	-50.71921	-131.2359		2.56631	-3300.16	-97.27222	-249.6307
3	2.62871	-662.77	-27.31275	-71.7973		2.59693	-1230.75	-37.67941	-97.85079
4	2.66992	-65.6015	-2.703438	-7.217963		2.62754	-1230.75	-37.67941	-99.00416
5	2.71113	0				2.65816	-662.77	-20.2907	-53.93594
Sum			-216.7515	-556.5876		2.68877	-65.6015	-2.00839	-5.400099
						2.71939	0		
					Sum			-217.5981	-563.3526
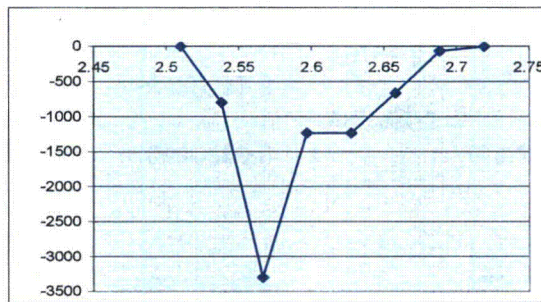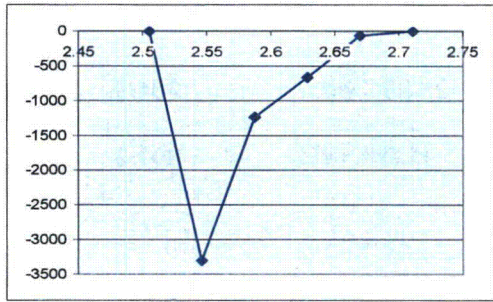
Load Case 2

		Side 1					Side 2		
Index	Radius	Szz	FORCEz	Force/Rad	Index	Radius	Szz	FORCEz	Force/Rad
0	2.50507	0				2.50964	0		
1	2.54629	301.824	12.43968	31.67502		2.53798	301.824	8.552183	21.70527
2	2.5875	-132.484	-5.459666	-14.12688		2.56631	100	2.9475	7.564199
3	2.62871	-398.673	-16.42931	-43.1879		2.59693	-132.484	-4.055998	-10.53314
4	2.66992	-1240.54	-51.12265	-136.4934		2.62754	-398.673	-12.20537	-32.07011
5	2.71113	0				2.65816	-1240.54	-37.97913	-100.9546
Sum			-60.57196	-162.1332		2.68877	-600	-18.369	-49.39002
						2.71939	0		
					Sum			-61.10982	-163.6784
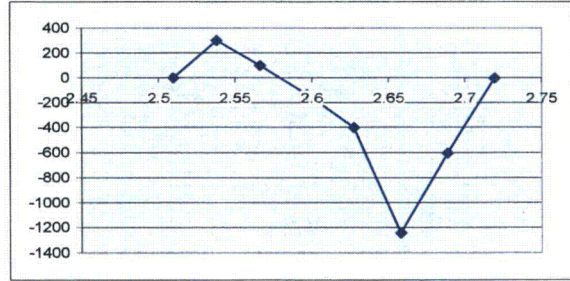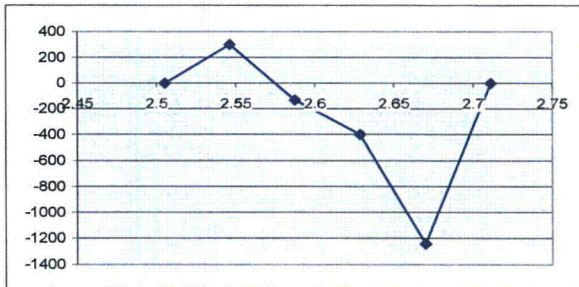
2-126

GENERAL DESIGN AND COMPUTATION SHEET

JOB Fatigue Analysis of ES-3100 CV Threads under Normal Conditions of Use		DATE 16 February 2005	SHEET 1 of 30
DAC NO. DAC-EA-900000-A007	REVISION NO. 0	COMPUTED C. R. Hammond	CHECKED BY M. L. Goins

1.0 TABLE OF CONTENTS

2-127

GENERAL DESIGN AND COMPUTATION SHEET

JOB Fatigue Analysis of ES-3100 CV Threads under Normal Conditions of Use	DATE 16 February 2005	SHEET 2 of 30
DAC NO. DAC-EA-900000-A007	REVISION NO. 0	COMPUTED C. R. Hammond	CHECKED BY M. L. Goins

2.0 OBJECTIVE

The 7°/45° Buttress threads, specified per ANSI B1.9-1973 7.0-8 Push, used to secure the lid of the ES-3100 Containment Vessel are evaluated for fatigue resistance under normal conditions of use. The evaluation is based on rules in NB-3232.3 from ASME B&PV Code, Section III.

3.0 EVALUATION INPUT (CRITERIA) AND SOURCE

3.1 REFERENCES USED

(B1.9) *Buttress Inch Screw Threads*, ANSI B1.9 – 1973, The American Society of Mechanical Engineers, 1973.

(Code) *Class 1 Components, Section III, Rules for Construction of Nuclear Power Plant Components*, Division 1, 2001 Edition with 2003 Addenda, The American Society of Mechanical Engineers, 2003.

(Drawing) "Containment Vessel Assembly," M2E801580A011, Rev. A, BWXT Y-12, 2003.

(Hammond) "ASME Code Subsection NB Stress Analysis of ES-3100 Containment Vessel," DAC-EA-900000-A006, Rev. 1, BWXT Y-12, 2004.

(Laughner & Hargan) *Handbook of Fastening and Joining of Metal Parts*, McGraw-Hill Book Company, 1956, pp. 167-168.

(Section II) *Section II, Materials*, Part D – Properties, 2001 Edition with 2003 Addenda, The American Society of Mechanical Engineers, 2003.

(SST/SGT) J. S. Cap, "Recommended Random Vibration and Shock Test Specifications for Cargo Transported on SST and SGT Trailers," letter to distribution, Sandia National Laboratory, Albuquerque, New Mexico, 2002.

3.2 DESIGN CONDITIONS

Hot NCT: Internal pressure of 17.786 psia at 190.06° F.

Cold NCT: Internal pressure of 11.13 psia at -40° F.

3.3 METHODS TO BE USED

A finite element model described in DAC-EA-900000-A006 by Hammond was used. The program was verified by running problems with known solutions. The file name for the model is ES3100CV1. Properties used in the model are shown in Appendix 2.

2-128

GENERAL DESIGN AND COMPUTATION SHEET

JOB Fatigue Analysis of ES-3100 CV Threads under Normal Conditions of Use		DATE 16 February 2005	SHEET 3 of 30
DAC NO. DAC-EA-900000-A007	REVISION NO. 0	COMPUTED C. R. Hammond	CHECKED BY M. L. Goins

4.0 ANALYSES AND/OR CALCULATIONS

The previous analysis (Hammond) followed ASME Code rules to validate the vessel design under a bounding internal pressure of 101.5 psi. The design margin of the vessel, including the vessel body, the lid, and the retaining nut but not including threads on the nut or vessel body, was limited by stress intensity calculated at the side wall to bottom transition of the vessel. The actual maximum expected internal pressure is 17.786 psia or 17.786 psia − 14.7 psia = 3.1 psig. Away from the contact region between the lid and vessel body, stresses are proportional to pressure so the stress in the body and at the center of the lid will be reduced to 3.1 psi/101.5 psi = 0.0305 or 3.05% of values calculated previously. The design margin in the vessel becomes limited by stresses in the clamping region primarily due to gasket seating load or the load produced by tightening the nut. These calculations determine the load from torquing the nut and their effects on stress in the vessel components in the contact or clamping region.

4.1 TIGHTENING TORQUE

The specified nut torque is 120 +/- 5 ft.-lb. From Laughtner & Hargan, the ratio of axial force, P (lb.), to torque, T (in.-lb.) is

$$\frac{P}{T} = \frac{2}{(D\,v + d_p\,m)}, \text{ where}$$

D = mean bearing diameter of nut (in.),

dp = pitch diameter of screw thread (in.),

v = coefficient of friction between nut and bearing surface,

$$m = \frac{\tan(\beta + \phi)}{\cos\alpha}, \text{ where}$$

α = one-half of thread profile angle (degrees),

β = helix angle (degrees), and

ϕ = friction angle the tangent of which is the friction coefficient.

The threads are 7 inch nominal diameter with 8 threads per inch or having a pitch of 0.125 in. From B1.9 the pitch diameter is

$$d_p = 7\,\text{in.} - 0.6\,(0.125\,\text{in.}) = 6.93\,\text{in.}$$

The helix angle on the pitch diameter is

$$\beta = \arctan\frac{0.125\,\text{in.}}{\pi(6.93\,\text{in.})} = 0.329°.$$

The thread profile angle at the mating surfaces is 7° so $\alpha = 3.5°$.

2-129

GENERAL DESIGN AND COMPUTATION SHEET

The mean effective bearing diameter of the nut is about 5.8 inches. That is D = 5.8 in.

The referenced drawing has the note: "During installation of container vessel lid assembly, apply a light coat of Krytox grease to the threads and under the nut." A typical value for coefficient of friction for lubricated threads is 0.11. In this case

$\phi = \arctan(0.11) = 6.3$.

$$m = \frac{\tan(0.329° + 6.3°)}{\cos(3.5°)} = 0.12.$$

$$P/T = 2/(5.8\,in.(0.11) + 6.93\,in.(0.12)) = 1.36.$$

The maximum and the minimum force, assuming that the friction coefficient 0.11 is correct are

Pmax = 1.36 T = 1.36 (125 ft.-lb)(12 in./ft.) = 2,000 lb., rounding to 2 significant figures, and

Pmin = 1.36 (115 ft.-lb.)(12 in./ft.) = 1,900 lb.

According to Hammond the force required to seat the gaskets is
$W_{m2} = 20\,lb./in.\,\pi[(5.359\,in. + 0.139\,in.) + (5.859\,in. + 0.139\,in.)] = 722.3\,lb$ and

the load due to the maximum allowable pressure, 101.5 psig, to the outer edge of the inner O-ring groove is

$$W_{m1} = \pi\frac{101.5\,psig\,(5.624\,in.)^2}{4} = 2521\,lb.$$

The sum of gasket seating and pressure forces is 3,244 lb. so the specified torque is not adequate for the bounding pressure. However, the highest expected internal pressure is 17.786 psia which is (17.786 psia – 14.7 psia =) 3.1 psig so

$$W_{m1} = \pi\frac{3.1\,psig\,(5.624\,in.)^2}{4} = 77\,lb.$$

The sum of gasket seating force and actual pressure force is 799 lb and there is a large margin on torque required to maintain a tight gasket and consequently the required torque is not sensitive to the coefficient of friction.

The minimum cross section area of the CV subject to the axial force from torquing the nut is at the undercut just below the threads. The inside diameter at the undercut is 6.85 in. +2(0.09 in.) = 7.03 in. The outside diameter in the same plane is 7.50 in. The minimum cross section area considering the tolerances listed on the drawing is $\pi((7.50\,in. - 0.01\,in.)^2 - (7.03\,in. + 0.01\,in.)^2))/4 = 5.14\,in^2$.

The average axial stress due to the force due to maximum torque at this section is

$\overline{\sigma}_{torque} = 2,000\,lb. / 5.14\,in^2 = 389\,psi.$

2-130

GENERAL DESIGN AND COMPUTATION SHEET

The maximum diameter at the root of a thread on the CV is 7.04 in. That is called the maximum major diameter of the internal thread which per B1.9 is $D - h + PDtol. + 0.80803\, p$, where D is the major diameter (7 in.), h is the basic height of thread engagement (0.6 p), PDtol. is tolerance on pitch diameter (0.0101 in.), and p is pitch (0.125 in.). The cross section area at the root of the thread is thus the same as the minimum area at the undercut (i.e. 7.03 in. + 0.01 in. including tolerance) and the average stress is the same.

The finite element model used by Hammond to evaluate pressure resistance was modified to simulate the effect of the axial force due to torquing the nut. The section of the vessel between the flange surface and the threads was forced to shrink in the axial direction by applying an artificial temperature drop of 100° F. and manipulating the axial coefficient of thermal expansion to produce an axial force of 2,000 lb. Fig. 1 shows the effected region of the vessel with dots at the locations where axial stresses were recorded. The O-ring elements were removed and the entire flange surface was held in place by stiff axial spring elements. Nodal axial stresses were obtained across the two horizontal sections. There were two stresses calculated at each point, one above and one below the section boundary. The stress in the section without the temperature-dependent properties was recorded to avoid including thermal strain in the stress calculation. The results from the final run are shown on the spreadsheet along with the axial stress calculated at each point across the two sections in Appendix 1.

The net axial forces across each section were calculated by multiplying the axial stress over the tributary area. There was a slight but acceptable difference (4%) between the upper and lower sections attributed to model coarseness. The net force across the section with the highest axial stress was about 2% greater than 2000 lb.

The plot of axial stress shown in Appendix 1 clearly indicates that the peak stress at the left edge is higher than an extrapolated equivalent linear bending stress. The value of peak stress due to preload from torque, 3,476 psi, is so low that we can substitute this peak stress for the sum of membrane and bending stress in combination with axial stress from other loads.

The gasket seating force between the lid and CV body is the sum of gasket seating forces at both O-rings or 722.3 lb. total. The pressure force due to the 101.5 psig from the earlier calculation over the area to the back side of the inner O-ring groove is

$$F_p = 101.5\,\text{psi}\,\pi\,(2.817\,\text{in.})^2 = 2530\,\text{lb.}$$

In general, stress intensities are not linear functions of applied force but in our case of the axial force due to torque on the nut alone, stress intensities will increase by the ratio 2000 lb./722.3 lb. = 2.77 . The calculated peak stress intensity due to gasket seating load alone (Load Case 2) were highest near points of high compression that would be affected by the applied torque. The peak values were 872 psi in the lid and 2224 psi in the nut (Hammond, pp. 18, 20). The stresses in these components due to torque would be 2.77(872 psi) = 2415 psi in the lid and 2.77(2224 psi) = 6158 psi in the nut.

Bending or radial stress near the center of the lid and stresses in the vessel body away from the contact region will be reduced to about 3.05% of previously calculated values.

2-131

GENERAL DESIGN AND COMPUTATION SHEET

JOB Fatigue Analysis of ES-3100 CV Threads under Normal Conditions of Use	DATE 16 February 2005	SHEET 6 of 30
DAC NO. DAC-EA-900000-A007	REVISION NO. 0	COMPUTED C. R. Hammond	CHECKED BY M. L. Goins

The effect of an internal 3.1 psig pressure plus the torque is shown in Fig. 3. Maximum stress intensity is 3501 psi. This is in the same location as for the pressure plus gasket seat case, in the transition between the side and bottom of the vessel. The axial stress in this region due to 3.1 psi pressure and torque is shown on Fig. 4. The peak axial stress is 3714 psi. The slight pressure causes just a slight increase in stress over the case with torque alone. The stress intensities in the clamping regions of the lid and nut will become about (3714 psi/3476 psi) 2415 psi = 2580 psi and (3714 psi/3476 psi) 6158 psi = 6580 psi, respectively.

4.2 DIFFERENTIAL THERMAL EXPANSION

The range of temperatures to which the CV may be exposed is -40° F. to 190.06° F. The average thermal expansion coefficient for the 304 material of the CV between 70 and 200 F. is 8.9 10^{-6} in./in./° F. and greater for higher upper temperatures per Section II. From the HP Alloys web site the average thermal expansion coefficient of the Nitronic 60 material of the nut between 75 and 200 F. is 8.8 10^{-6} in./in./° F. and greater for higher upper temperatures. Since the temperatures on opposite sides of the thread mating surface are expected to be the same an upper bound on the stress due to differential thermal expansion is

$$\sigma_t = E_c \Delta T (\alpha_{CV} - \alpha_N),$$ where E_c is the cold elastic modulus of either part, T is temperature, and α is average thermal expansion coefficient.

In the CV the stress, using a modulus interpolated from Table TM-1 in Section II, is

$$\sigma_{tCV} = 28.8 \times 10^6 \, psi (190.06° - (-40°))(8.9 \times 10^{-6} \, in./in./\circ - 8.8 \times 10^{-6} \, in./in/\circ)$$
$$= 663 \, psi.$$

The nut material has a slightly lower modulus listed so the stress in the nut will be slightly less. The room temperature modulus of the nut material is 26.2×10^6 psi per the HP Alloy website. The cold temperature modulus is not available but an approximation is obtained by comparing the modulus of Nitronic 60 at room temperature with the modulus of 304 at room temperature. From Table TM-1, the modulus of 304 at 70F. is 28.3×106 psi. Stress in the nut at the threads is about

$$\sigma_{tN} = \frac{26.2 \times 10^6 \, psi}{28.3 \times 10^6 \, psi} 663 \, psi = 613 \, psi.$$

The CV material has the higher thermal expansion coefficient so the effect of temperature increase is to reduce preload on the lid. Consider the mid-height of the threads to be fixed. The fixed plane is 1.100 in. − 0.55 in. / 2 = 0.825 in. above the mating plane. The lid is 0.5 in. thick under the nut and the lid will grow the same amount as the CV. The nut has 0.325 in. of material below the fixed plane and the difference in growth between the CV and the nut is

$$0.325 \, in. (190.06° - (-40°))(8.9 \times 10^{-6} \, in./in./\circ - 8.8 \times 10^{-6} \, in./in./\circ)$$
$$= 0.0000075 \, in.$$

2-132

GENERAL DESIGN AND COMPUTATION SHEET

Even if the torque load in the metal is ignored, the O-rings are compressed at least

Comp. = (0.139 in.-0.004 in.) – (0.114 in.+0.001 in.) = 0.020 in.

and a reduction in compression of 0.004% due to temperature change is insufficient to unload the O-rings enough to allow leakage.

4.3 TRANSPORTATION LOADS

The highest shock acceleration expected during transport is 11g in the vertical direction compared to a maximum horizontal acceleration of 5g per SST/SGT. The contents of the CV are specified to not exceed 90 lbs. The lid can be viewed as three disks, the volumes of which are:

Disk	Volume Formula	Volume, in^3
Top	$\pi(3.98\,\text{in.})^2 (0.56\,\text{in.})/4$	6.97
Middle	$\pi(6.741\,\text{in.})^2 (0.500\,\text{in.})/4$	17.84
Bottom	$\pi(5.00\,\text{in.})^2 (0.05\,\text{in.})/4$	0.98
Sum		25.8

The weight density of the lid material is about 0.29 lb./cu. in. so the weight of the lid is about 7.5 lb. Assume the threads must restrain 100 lbs. as the package is transported. Assuming the CV is upright, gravity provides 1g downward acceleration so the nut must restrain at most a net of 100 lbm. (11g – 1g) = 1,000 lbf. The average stress at the minimum cross section due to shock load is 1,000 lb. / 5.14 in^2 = 195 psi.

4.4 FATIGUE ANALYSIS

For each use of the vessel, the part of the CV equivalent to a bolt is loaded in tension by a torque producing a maximum axial load of 2,000 lb., an average stress of 389 psi and a peak stress (including bending) of 3,563 psi. When the vessel is pressurized to 3.1 psi the peak axial stress is 3,714 psi. This is the peak stress at the undercut which has a stress concentration factor of about 3. Per the Code, paragraph NB-3232.3 (c), the fatigue strength reduction factor for the threads shall not be less than 4 so the fatigue stress on the threads is 3,714 psi (4/3) = 4,952 psi.

Conservatively ignoring the interplay between the CV and the nut and lid, the stress due to impact during transportation is added to produce a maximum tensile stress of 4,952 psi + 195 psi = 5,147 psi. The thermal expansion reduces the preload so it will not extend the stress range. The range is zero to 5,147 psi and the alternating stress is half of the range or 5,147 psi / 2 = 2,574 psi.

2-133

GENERAL DESIGN AND COMPUTATION SHEET

The threads are evaluated for cyclic service by comparison with the design Curve A on Table I—9.2.2. For alternating stresses below 23,700 psi the allowable number of cycles exceeds 10^{11}. In every case the stress in the nut has been less than in the CV and since the nut material is also austenitic it does not limit fatigue design.

5.0   CONCLUSIONS

Force due to torquing the nut on the vessel was determined. The actual maximum expected internal pressure is low so the torque load produces much higher stresses in the vessel than pressure but the combined effect of torque and actual pressure was less than the conditions including bounding pressure used in the previous evaluation of the vessel design.

Thermal loads were evaluated relative to gasket compression it was shown that gaskets would remain seated through the maximum expected temperature change.

The threaded components of the ES-3100 Containment Vessel were evaluated per ASME Section III requirements and were found to have an allowable fatigue life in excess of 10^{11} cycles. Since the allowable life of the vessel is limited to a mere 30,000 cycles, the threads do not limit the life of the vessel.

GENERAL DESIGN AND COMPUTATION SHEET

JOB Fatigue Analysis of ES-3100 CV Threads under Normal Conditions of Use		DATE 16 February 2005	SHEET 9 of 30
DAC NO. DAC-EA-900000-A007	REVISION NO. 0	COMPUTED C. R. Hammond	CHECKED BY M. L. Goins

Stress
Tensor Z-Z
lbf/(in^2)

3562.71
3082.065
2601.419
2120.774
1640.128
1159.483
678.8375
198.192
-282.4535
-763.099
-1243.744

Load Case: 3 of 4

Maximum Value: 3562.71 lbf/(in^2)

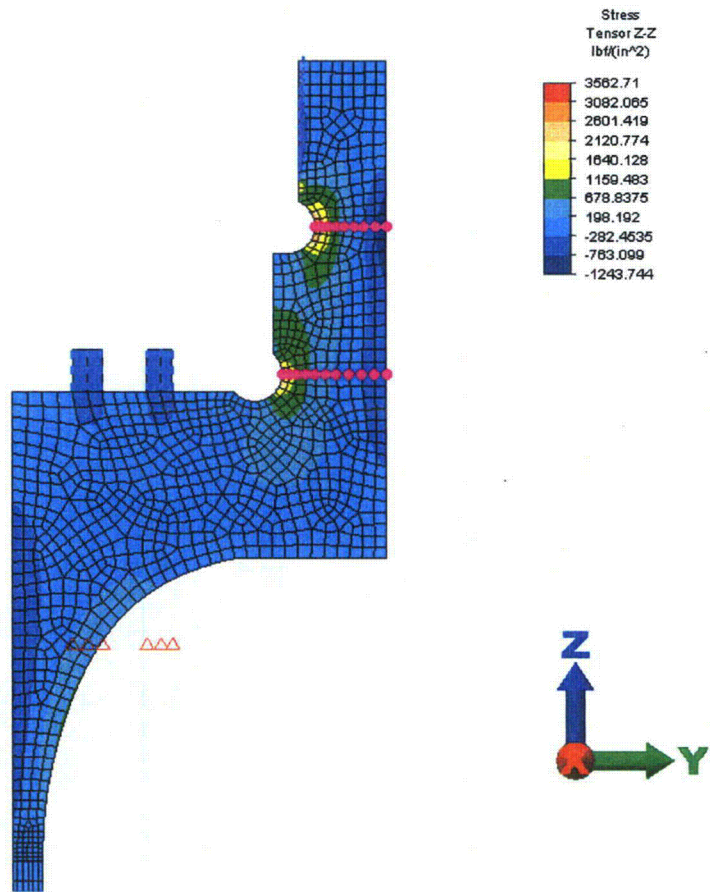Minimum Value: -1243.74 lbf/(in^2)

Fig. 1 – Axial Stress Due to Torque Load in Containment Vessel Neck

GENERAL DESIGN AND COMPUTATION SHEET

JOB Fatigue Analysis of ES-3100 CV Threads under Normal Conditions of Use		DATE 16 February 2005	SHEET 10 of 30
DAC NO. DAC-EA-900000-A007	REVISION NO. 0	COMPUTED C. R. Hammond	CHECKED BY M. L. Goins

Load Case: 2 of 4

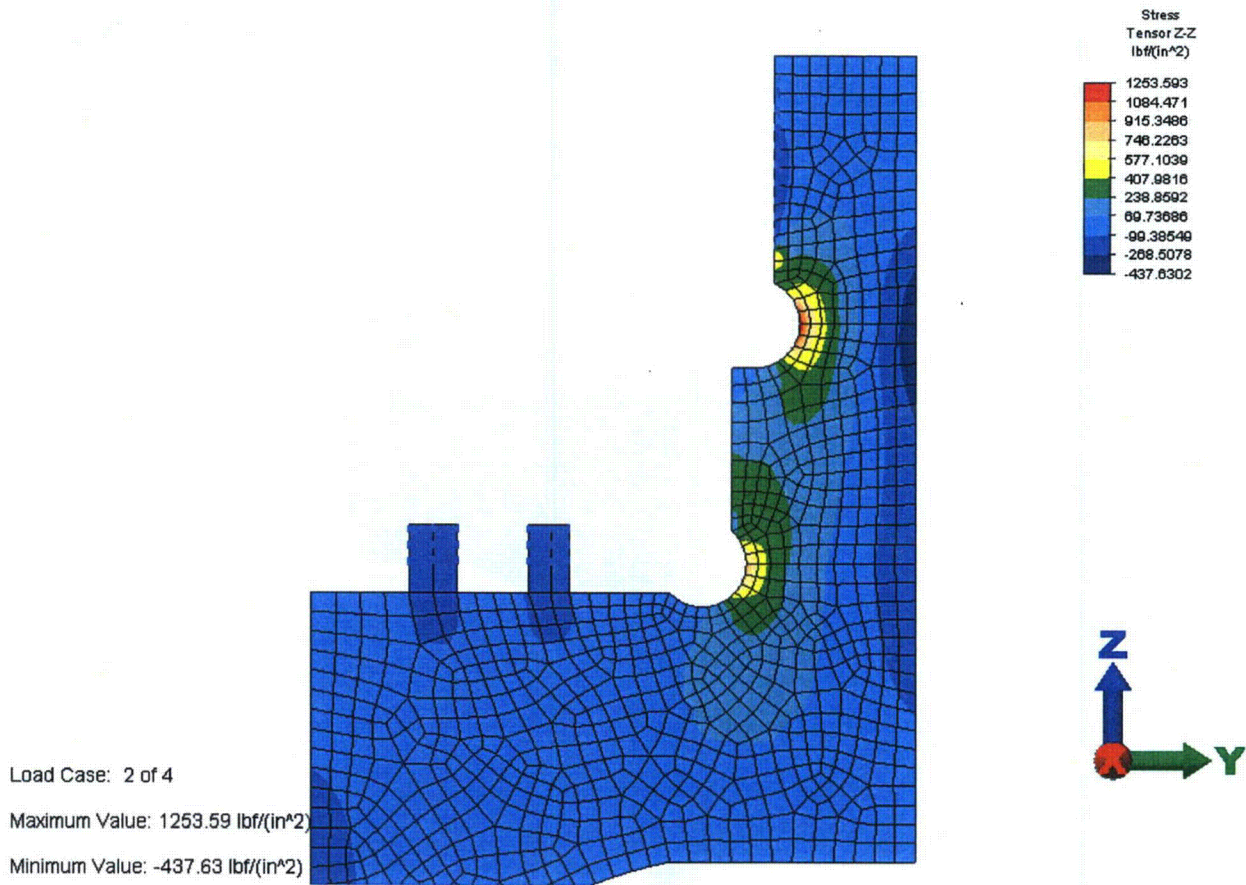Maximum Value: 1253.59 lbf/(in^2)

Minimum Value: -437.63 lbf/(in^2)

Fig. 2 – Axial Stress below the Threads in the Containment Vessel due to Gasket Seating Load
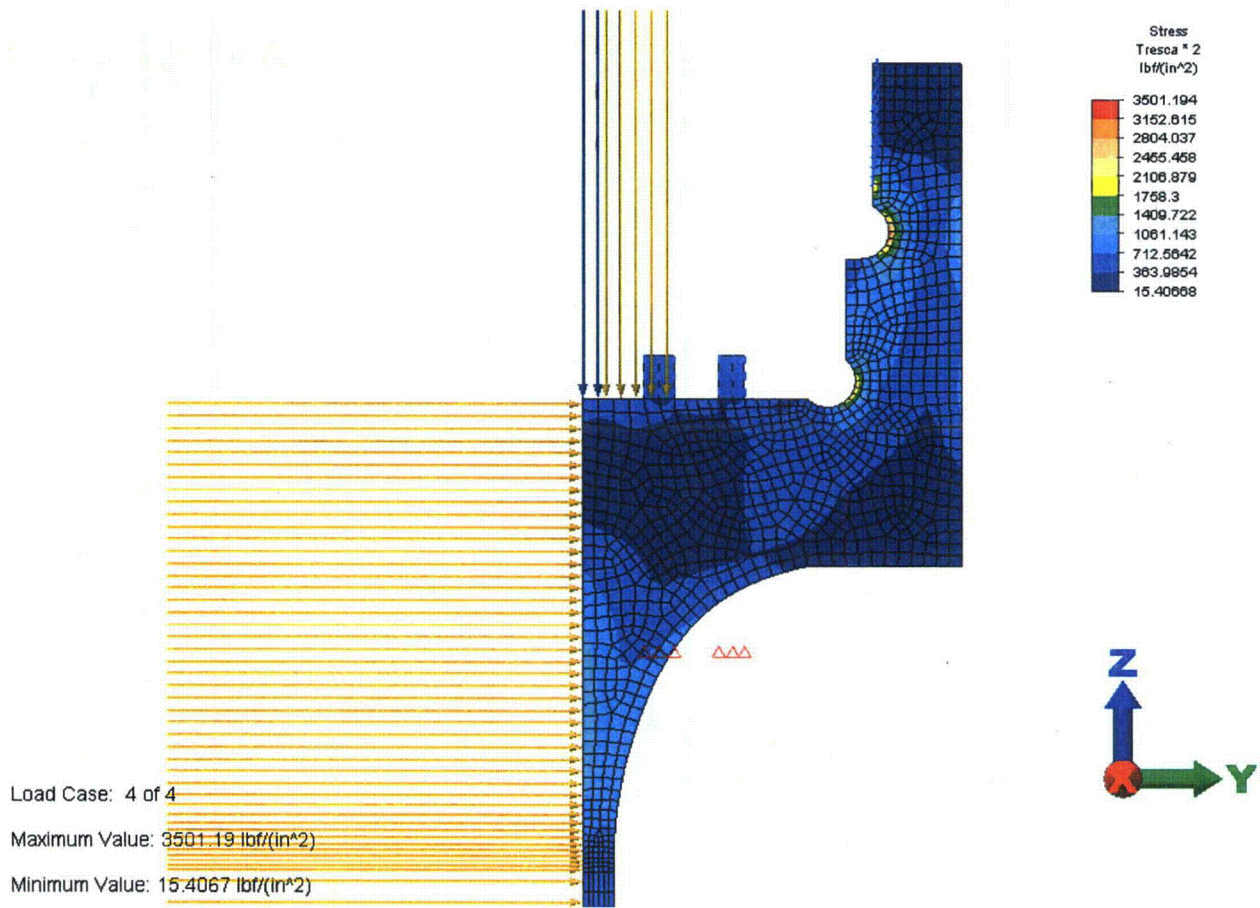
GENERAL DESIGN AND COMPUTATION SHEET

Fig. 3 –Stress Intensity below the Threads in the Containment Vessel due to 3.1 psi Pressure and Torque Loads

JOB Fatigue Analysis of ES-3100 CV Threads under Normal Conditions of Use		DATE 16 February 2005	SHEET 12 of 30
DAC NO. DAC-EA-900000-A007	REVISION NO. 0	COMPUTED C. R. Hammond	CHECKED BY M. L. Goins

Stress
Tensor Z-Z
lbf/(in^2)

3713.765
3212.392
2711.018
2209.645
1708.271
1206.898
705.5247
204.1512
-297.2222
-798.5956
-1299.969

Load Case: 4 of 4

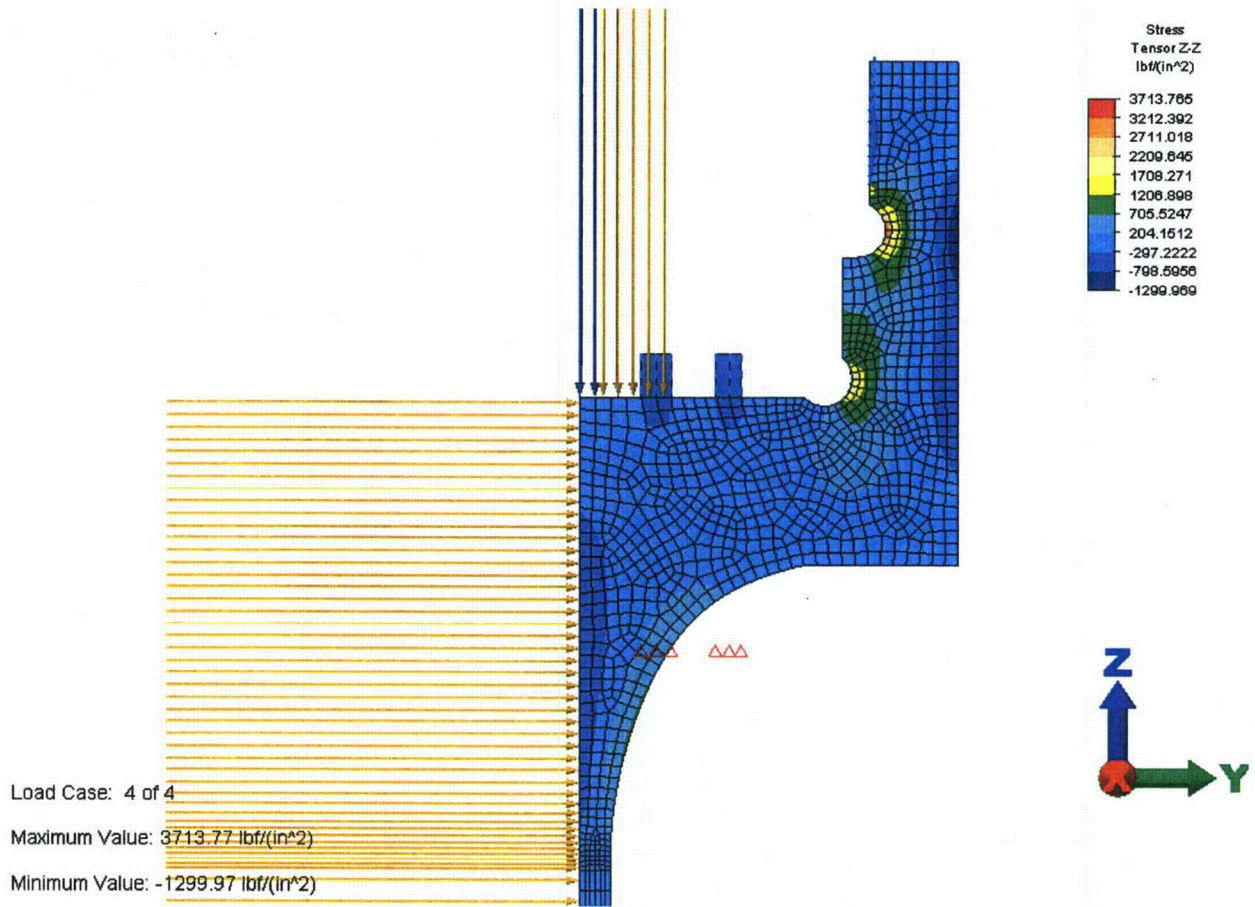Maximum Value: 3713.77 lbf/(in^2)

Minimum Value: -1299.97 lbf/(in^2)

Fig. 4 – Axial Stress in Containment Vessel Due to 3.1 psi Pressure and Torque

GENERAL DESIGN AND COMPUTATION SHEET

Appendix 1 – Axial Stresses across Neck of ES-3100 due to Torque

Top Section

Current Load Case = 3

Node # 1894 (X = 0, Y = 3.515, Z = 9.45)

    Displaced Position : X = 0, Y = 3.51496, Z = 9.44997

    Displacement = DX: 0, DY: -4.55757e-005, DZ: -2.7064e-005, Magnitude: 5.30057e-005

    appears in 2 Elements

    Part: 8   Element: 1

    Current Result Value: 3476.397428 lbf/(in^2)

    Part: 6   Element: 152

    Current Result Value: 3562.710297 lbf/(in^2)

Node # 1895 (X = 0, Y = 3.53702, Z = 9.45)

    Displaced Position : X = 0, Y = 3.53697, Z = 9.44998

    Displacement = DX: 0, DY: -4.64674e-005, DZ: -1.54912e-005, Magnitude: 4.89816e-005

    appears in 4 Elements

    Part: 8   Element: 1

    Part: 8   Element: 2

    Current Result Value: 2076.571725 lbf/(in^2)

    Part: 6   Element: 151

    Part: 6   Element: 152

    Current Result Value: 2150.404851 lbf/(in^2)

Node # 1896 (X = 0, Y = 3.55903, Z = 9.45)

    Displaced Position : X = 0, Y = 3.55898, Z = 9.44998

    Displacement = DX: 0, DY: -4.70825e-005, DZ: -1.69066e-005, Magnitude: 5.0026e-005

    appears in 4 Elements

    Part: 8   Element: 2

    Part: 8   Element: 3

    Current Result Value: 1338.334401 lbf/(in^2)

2-139

GENERAL DESIGN AND COMPUTATION SHEET

JOB Fatigue Analysis of ES-3100 CV Threads under Normal Conditions of Use	DATE 16 February 2005	SHEET 14 of 30
DAC NO. DAC-EA-900000-A007	REVISION NO. 0	COMPUTED C. R. Hammond	CHECKED BY M. L. Goins

```
    Part: 6      Element: 150

    Part: 6      Element: 151

    Current Result Value: 1388.726762 lbf/(in^2)

Node # 1897 ( X = 0, Y = 3.58545, Z = 9.45 )

    Displaced Position : X = 0, Y = 3.5854, Z = 9.44998

    Displacement = DX: 0, DY: -4.7175e-005, DZ: -1.82265e-005, Magnitude: 5.05735e-005

    appears in 4 Elements

    Part: 8      Element: 3

    Part: 8      Element: 4

    Current Result Value: 815.1134205 lbf/(in^2)

    Part: 6      Element: 149

    Part: 6      Element: 150

    Current Result Value: 856.9278605 lbf/(in^2)

Node # 1898 ( X = 0, Y = 3.61186, Z = 9.45 )

    Displaced Position : X = 0, Y = 3.61182, Z = 9.44998

    Displacement = DX: 0, DY: -4.7039e-005, DZ: -1.97662e-005, Magnitude: 5.10232e-005

    appears in 4 Elements

    Part: 8      Element: 4

    Part: 8      Element: 5

    Current Result Value: 422.3549006 lbf/(in^2)

    Part: 6      Element: 148

    Part: 6      Element: 149

    Current Result Value: 454.1958936 lbf/(in^2)

Node # 1899 ( X = 0, Y = 3.64356, Z = 9.45 )

    Displaced Position : X = 0, Y = 3.64352, Z = 9.44998

    Displacement = DX: 0, DY: -4.6803e-005, DZ: -2.12778e-005, Magnitude: 5.14127e-005

    appears in 4 Elements

    Part: 8      Element: 5
```

2-140

Part: 8   Element: 6

Current Result Value: 60.92361234 lbf/(in^2)

Part: 6   Element: 147

Part: 6   Element: 148

Current Result Value: 92.87579812 lbf/(in^2)

Node # 1900 (X = 0, Y = 3.67526, Z = 9.45)

    Displaced Position : X = 0, Y = 3.67522, Z = 9.44998

    Displacement = DX: 0, DY: -4.64719e-005, DZ: -2.30637e-005, Magnitude: 5.18804e-005

    appears in 4 Elements

    Part: 6   Element: 145

    Part: 6   Element: 147

    Current Result Value: -276.2872177 lbf/(in^2)

    Part: 8   Element: 6

    Part: 8   Element: 7

    Current Result Value: -291.8618414 lbf/(in^2)

Node # 1901 (X = 0, Y = 3.71263, Z = 9.45)

    Displaced Position : X = 0, Y = 3.71258, Z = 9.44997

    Displacement = DX: 0, DY: -4.6099e-005, DZ: -2.48703e-005, Magnitude: 5.23798e-005

    appears in 4 Elements

    Part: 8   Element: 7

    Part: 8   Element: 8

    Current Result Value: -690.1878235 lbf/(in^2)

    Part: 6   Element: 145

    Part: 6   Element: 146

    Current Result Value: -699.5449043 lbf/(in^2)

Node # 1902 (X = 0, Y = 3.75, Z = 9.45)

    Displaced Position : X = 0, Y = 3.74996, Z = 9.44997

    Displacement = DX: 0, DY: -4.48856e-005, DZ: -2.93433e-005, Magnitude: 5.3626e-005

2-141

GENERAL DESIGN AND COMPUTATION SHEET

JOB Fatigue Analysis of ES-3100 CV Threads under Normal Conditions of Use	DATE 16 February 2005	SHEET 16 of 30
DAC NO. DAC-EA-900000-A007	REVISION NO. 0	COMPUTED C. R. Hammond	CHECKED BY M. L. Goins

```
appears in 2 Elements

Part: 8    Element: 8

Current Result Value: -1189.038154 lbf/(in^2)

Part: 6    Element: 146

Current Result Value: -1243.744425 lbf/(in^2)
```

Lower Section

```
Current Load Case = 3


Node # 1718 ( X = 0, Y = 3.4065, Z = 8.96 )

    Displaced Position : X = 0, Y = 3.40646, Z = 9.03102

    Displacement = DX: 0, DY: -3.86154e-005, DZ: 0.0710243, Magnitude: 0.0710243

    appears in 2 Elements

    Part: 6    Element: 1

    Current Result Value: 2381.970074 lbf/(in^2)

    Part: 3    Element: 713

    Current Result Value: 2573.760605 lbf/(in^2)

Node # 1719 ( X = 0, Y = 3.43091, Z = 8.96 )

    Displaced Position : X = 0, Y = 3.43087, Z = 9.03103

    Displacement = DX: 0, DY: -3.82805e-005, DZ: 0.071027, Magnitude: 0.071027

    appears in 4 Elements

    Part: 6    Element: 1

    Part: 6    Element: 2

    Current Result Value: 1429.725908 lbf/(in^2)

    Part: 3    Element: 712

    Part: 3    Element: 713 .

    Current Result Value: 1507.238598 lbf/(in^2)
```

2-142

GENERAL DESIGN AND COMPUTATION SHEET

Node # 1720 (X = 0, Y = 3.45532, Z = 8.96)

   Displaced Position : X = 0, Y = 3.45529, Z = 9.03102

   Displacement = DX: 0, DY: -3.93058e-005, DZ: 0.0710167, Magnitude: 0.0710167

   appears in 4 Elements

   Part: 3   Element: 711

   Part: 3   Element: 712

   Current Result Value: 1015.779644 lbf/(in^2)

   Part: 6   Element: 2

   Part: 6   Element: 3

   Current Result Value: 1035.108104 lbf/(in^2)

Node # 1721 (X = 0, Y = 3.48462, Z = 8.96)

   Displaced Position : X = 0, Y = 3.48458, Z = 9.03103

   Displacement = DX: 0, DY: -3.78762e-005, DZ: 0.0710297, Magnitude: 0.0710297

   appears in 4 Elements

   Part: 3   Element: 710

   Part: 3   Element: 711

   Current Result Value: 699.5787633 lbf/(in^2)

   Part: 6   Element: 3

   Part: 6   Element: 4

   Current Result Value: 752.6151572 lbf/(in^2)

Node # 1722 (X = 0, Y = 3.51391, Z = 8.96)

   Displaced Position : X = 0, Y = 3.51388, Z = 9.03103

   Displacement = DX: 0, DY: -3.73704e-005, DZ: 0.0710323, Magnitude: 0.0710323

   appears in 4 Elements

   Part: 3   Element: 707

   Part: 3   Element: 710

   Current Result Value: 479.8616501 lbf/(in^2)

   Part: 6   Element: 4

GENERAL DESIGN AND COMPUTATION SHEET

JOB Fatigue Analysis of ES-3100 CV Threads under Normal Conditions of Use	DATE 16 February 2005	SHEET 18 of 30
DAC NO. DAC-EA-900000-A007	REVISION NO. 0	COMPUTED C. R. Hammond	CHECKED BY M. L. Goins

```
Part: 6      Element: 5

Current Result Value: 524.8054716 lbf/(in^2)

Node # 1723 ( X = 0, Y = 3.54907, Z = 8.96 )

   Displaced Position : X = 0, Y = 3.54903, Z = 9.03101

   Displacement = DX: 0, DY: -3.89625e-005, DZ: 0.0710096, Magnitude: 0.0710096

   appears in 4 Elements

   Part: 3      Element: 704

   Part: 3      Element: 707

   Current Result Value: 286.7099034 lbf/(in^2)

   Part: 6      Element: 5

   Part: 6      Element: 6

   Current Result Value: 319.4018001 lbf/(in^2)

Node # 1724 ( X = 0, Y = 3.58422, Z = 8.96 )

   Displaced Position : X = 0, Y = 3.58418, Z = 9.03101

   Displacement = DX: 0, DY: -3.94127e-005, DZ: 0.071011, Magnitude: 0.071011

   appears in 4 Elements

   Part: 3      Element: 704

   Part: 3      Element: 705

   Current Result Value: 104.2072763 lbf/(in^2)

   Part: 6      Element: 6

   Part: 6      Element: 7

   Current Result Value: 126.0936862 lbf/(in^2)

Node # 1725 ( X = 0, Y = 3.62567, Z = 8.96 )

   Displaced Position : X = 0, Y = 3.62563, Z = 9.03101

   Displacement = DX: 0, DY: -3.94951e-005, DZ: 0.0710126, Magnitude: 0.0710126

   appears in 4 Elements

   Part: 6      Element: 7

   Part: 6      Element: 8
```

2-144

GENERAL DESIGN AND COMPUTATION SHEET

JOB Fatigue Analysis of ES-3100 CV Threads under Normal Conditions of Use	DATE 16 February 2005	SHEET 19 of 30
DAC NO. DAC-EA-900000-A007	REVISION NO. 0	COMPUTED C. R. Hammond	CHECKED BY M. L. Goins

Current Result Value: -69.65167919 lbf/(in^2)

Part: 3   Element: 705

Part: 3   Element: 706

Current Result Value: -87.34285327 lbf/(in^2)

Node # 1726 (X = 0, Y = 3.66711, Z = 8.96)

Displaced Position : X = 0, Y = 3.66707, Z = 9.03101

Displacement = DX: 0, DY: -3.94338e-005, DZ: 0.0710146, Magnitude: 0.0710146

appears in 4 Elements

Part: 6   Element: 8

Part: 6   Element: 9

Current Result Value: -274.1379622 lbf/(in^2)

Part: 3   Element: 706

Part: 3   Element: 708

Current Result Value: -286.8211743 lbf/(in^2)

Node # 1727 (X = 0, Y = 3.70856, Z = 8.96)

Displaced Position : X = 0, Y = 3.70852, Z = 9.03102

Displacement = DX: 0, DY: -3.91153e-005, DZ: 0.0710191, Magnitude: 0.0710191

appears in 4 Elements

Part: 6   Element: 9

Part: 6   Element: 10

Current Result Value: -489.6421277 lbf/(in^2)

Part: 3   Element: 708

Part: 3   Element: 709

Current Result Value: -498.9915546 lbf/(in^2)

Node # 1728 (X = 0, Y = 3.75, Z = 8.96)

Displaced Position : X = 0, Y = 3.74996, Z = 9.03102

Displacement = DX: 0, DY: -3.89012e-005, DZ: 0.0710215, Magnitude: 0.0710215

appears in 2 Elements

2-145

GENERAL DESIGN AND COMPUTATION SHEET

JOB Fatigue Analysis of ES-3100 CV Threads under Normal Conditions of Use		DATE 16 February 2005	SHEET 20 of 30
DAC NO. DAC-EA-900000-A007	REVISION NO. 0	COMPUTED C. R. Hammond	CHECKED BY M. L. Goins

Part: 6   Element: 10

Current Result Value: -726.5076374 lbf/(in^2)

Part: 3   Element: 709

Current Result Value: -737.209287 lbf/(in^2)

2-146

GENERAL DESIGN AND COMPUTATION SHEET

JOB Fatigue Analysis of ES-3100 CV Threads under Normal Conditions of Use		DATE 16 February 2005	SHEET 21 of 30
DAC NO. DAC-EA-900000-A007	REVISION NO. 0	COMPUTED C. R. Hammond	CHECKED BY M. L. Goins

**Appendix 1 - Axial stress across neck of ES-3100 CV due to torque**

Top section - Part 8

Y, in.	Sigma ZZ, psi	Delta R, in.	Force, lb.	Force (hard way), lb.
3.515	3476.397428	0.01101	845.3215421	846.6454383
3.53702	2076.571725	0.022015	1015.974973	1015.974255
3.55903	1338.334401	0.024215	724.7039558	724.9284512
3.58545	815.1134205	0.026415	485.0563535	485.0560153
3.61186	422.3549006	0.029055	278.4897363	278.5917067
3.64356	60.92361234	0.0317	44.21307309	44.21307309
3.67526	-291.8618414	0.034535	-232.7580525	-232.8478243
3.71263	-690.1878235	0.03737	-601.6610939	-601.6610939
3.75	-1189.038154	0.018685	-523.4799217	-522.1757588
		Sum	2035.860566	2038.724263

Lower section - Part 3

Y, in.	Sigma ZZ, psi	Delta R, in.	Force, lb.	Force (hard way), lb.
3.4065	2573.760605	0.012205	672.3481194	673.5525828
3.43091	1507.238598	0.02441	793.1201445	793.1201445
3.45532	1015.779644	0.026855	592.2332744	592.4428079
3.48462	699.5787633	0.029295	448.7096535	448.7093316
3.51391	479.8616501	0.032225	341.4125422	341.5551249
3.54907	286.7099034	0.035155	224.7626947	224.7625364
3.58422	104.2072763	0.0383	89.88171407	89.92121045
3.62567	-87.34285327	0.041445	-82.46461971	-82.46456285
3.66711	-286.8211743	0.041445	-273.8969268	-273.8971135
3.70856	-498.9915546	0.041445	-481.8928886	-481.8925638
3.75	-737.209287	0.02072	-359.9081529	-358.9138467
		Sum	1964.305555	1966.895652

Section difference = 0.036518771
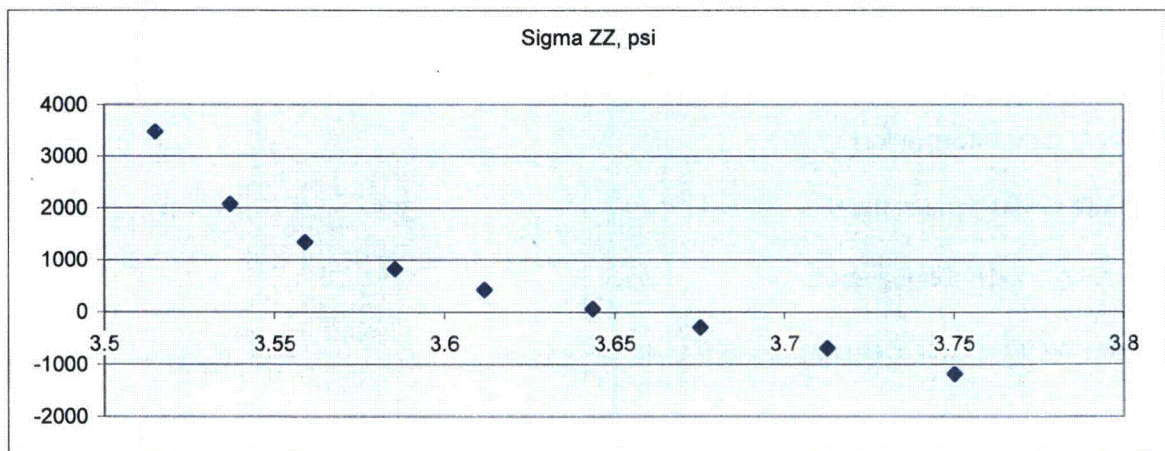
Sigma ZZ, psi

2-147

GENERAL DESIGN AND COMPUTATION SHEET

JOB Fatigue Analysis of ES-3100 CV Threads under Normal Conditions of Use	DATE 16 February 2005	SHEET 22 of 30
DAC NO. DAC-EA-900000-A007	REVISION NO. 0	COMPUTED C. R. Hammond	CHECKED BY M. L. Goins

Appendix 2 – Finite Element Data

Summary

Description

Thread Analysis

Model Information

Analysis Type - Static Stress with Linear Material Models
Units - English (in) - (lbf, in, s, deg F, deg R, V, ohm, A, in*lbf)
Model location - C:\ALGOR12\es3100CV1

Analysis Parameters Information

Load Case Multipliers

Static Stress with Linear Material Models may have multiple load cases. This allows a model to be analyzed with multiple loads while solving the equations a single time. The following is a list of load case multipliers that were analyzed with this model.

Load Case	Pressure/ Surface Forces	Acceleration/ Gravity	Displaced Boundary	Thermal	Voltage
1	1	0	1	0	0
2	0	0	1	0	0
3	0	0	0	1	0
4	0.0305	0	0	1	0

Multiphysics Information

Default Nodal Temperature	70°F
Source of Nodal Temperature	None
Time step from Heat Transfer Analysis	Last

2-148

GENERAL DESIGN AND COMPUTATION SHEET

Processor Information

Type of Solver	Sparse
Disable Calculation and Output of Strains	No
Calculate Reaction Forces	Yes
Invoke Banded Solver	Yes
Avoid Bandwidth Minimization	No
Stop After Stiffness Calculations	No
Displacement Data in Output File	No
Stress Data in Output File	No
Equation Numbers Data in Output File	No
Element Input Data in Output File	No
Nodal Input Data in Output File	No
Centrifugal Load Data in Output File	No

Part Information

Part ID	Part Name	Element Type	Material Name
1	Plate & shell	2-D	[Customer Defined] (Part 1)
2	Bottom corner	2-D	[Customer Defined] (Part 2)
3	Top transition	2-D	[Customer Defined] (Part 3)
4	Outer O-ring	2-D	[Customer Defined] (Part 4)
5	Inner O-ring	2-D	[Customer Defined] (Part 5)
6	Top flange neck	2-D	[Customer Defined] (Part 6)
8	Thread region	2-D	[Customer Defined] (Part 8)

2-149

GENERAL DESIGN AND COMPUTATION SHEET

Element Properties used for:

- Plate & shell

- Bottom corner

- Top transition

- Thread region

Element Type	2-D
Geometry Type	Axisymmetric
Material Model	Isotropic
Thickness	1 in
Stress Free Reference Temperature	70°F
Principle Axes Transformational Angle	0°
Nodal Order Method	Default
Nodal Order Y Coordinate	0 in
Nodal Order Z Coordinate	0 in

Element Properties used for:

- Outer O-ring

- Inner O-ring

Element Type	2-D
Geometry Type	Axisymmetric
Material Model	Isotropic
Thickness	1 in
Stress Free Reference Temperature	0°F
Principle Axes Transformational Angle	0°
Nodal Order Method	Default
Nodal Order Y Coordinate	0 in
Nodal Order Z Coordinate	0 in

2-150

GENERAL DESIGN AND COMPUTATION SHEET

Element Properties used for:

- Top flange neck

Element Type	2-D
Geometry Type	Axisymmetric
Material Model	Orthotropic
Thickness	1 in
Stress Free Reference Temperature	170°F
Principle Axes Transformational Angle	0°
Nodal Order Method	Default
Nodal Order Y Coordinate	0 in
Nodal Order Z Coordinate	0 in

Material Information

[Customer Defined] (Part 1) - 2-D

Material Model	Standard
Material Source	Not Applicable
Material Source File	
Date Last Updated	2004/09/28-14:35:06
Material Description	Customer defined material properties
Mass Density	7.50e-4 lbf*s^2/in/in³
Modulus of Elasticity	27e6 lbf/in²
Poisson's Ratio	0.3
Thermal Coefficient of Expansion	9.2e-6 1/°F
Shear Modulus of Elasticity	10384615 lbf/in²

2-151

GENERAL DESIGN AND COMPUTATION SHEET

[Customer Defined] (Part 2) - 2-D

Material Model	Standard
Material Source	Not Applicable
Material Source File	
Date Last Updated	2004/09/28-14:36:43
Material Description	Customer defined material properties
Mass Density	7.50e-4 lbf*s^2/in/in³
Modulus of Elasticity	27e6 lbf/in²
Poisson's Ratio	0.3
Thermal Coefficient of Expansion	9.2e-6 1/°F
Shear Modulus of Elasticity	10384615 lbf/in²

[Customer Defined] (Part 3) - 2-D

Material Model	Standard
Material Source	Not Applicable
Material Source File	
Date Last Updated	2004/09/28-14:38:39
Material Description	Customer defined material properties
Mass Density	7.50e-4 lbf*s^2/in/in³
Modulus of Elasticity	27e6 lbf/in²
Poisson's Ratio	0.30
Thermal Coefficient of Expansion	9.2e-6 1/°F
Shear Modulus of Elasticity	10384615 lbf/in²

2-152

GENERAL DESIGN AND COMPUTATION SHEET

[Customer Defined] (Part 4) - 2-D

Material Model	Standard
Material Source	Not Applicable
Material Source File	
Date Last Updated	2004/09/28-14:39:52
Material Description	Customer defined material properties
Mass Density	0 lbf*s^2/in/in³
Modulus of Elasticity	1321 lbf/in²
Poisson's Ratio	0
Thermal Coefficient of Expansion	0 1/°F
Shear Modulus of Elasticity	660.5 /²

[Customer Defined] (Part 5) - 2-D

Material Model	Standard
Material Source	Not Applicable
Material Source File	
Date Last Updated	2004/09/28-14:40:41
Material Description	Customer defined material properties
Mass Density	0 lbf*s^2/in/in³
Modulus of Elasticity	1122 lbf/in²
Poisson's Ratio	0
Thermal Coefficient of Expansion	0 1/°F
Shear Modulus of Elasticity	561. /²

2-153

GENERAL DESIGN AND COMPUTATION SHEET

JOB Fatigue Analysis of ES-3100 CV Threads under Normal Conditions of Use		DATE 16 February 2005	SHEET 28 of 30
DAC NO. DAC-EA-900000-A007	REVISION NO. 0	COMPUTED C. R. Hammond	CHECKED BY M. L. Goins

[Customer Defined] (Part 6) - 2-D

Material Model	OrthotropicTempDep
Material Source	Not Applicable
Material Source File	
Date Last Updated	2004/10/14-14:27:16
Material Description	Customer defined material properties
Mass Density	7.50e-4 lbf*s^2/in/in³
Index 1 - Temperature	170 °F
Index 1 - E1	27e6 lbf/in²
Index 1 - E2	27e6 lbf/in²
Index 1 - E3	27e6 lbf/in²
Index 1 - V12	.3
Index 1 - V13	.3
Index 1 - V23	.3
Index 1 - G12	10384615 lbf/in²
Index 1 - G13	10384615 lbf/in²
Index 1 - G23	10384615 lbf/in²
Index 1 - Alpha 1	0 1/°F
Index 1 - Alpha 2	1.45e-3 1/°F
Index 1 - Alpha 3	0 1/°F

2-154

GENERAL DESIGN AND COMPUTATION SHEET

[Customer Defined] (Part 8) - 2-D

Material Model	Standard
Material Source	Not Applicable
Material Source File	
Date Last Updated	2004/09/28-14:43:25
Material Description	Customer defined material properties
Mass Density	7.50e-4 lbf*s^2/in/in³
Modulus of Elasticity	27e6 lbf/in²
Poisson's Ratio	0.30
Thermal Coefficient of Expansion	9.2e-6 1/°F
Shear Modulus of Elasticity	10384615 lbf/in²

Processor Output

Processor Summary

```
ALGOR (R) Static Stress with Linear Material Models
Version 16.00-WIN 29-SEP-2004
Copyright (c) 1984-2004 ALGOR, Inc. All rights reserved.

-----------------------------------------------
                      DATE: FEBRUARY 16, 2005
                      TIME: 07:55 AM
               INPUT MODEL: C:\ALGOR12\es3100CV1

          PROGRAM VERSION: 16000001
            ALG.DLL VERSION: 13240000
       AlgConfig.DLL VERSION: 15000000
        agsdb_ar.DLL VERSION: 14000004
        amgsolve.DLL VERSION: 03220000
-----------------------------------------------

     Linear Stress

1**** CONTROL INFORMATION

     number of node points      (NUMNP)   =        2061
     number of element types    (NELTYP)  =           8
     number of load cases       (LL)      =           4
```

GENERAL DESIGN AND COMPUTATION SHEET

JOB Fatigue Analysis of ES-3100 CV Threads under Normal Conditions of Use	DATE 16 February 2005	SHEET 30 of 30

DAC NO. DAC-EA-900000-A007	REVISION NO. 0	COMPUTED C. R. Hammond	CHECKED BY M. L. Goins

```
         number of frequencies          (NF)     =            0
         analysis type code             (NDYN)   =            0
         equations per block            (KEQB)   =            0
         bandwidth minimization flag    (MINBND) =            0
         gravitational constant         (GRAV)   =    3.8640E+02
         number of equations            (NEQ)    =         4092

****  PRINT OF NODAL DATA SUPPRESSED
****  PRINT OF EQUATION NUMBERS SUPPRESSED
****  PRINT OF TYPE-4 ELEMENT DATA SUPPRESSED
****  PRINT OF TYPE-4 ELEMENT DATA SUPPRESSED
****  PRINT OF TYPE-4 ELEMENT DATA SUPPRESSED
****  PRINT OF TYPE-4 ELEMENT DATA SUPPRESSED
****  PRINT OF TYPE-4 ELEMENT DATA SUPPRESSED
****  PRINT OF TYPE-4 ELEMENT DATA SUPPRESSED
****  PRINT OF TYPE-4 ELEMENT DATA SUPPRESSED
****  PRINT OF TYPE-7 ELEMENT DATA SUPPRESSED
****  Hard disk file size information for processor:

      Available hard disk space on current drive =   3849.848 megabytes

1****  NODAL LOADS (STATIC) OR MASSES (DYNAMIC)

   NODE  LOAD     X-AXIS       Y-AXIS        Z-AXIS        X-AXIS        Y-AXIS        Z-AXIS
  NUMBER CASE     FORCE        FORCE         FORCE         MOMENT        MOMENT        MOMENT

    1685   1  0.000E+00   0.000E+00  -6.362E+00   0.000E+00   0.000E+00   0.000E+00
    1685   4  0.000E+00   0.000E+00  -1.943E-01   0.000E+00   0.000E+00   0.000E+00
    1686   1  0.000E+00   0.000E+00  -6.424E+00   0.000E+00   0.000E+00   0.000E+00
    1686   4  0.000E+00   0.000E+00  -1.962E-01   0.000E+00   0.000E+00   0.000E+00

1****  ELEMENT LOAD MULTIPLIERS

      load case      case A       case B       case C       case D       case E
      ---------    ----------   ----------   ----------   ----------   ----------

          1        1.000E+00    0.000E+00    1.000E+00    0.000E+00    0.000E+00
          2        0.000E+00    0.000E+00    1.000E+00    0.000E+00    0.000E+00
          3        0.000E+00    0.000E+00    0.000E+00    1.000E+00    0.000E+00
          4        3.050E-02    0.000E+00    0.000E+00    1.000E+00    0.000E+00
```

Appendix 2.10.2

IMPACT ANALYSES OF ES-3100 DESIGN CONCEPTS USING BOROBOND AND CAT 277-4 NEUTRON ABSORBERS

2-157

2-158

Index

Part B - Design with HABC Cylinder (continued)

1.0   Problem Statement

This calculation summarizes the impact simulation computer runs made in support of the ES-3100 shipping package design effort. From the summer of 2003 through the spring of 2004 the design impact simulations were run with borobond as the neutron absorber. During the summer of 2004, the ES-3100 with the borobond neutron absorber was tested to the 10CFR71 impact requirements. In August 2004 a decision was made to change the neutron absorber material to a high alumina borated cement (HABC). The HABC material is also known as "Catalog 277-4" or just "277-4", but the HABC notation is used in this report. The August 2004 absorber change also involved some minor design changes to the configuration of the package liners surrounding the HABC material. Material testing on the HABC material occurred during the Fall of 2004. The simulation impacts were run in the late Fall of 2004.

This calculation is presented in two parts, Part A and Part B. Part A summarizes the impact simulations made for the initial borobond design. Part B summarizes the impact analyses made with the HABC design. A beginning section, Section 1.0 and an ending section, Section 9.0, address both designs. The Part A borobond design simulations are documented in Sections 2 through 5. The Part B, HABC simulations are documented in Sections 6 through 8. A detailed explanation of changes to the Part A, borobond models to develop the Part B HABC models is given in Part B, Section 6.1.

A qualitative, cross sectional view of a ES-3100 package with the initial design borobond neutron absorber (presented in Part A) is shown in Figure 1.1. The ES-3100 shipping package is a stainless steel drum with kaolite insulation material. The overall dimensions of the overpack are a height of about 44 inches and a diameter of about 19.4 inches. At the top of the overpack is a bolted lid restrained by eight, 5/8 inch welded studs. The lid restrains a removable plug filled with the kaolite material. The plug covers a cavity in which the stainless steel containment vessel (CV) is placed. The CV is about 32.9 inches tall with a 5.4 inch inside diameter and a body wall thickness of 0.1 inches. The CV closure is a flat plate constrained by a threaded ring. In the shipping package, and immediately surrounding the CV cavity is a 0.90 inch thick layer of borobond, a neutron absorbing cast material. All the kaolite and borobond materials are wrapped by stainless steel liners. In this model, there is a slight indentation (about 0.32 in) of the liner near the CV flange region into the kaolite, as can be seen in Figure 1.1.
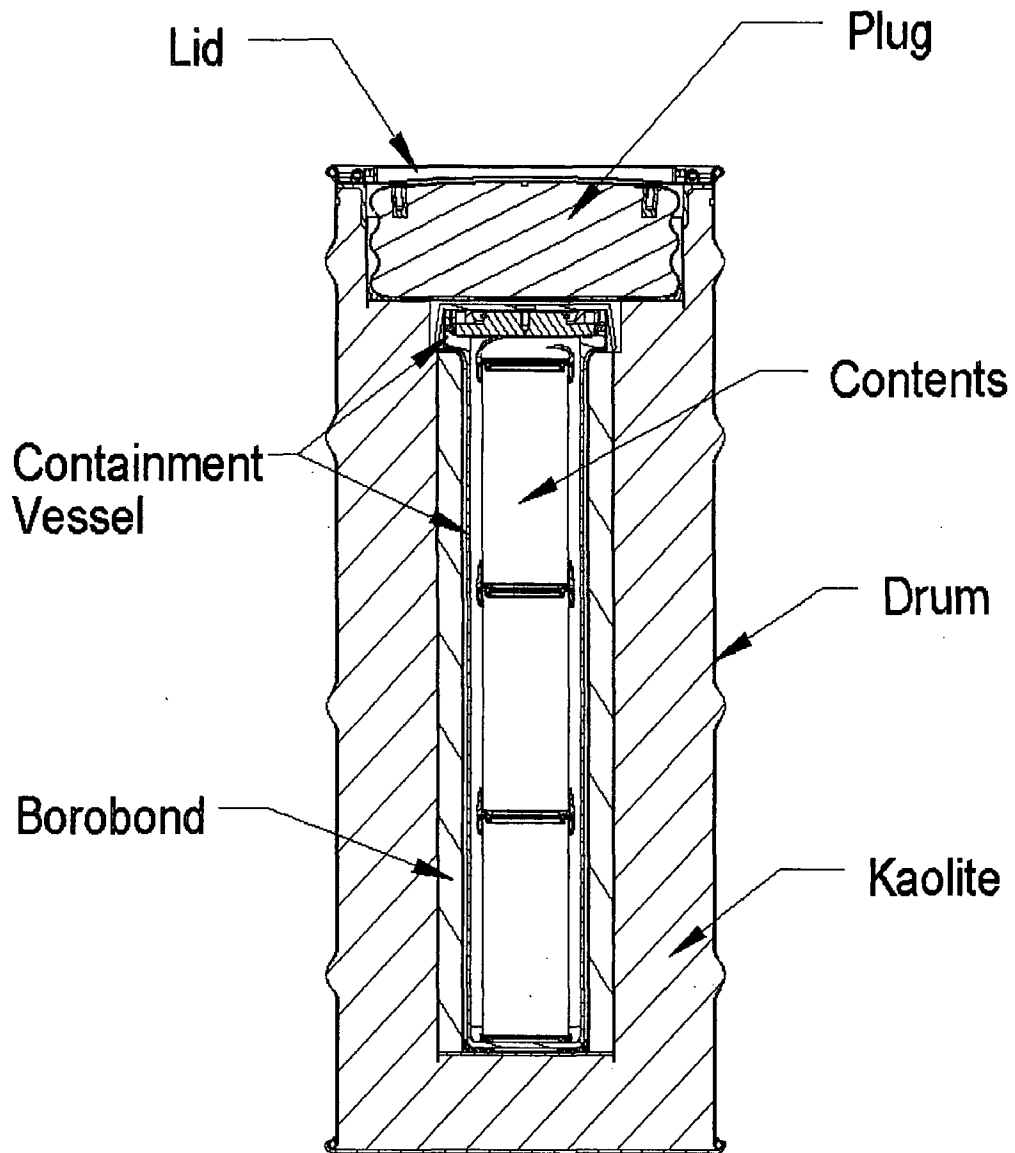
Figure 1.1 - Configuration of the Initial, Borobond Neutron Absorber ES-3100 Package, Presented in Part A

The redesigned package with the HABC (Part B) is shown in Figure 1.2. As can be qualitatively seen in the figure, the liner between the HABC and the kaolite is moved out slightly and there is no indentation into the kaolite near the CV flange. The HABC design changes are minor as shown by qualitatively comparing Figures 1.1 and 1.2. The detailed differences between the Part A borobond model and the Part B, HABC model are presented in Part B, Section 6.
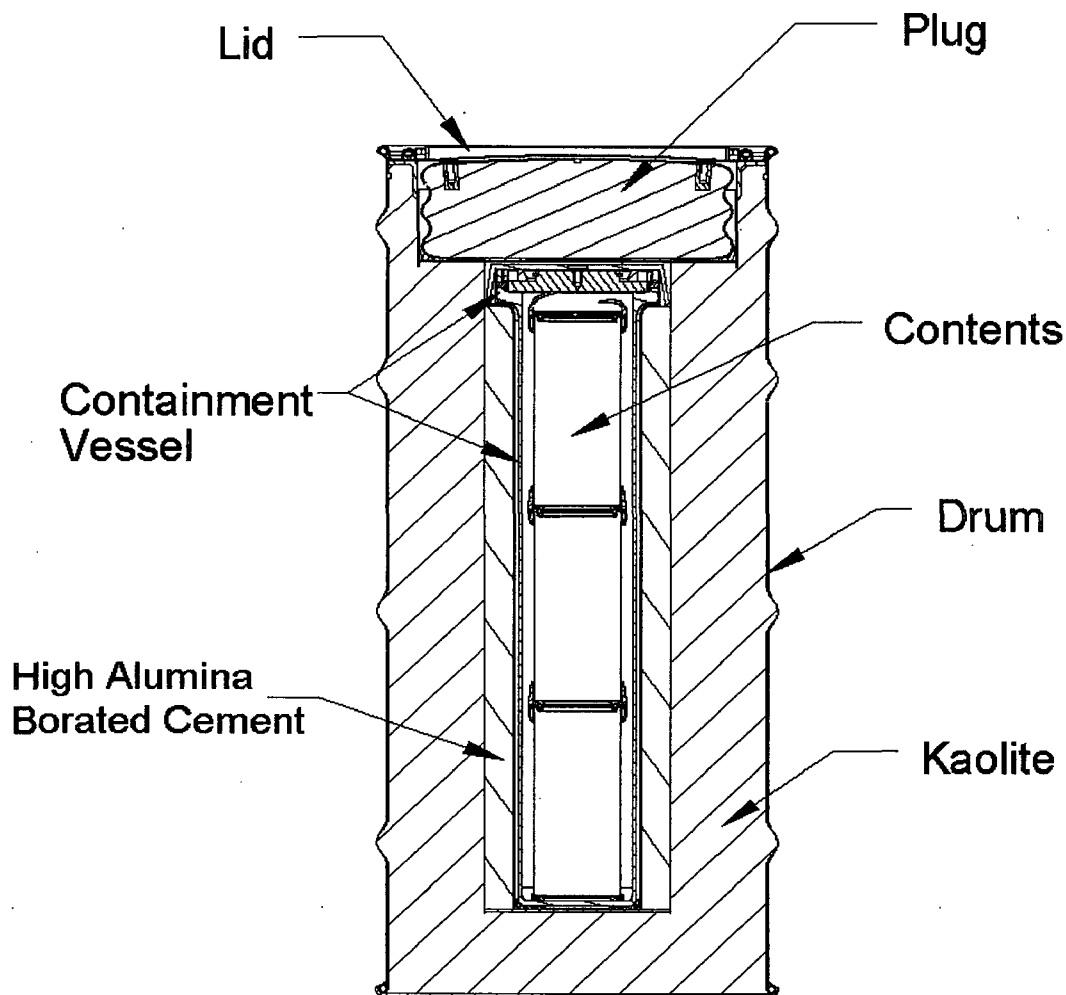
Figure 1.2 - Configuration of the Redesigned ES-3100 with the HABC as the Neutron Absorber, Presented in Part B

The Part A and Part B impact simulations were modeled with the pre-processor software TrueGrid (reference 5.1), solved with the software LS-Dyna (reference 5.2), and results obtained with the post-processor LS-Post (reference 5.3). The computers used for these simulations were Dell dual processor machines (Y12 machines ep0134, ep0141 and ep0142). TrueGrid was run on a Silicon Graphics Workstation (Y12 machine ew204). Typical solution times for one impact ranged from 1 to 4 days.

The impact simulations of the ES3100 package are driven by the 10CFR71, subpart F, sections 71.71 and 71.73 impact requirements. LS-Dyna allows successive restarts to be made which enables cumulative damage to be obtained in the shipping package model. Part A, Section 2.1, describes the specific impact simulations performed for the initial borobond design. Part B, Section 6.1, describes the simulations performed for the HABC design. Sections 3.12 and 7.7 compare the respective model results to physical test results.

2.0   Analytical Model

Two models were used in the dynamic impact runs for the borobond design of the ES-3100 shipping container; a detailed model and a simplified model. A detailed model included the drum closure details, CV details and generally a finer element mesh. The detailed model was used for all the runs, except the study which evaluated the response of the drum to various punch angles. A simplified model was used to investigate the variation in punch angles. The detailed model is discussed in Section 2.1 and the simplified model is discussed in Section 2.2.

Design drawings were used to develop the ES-3100 analytical models. The reference 5.5 AutoSketch software was used as an aid in the creation of the TrueGrid input file. The running of TrueGrid created the bulk of the LS-Dyna input file (e.g., the nodal data, element data, contact surfaces, etc). The LS-Dyna command lines and material properties were created in a separate file and edited into the TrueGrid created LS-Dyna input file. The resulting file was a complete LS-Dyna input file which was then submitted for execution.

2.1   Model Description - Detailed Model

Figure 2.1.1 shows the typical detailed model assembly for the ES-3100. All of the entities shown (rigid surface, crush plate, shipping package and punch) exist in the model, however, only the entities of concern in an impact were active in that impact. In the 4-foot impact and 30-foot impact only the shipping package and the rigid plate were in contact. The crush plate and the punch existed in the model, however, there was no contact between them and the shipping package. During the crush impact, the crush plate contacts the shipping package, which then contacts the rigid plate. During the crush impact, the punch exists, but is not contacted. During the punch impact, the crush plate and the rigid surface are deleted from the model, allowing contact to be made between the shipping package and the punch.

Figure 2.1.2 shows the components of the detailed model in an exploded view. The element mesh is not included in Figure 2.1.1, nor in Figure 2.1.2 for clarity. Representative element meshes for the detailed model are shown in Figures 2.1.3 and 2.1.4.

Various impact configurations of the ES-3100 detailed model are documented in this calculation. Figure 2.1.5 shows icons representing the impact configurations run for the design effort. The 4-foot impact and the punch impact are not as structurally demanding as is the 30-foot free fall impact, nor the 30-foot crush impact. Therefore, only the 30-foot impact and the crush impact were performed in the design effort runs. Figure 2.1.6
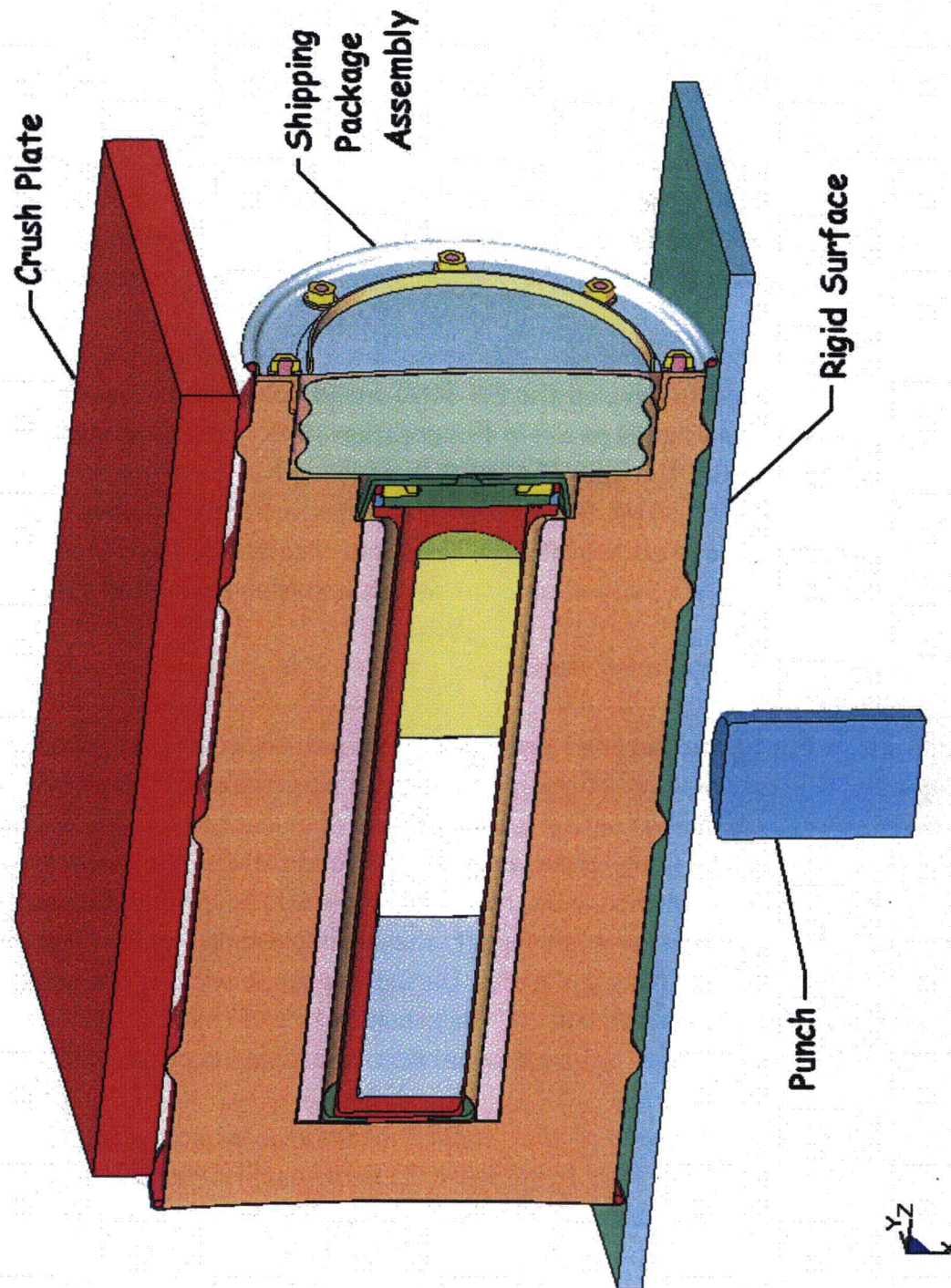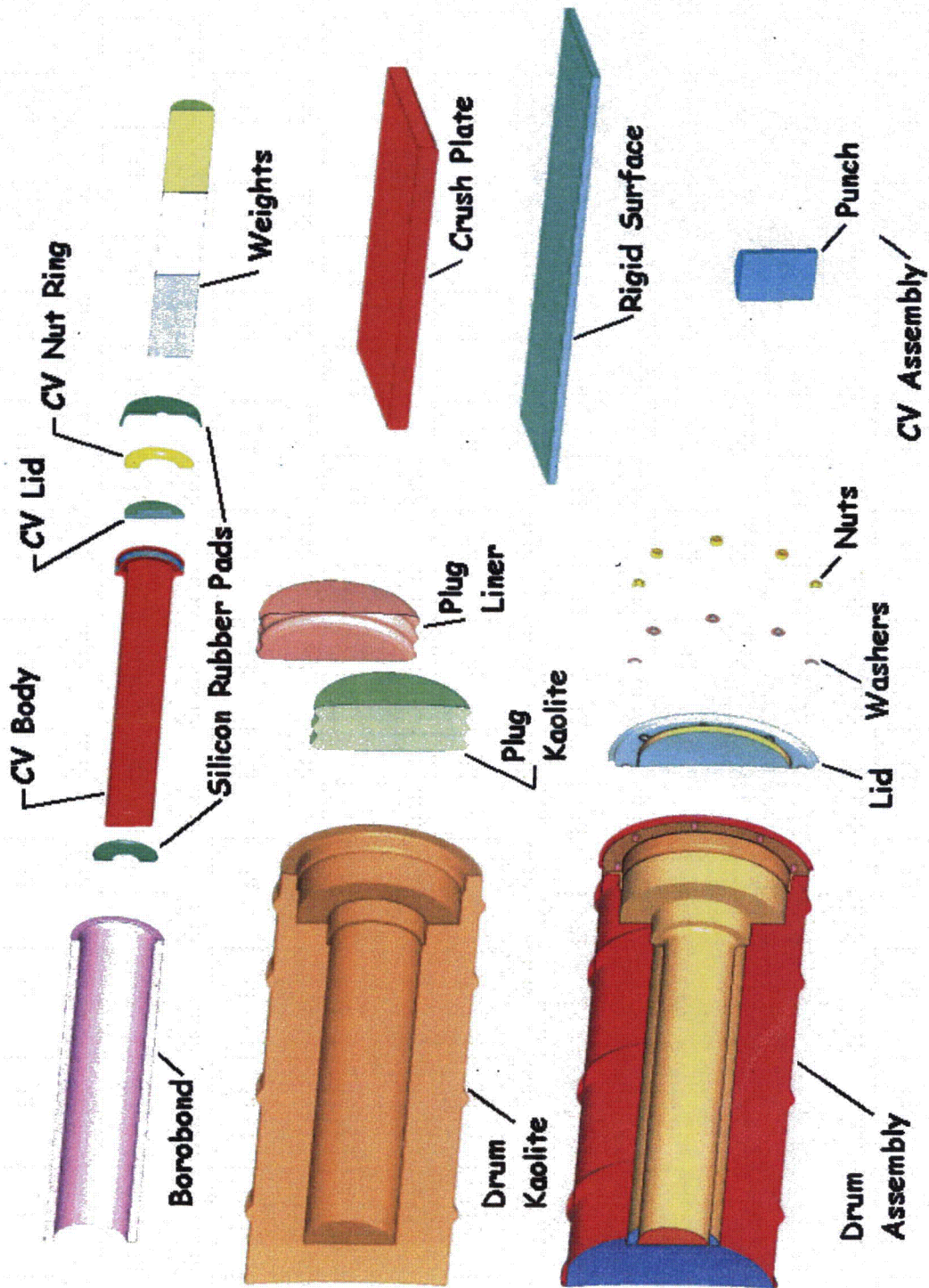
Figure 2.1.1 - Typical ES-3100 Detailed Model Assembly

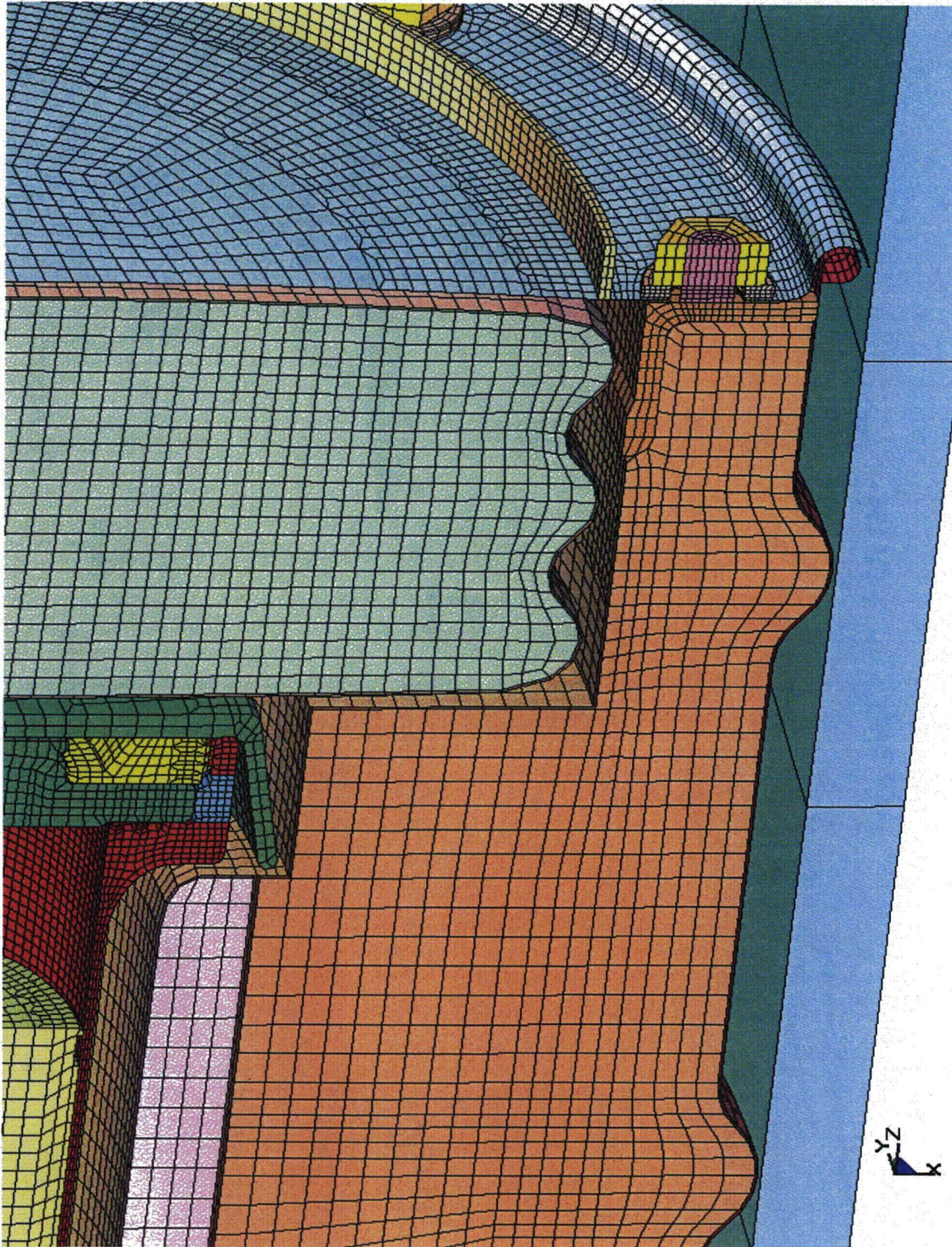Figure 2.1.2 - ES-3100 Detailed Model Components

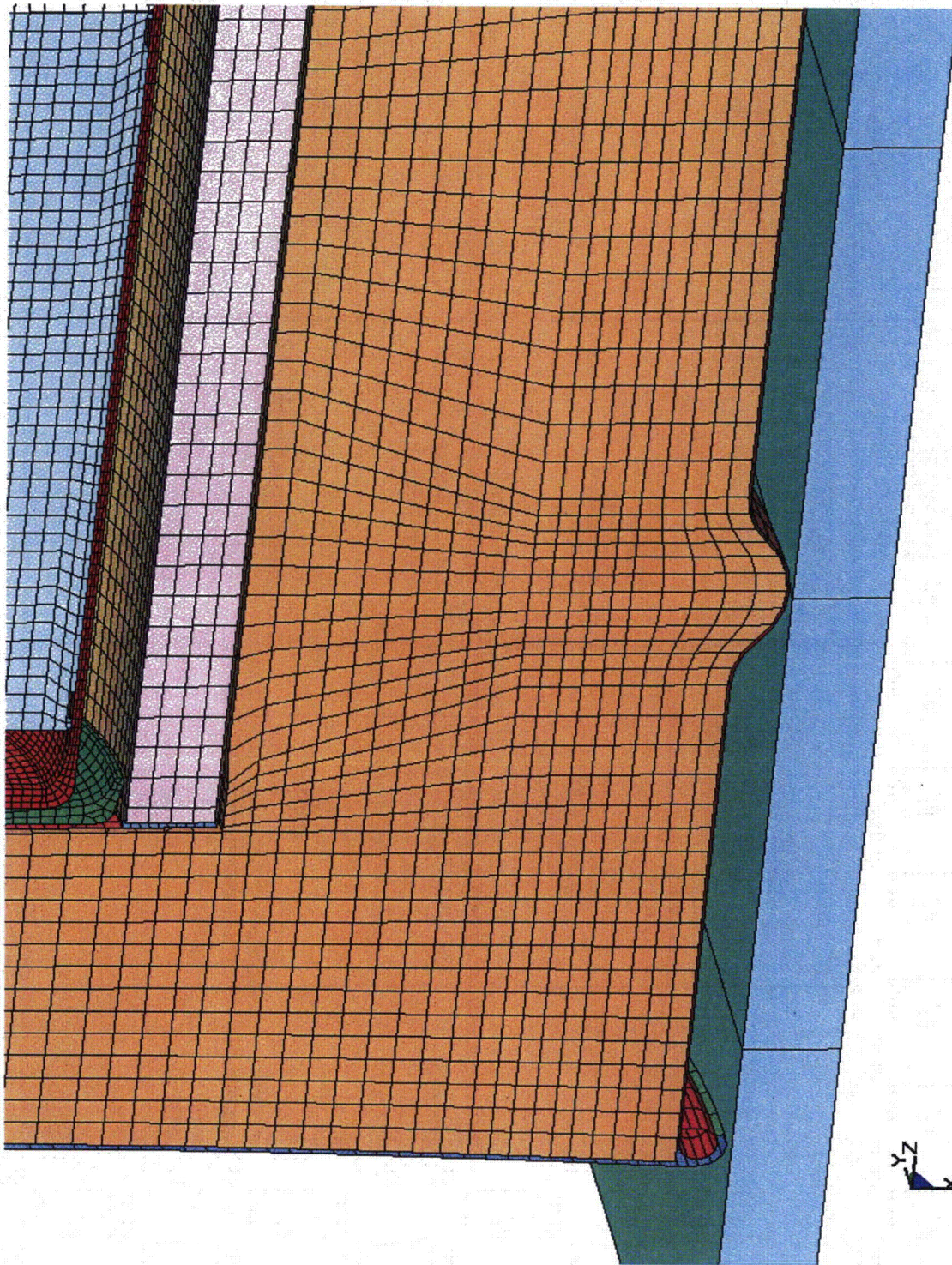Figure 2.1.3 - Typical Element Mesh in the Upper Container Region of the Detailed Model

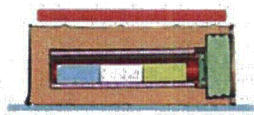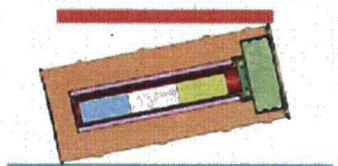Figure 2.1.4 - Typical Element Mesh in the Lower Container Region of the Detailed Model
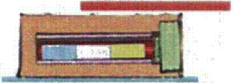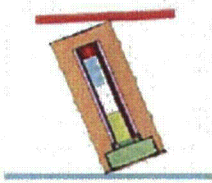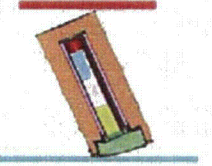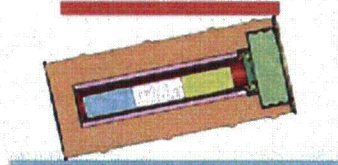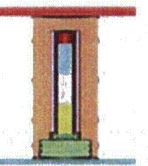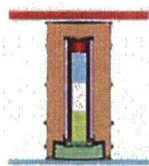
ES-3100 Dynamic Analysis

30-Foot Impact	Crush	30-Foot Impact	Crush
Side (run1g, 1ga)	Centered (run1g)	12 Degree Slapdown(run4g,ga) Bolts on Symmetry Plane	Offset (run4g)
	Offset (run1ga)		Centered (run4ga)
Lid Corner (run2e)	Bottom Corner (run2e)	12 Degree Slapdown (run4h) Bolts off Symmetry Plane	Offset (run4h)
Top End Down (run3b)	Bottom End Crush (run3b)		Centered (run4ha)

Figure 2.1.5 - LS-Dyna Design Runs for Successive 30-Foot and 30-Foot Crush Impacts
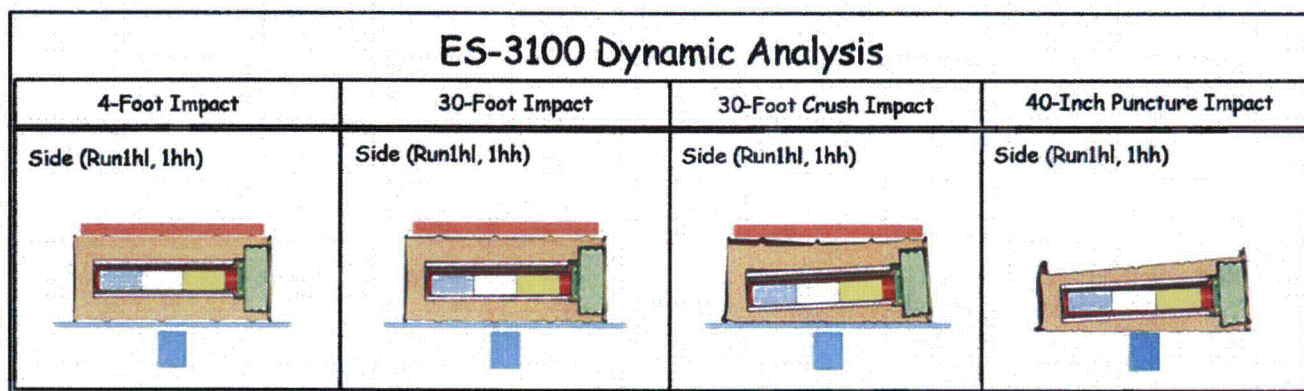
Figure 2.1.6 - Four Successive Impacts with the ES-3100 Bounding Kaolite Stiffness Models

shows icons representing the configurations run for the successive 4-foot + 30-foot + 30-foot crush + 40-inch punch impacts. The Figure 2.1.6 impacts were performed with the upper (-40°F, run1hh) and lower bound (100°F, run1hl) kaolite properties (see Section 2.3.5). The Figure 2.1.5 design runs were made with averaged kaolite properties (see Section 2.3.5). The run numbers (e.g., run1g, etc) are listed in Table 2.1.1 along with a verbal description of the impacts. Table 2.1.1 also identifies the Kaolite material model used for each run (see Section 2.3.5 for definition of the material properties).

Cumulative damage to the shipping package is obtained through successive impact restart solutions of LS-Dyna. At the beginning of the first impact, the initial velocity is assigned to the appropriate model nodes for the first impact. The solution is initiated and is considered over, when the kinetic energy reaches a constant value (after a minimum is reached) and when the rebound velocity reaches a constant value. Consideration was also given to the motion of the masses internal to the CV with regard to a primary impacts against the CV wall. When a run is considered over, the solution is halted and a restart file is written by LS-Dyna. The restart file captures the state of the container assembly at that point in the execution (including nodal velocities and element strains). A restart input file (text file) is then created which defines changes to be made to the model. The restart input file is used to redefine the velocity for the nodes of interest in a successive impact, or delete materials (components) if desired. The redefined velocity becomes the initial velocity, for the successive impact. The successive impact solution is then initiated with the restart file written by the halting of the previous impact and the restart input file. The velocities used in this analysis are: 193 in/sec for the 4-foot impact; 528 in/sec for the 30-foot impact; and 176 in/sec for the 40-inch punch impact.

Table 2.1.1 - Description of the ES-3100 Impacts Using the Detailed Model		
Run ID	Description	Kaolite Model[†]
Run1g	30-foot side impact + 30-foot crush with plate centered on drum	Average stiffness, 22.4 lb/0ft³
Run1ga	30-foot side impact + 30-foot crush with plate centered on CV flange	Average stiffness, 22.4 lb/ft³
Run1hl	4-foot side impact + 30-foot side impact + 30-foot crush impact + 40-inch punch impact	Lower bound stiffness, 27 lb/ft³
Run1hh	4-foot side impact + 30-foot side impact + 30-foot crush impact + 40-inch punch impact	Upper bound stiffness, 27 lb/ft³
Run2e	30-foot CG over lid corner impact + 30-foot crush on bottom corner	Average stiffness, 22.4 lb/ft³
Run3b	30-foot top end impact + 30-foot bottom end crush	Average stiffness, 22.4 lb/ft³
Run4g	30-foot, 12° slapdown with lid studs on plane of symmetry + 30-foot crush with plate centered on CV flange	Average stiffness, 22.4 lb/ft³
Run4ga	30-foot, 12° slapdown with lid studs on plane of symmetry + 30-foot crush with plate centered on drum	Average stiffness, 22.4 lb/ft³
Run4h	30-foot, 12° slapdown with lid studs off plane of symmetry + 30-foot crush with plate centered on the CV flange	Average stiffness, 22.4 lb/ft³
Run4ha	30-foot, 12° slapdown with lid studs off plane of symmetry + 30-foot crush with plate centered on the drum	Average stiffness, 22.4 lb/ft³
† - Defined in Section 2.3.5		

In the successive design impacts (Figure 2.15), a 30-foot impact was followed by a 30-foot crush impact. For these runs, the initial velocities of the shipping package assembly nodes were all defined as 528 in/sec in a direction normal and toward the rigid surface. When the initial impact was over, the run was halted and the velocities of the shipping package assembly nodes were all re-defined as 0.0 in/sec in the restart input file. This file also defined the velocity of the crush plate nodes as 528 in/sec in a direction towards the shipping package.

For the bounding kaolite stiffness runs (Figure 2.1.6), the impacts were successive 4-foot, 30-foot, 30-foot crush and 40-inch punch impacts. The 4-foot, 30-foot and 30-foot crush impacts were carried out as defined previously. The successive punch impact was initiated with the restart input file deleting the crush plate and the rigid plate from the model. The restart input file also redefined the velocity of the shipping package nodes to be towards the punch. This allowed the shipping package to pass through the original position of the rigid surface and impact the punch.

Table 2.1.2 gives the shipping package component masses and weights used in the detailed model analyses. Summations for assembly weights are also listed along with a total assembly weight. As discussed in the Section 2.3 on material models, an initial mass based on preliminary information supplied by the designer is adjusted to match expected hardware weights. This adjustment is required due to the faceted element faces on the inner and outer radius surfaces and the fact that small details are not explicitly modeled (holes, notches, etc). The total weight (full model) of the model is about 427.85 pounds, with 22.4 lb/ft^3 kaolite. The mass moment of inertia for the package is 90.84 in*lb*sec^2 about the global Y axis and the CG is located at Z = 22.4 inches.

Contact surfaces are used to allow adjacent components to separate, bear and/or slide along an adjacent surface. The contact used between the metal components of the model is a LS-Dyna single surface contact. Each node is reactive against every other element in the defined set. The contact between the borobond and its stainless steel liners; and the kaolite and its stainless steel liners is a surface to surface contact. All package nodes are defined as reactive to the rigid surface.

Table 2.1.2 - Analysis Weights for ES-3100

Material Number	Component Description	Run1g-Side mass*	weight**	Run1hl-Side mass*	weight**	Run1hh-Side mass*	weight**	Run2e-Lid Corner mass*	weight**	Run3b-Lid End mass*	weight**	Run4g-Slapdown mass*	weight**	Run4h-Slapdown mass*	weight**
m 1	CV body	2.73E-02	21.10	2.73E-02	21.10	2.73E-02	21.10	2.73E-02	21.10	2.73E-02	21.10	2.73E-02	21.10	2.73E-02	21.10
m 2	CV body at flange	1.73E-03	1.34	1.73E-03	1.34	1.73E-03	1.34	1.73E-03	1.34	1.73E-03	1.34	1.73E-03	1.34	1.73E-03	1.34
m 3	CV lid	9.57E-03	7.39	9.57E-03	7.39	9.57E-03	7.39	9.57E-03	7.39	9.57E-03	7.39	9.57E-03	7.39	9.57E-03	7.39
m 4	CV screw ring	4.27E-03	3.30	4.27E-03	3.30	4.27E-03	3.30	4.27E-03	3.30	4.27E-03	3.30	4.27E-03	3.30	4.27E-03	3.30
m 5	angle	1.69E-02	13.02	1.69E-02	13.02	1.69E-02	13.02	1.69E-02	13.02	1.69E-02	13.02	1.69E-02	13.02	1.69E-02	13.02
m 6	drum	6.02E-02	46.50	6.02E-02	46.50	6.02E-02	46.50	6.02E-02	46.50	6.02E-02	46.50	6.02E-02	46.50	6.02E-02	46.50
m 7	drum bottom head	1.22E-02	9.42	1.22E-02	9.42	1.22E-02	9.42	1.22E-02	9.42	1.22E-02	9.42	1.22E-02	9.42	1.22E-02	9.42
m 8	weld drum to drum bottom head	1.18E-04	0.09	1.18E-04	0.09	1.18E-04	0.09	1.18E-04	0.09	1.18E-04	0.09	1.18E-04	0.09	1.18E-04	0.09
m 9	liner overlap to angle (0.03)	1.36E-04	0.11	1.36E-04	0.11	1.36E-04	0.11	1.36E-04	0.11	1.36E-04	0.11	1.36E-04	0.11	1.36E-04	0.11
m 10	liner (0.06)	3.95E-02	30.51	3.95E-02	30.51	3.95E-02	30.51	3.95E-02	30.51	3.95E-02	30.51	3.95E-02	30.51	3.95E-02	30.51
m 11	liner bottom (0.120) (see m 27 for	1.40E-03	1.08	1.40E-03	1.08	1.40E-03	1.08	1.40E-03	1.08	1.40E-03	1.08	1.40E-03	1.08	1.40E-03	1.08
m 12	lid shells (0.06)	7.25E-03	5.59	7.25E-03	5.59	7.25E-03	5.59	7.25E-03	5.59	7.25E-03	5.59	7.25E-03	5.59	7.25E-03	5.59
m 13	thin lid shell at bolts	1.37E-05	0.01	1.37E-05	0.01	1.37E-05	0.01	1.37E-05	0.01	1.37E-05	0.01	1.37E-05	0.01	1.37E-05	0.01
m 14	lid solids at the lid bolts	5.03E-05	0.04	5.03E-05	0.04	5.03E-05	0.04	5.03E-05	0.04	5.03E-05	0.04	5.03E-05	0.04	5.03E-05	0.04
m 15	lid stiffener	1.39E-03	1.07	1.39E-03	1.07	1.39E-03	1.07	1.39E-03	1.07	1.39E-03	1.07	1.39E-03	1.07	1.39E-03	1.07
m 16	drum bolts	5.06E-04	0.39	5.06E-04	0.39	5.06E-04	0.39	5.06E-04	0.39	5.06E-04	0.39	5.06E-04	0.39	5.06E-04	0.39
m 17	drum bolt nuts	1.20E-03	0.93	1.20E-03	0.93	1.20E-03	0.93	1.20E-03	0.93	1.20E-03	0.93	1.20E-03	0.93	1.20E-03	0.93
m 18	drum bolt washers	4.71E-04	0.36	4.71E-04	0.36	4.71E-04	0.36	4.71E-04	0.36	4.71E-04	0.36	4.71E-04	0.36	4.71E-04	0.36
m 19	plug liner	1.29E-02	10.00	1.29E-02	10.00	1.29E-02	10.00	1.29E-02	10.00	1.29E-02	10.00	1.29E-02	10.00	1.29E-02	10.00
m 20	plug kaolite	1.26E-02	9.70	1.52E-02	11.70	1.52E-02	11.70	1.26E-02	9.70	1.26E-02	9.70	1.26E-02	9.70	1.26E-02	9.70
m 21	drum kaolite	1.43E-01	110.08	1.72E-01	133.03	1.72E-01	133.03	1.43E-01	110.08	1.43E-01	110.08	1.43E-01	110.08	1.43E-01	110.08
m 22	drum borobond	5.66E-02	43.70	5.66E-02	43.70	5.66E-02	43.70	5.66E-02	43.70	5.66E-02	43.70	5.66E-02	43.70	5.66E-02	43.70
m 24	lower internal cv mass	4.75E-02	36.69	4.75E-02	36.69	4.75E-02	36.69	4.75E-02	36.69	4.75E-02	36.69	4.75E-02	36.69	4.75E-02	36.69
m 25	middle internal cv mass	4.75E-02	36.69	4.75E-02	36.69	4.75E-02	36.69	4.75E-02	36.69	4.75E-02	36.69	4.75E-02	36.69	4.75E-02	36.69
m 26	upper internal cv mass	4.75E-02	36.69	4.75E-02	36.69	4.75E-02	36.69	4.75E-02	36.69	4.75E-02	36.69	4.75E-02	36.69	4.75E-02	36.69
m 27	liner bottom solids	9.87E-04	0.76	9.87E-04	0.76	9.87E-04	0.76	9.87E-04	0.76	9.87E-04	0.76	9.87E-04	0.76	9.87E-04	0.76
m 29	visual rigid plane	7.80E-04	0.60	7.80E-04	0.60	7.80E-04	0.60	9.00E-04	0.69	8.00E-04	0.62	9.00E-04	0.69	9.00E-04	0.69
m 30	crush plate	1.42E+00	1099.99	1.42E+00	1099.99	1.42E+00	1099.99	1.42E+00	1099.99	1.42E+00	1099.99	1.42E+00	1099.99	1.42E+00	1099.99
m 31	punch	8.24E-02	63.62	8.24E-02	63.62	8.24E-02	63.62	8.24E-02	63.62	8.24E-02	63.62	8.24E-02	63.62	8.24E-02	63.62
m32	silicon rubber	1.65E-03	1.27	1.65E-03	1.27	1.65E-03	1.27	1.65E-03	1.27	1.65E-03	1.27	1.65E-03	1.27	1.65E-03	1.27
	dyna total model weight	2.06E+00	1592.05	2.09E+00	1617.00	2.09E+00	1617.00	2.06E+00	1592.15	2.06E+00	1592.07	2.06E+00	1592.15	2.06E+00	1592.15
	CV lid and nut ring		10.68		10.68		10.68		10.68		10.68		10.68		10.68
	CV body wt		22.44		22.44		22.44		22.44		22.44		22.44		22.44
	CV total wt		33.12		33.12		33.12		33.12		33.12		33.12		33.12
	plug liner and kaolite		19.70		21.69		21.69		19.70		19.70		19.70		19.70
	liner + angle		45.49		45.49		45.49		45.49		45.49		45.49		45.49
	drum body + kaolite + borobond4		256.94		279.90		279.90		256.94		256.94		256.94		256.94
	drum + lid + plug + kaolite + borobond4		284.65		309.60		309.60		284.65		284.65		284.65		284.65
	internal cv masses		110.08		110.08		110.08		110.08		110.08		110.08		110.08
	Total Package Weight		427.85		452.79		452.79		427.85		427.85		427.85		427.85
	Crush Plate Weight		1099.99		1099.99		1099.99		1099.99		1099.99		1099.99		1099.99
	Punch Weight		63.62		63.62		63.62		63.62		63.62		63.62		63.62
	Visual Rigid Plane		0.60		0.60		0.60		0.69		0.62		0.69		0.69
	Total Model Weight		1592.05		1617.00		1617.00		1592.15		1592.07		1592.15		1592.15

* - Mass is for the 1/2 model and is units of (pound * second^2) / inch
** - Weight is for the total package (2 x model weight) and is in units of pounds.

Friction factors are used in the contact surfaces of the models. Generally speaking, a static coefficient of 0.3 and a dynamic value of 0.2 is used. For the silicon rubber parts, a static coefficient of 0.6 and a dynamic value of 0.5 is assumed. The general factors of 0.3 (static) and 0.2 (dynamic) are also used for the shipping package contact with the rigid surface.

The design of the ES-3100 and the impact configurations are symmetrical. An analytical half model is used with conditions of symmetry defined for all nodes initially on the plane of symmetry. The drum bolting and the CV nut ring are modeled with surfaces initially in contact, but not pre-loaded. The CV is not pressurized. Gravity is included in the models.

The model typically used for a drum welded stud which secures the lid is shown in Figure 2.1.7. The mesh footprint in the stud is mirrored in the angle such that there is a one-to-one match of the stud nodes to angle nodes on the mating surface. The lower nodes on the studs are allowed to merge with the angle nodes. This is structurally conservative at the stud/angle intersection due to the fact that in the stud arc welding process a shoulder boss (area greater than the nominal stud area) is formed. The radius of the modeled studs is such that the faceted area of the stud model equates to the tensile stress area of the studs. Similarly to the stud/angle nodes, the nut/stud nodes are positioned and allowed to merge. The lid is modeled with shell elements, however, at the radius around each stud a transition to brick elements is made. This allows frictional bearing of the lid thickness onto the stud shank to be modeled. This modeling approach has been used and accepted for NNSA-licensed shipping packages that were subject to independent review and verification analysis (i.e., DPP-2 and ES-2100).
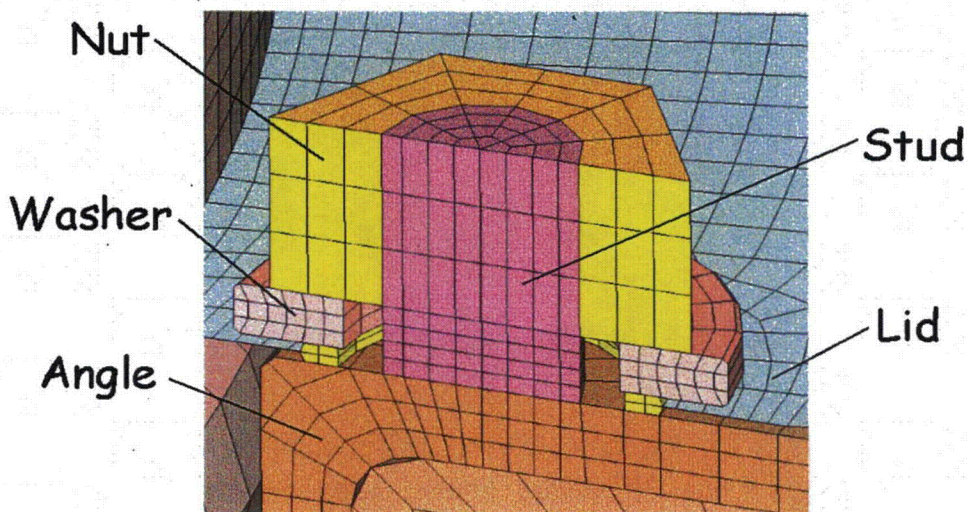
Figure 2.1.7 - Localized Model of a Stud

2.2   Model Description - Simplified Model

A series of punch impact runs were made on a simple model of the ES-3100 shipping container by varying the angle between the container liner and the punch, see Figure 2.2.1. In Figure 2.2.1, the position of the punch relative to the drum is shown with the angles in degrees. The purpose of the punch runs was to determine the response of the stainless steel drum liner due to the angled punch impacts. A series of eight, angled drops as shown in Figure 2.2.2 and described in Table 2.2.1 were made. In Figure 2.2.2, the punch is held stationary and the drum is positioned relative to the punch. The center of gravity of the shipping package was located directly above the side of the punch as shown in Figure 2.2.1. The initial velocity of the container is parallel to the axis of the punch as shown in Figure 2.2.2.
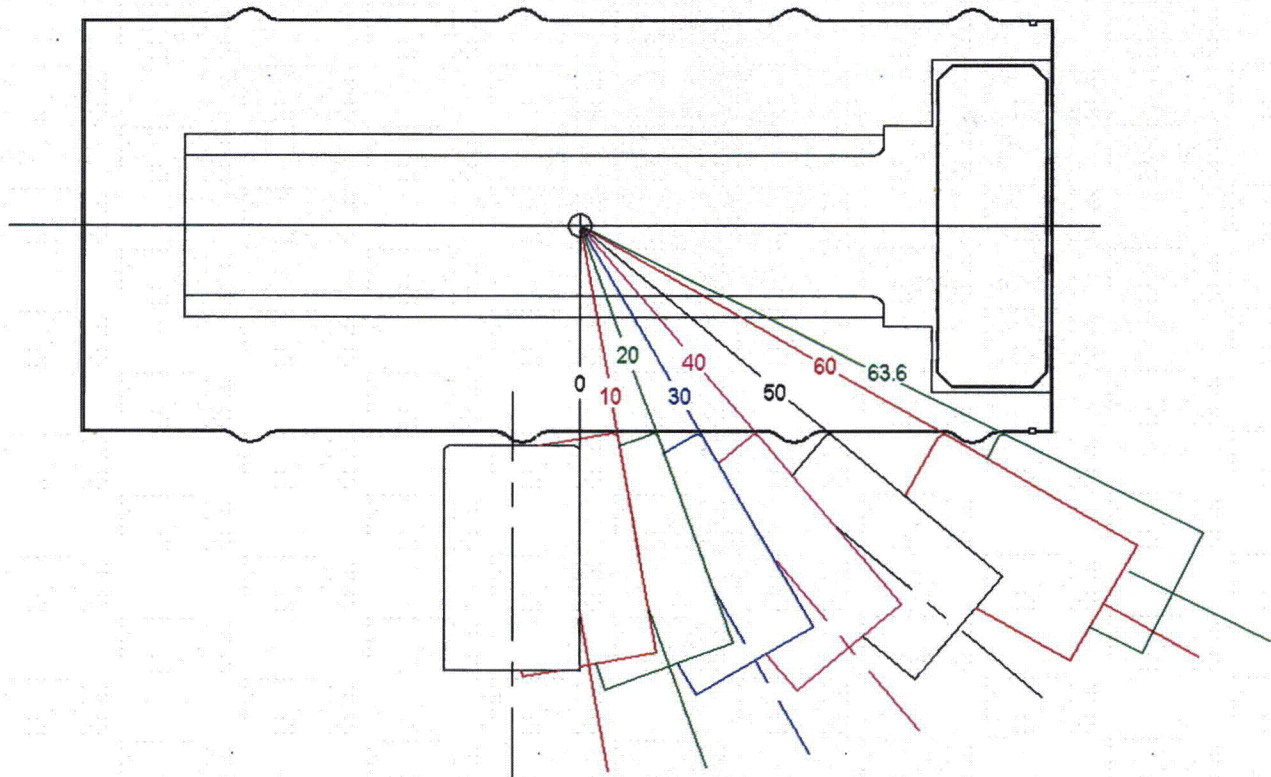
Figure 2.2.1 - Punch Angles on the Drum Liner

A simplified model of the ES-3100 was derived from the more detailed model (described in Section 2.1) for this series of runs. The model detail needed in the 4-foot, 30-foot, crush, and successive punch impact is not needed for the series of punch impacts. The purpose of the series of punch impacts is to evaluate the response of the drum skin to various punch angles.

The detailed model (section 2.1) was simplified (see below) to form the simple model. The detailed model was simplified except for the drum skin and the drum kaolite mesh nearest the punch impact. Figure 2.2.3 shows the simplified shipping package model used for the series of punch impacts. Figure 2.2.4 shows an exploded view of the simple model components.
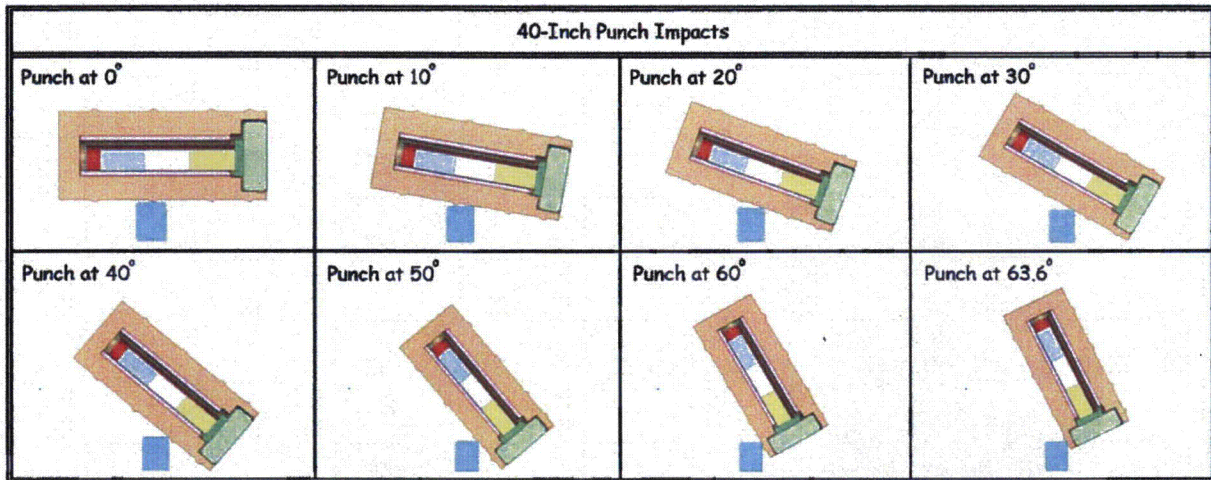

Figure 2.2.2 - ES-3100 Punch Configurations for the Series of Punch Impacts

Table 2.2.1 - Description of the ES-3100 Impacts with the Simplified Model Summarized in this DAC		
Run ID [†]	Description [†]	Kaolite Model
Punch at 0°	40-inch punch impact at 0°	Average stiffness, 22.4 lb/ft³ (note the density is altered slightly so that the punch model weights approximate the full model runs)
Punch at 10°	40-inch punch impact at 10°	
Punch at 20°	40-inch punch impact at 20°	
Punch at 30°	40-inch punch impact at 30°	
Punch at 40°	40-inch punch impact at 40°	
Punch at 50°	40-inch punch impact at 50°	
Punch at 60°	40-inch punch impact at 60°	
Punch at 63.6°	40-inch punch impact at 63.6°	
† - Angles in degrees, measured from a perpendicular to the drum axis as shown in Figure 2.2.1		

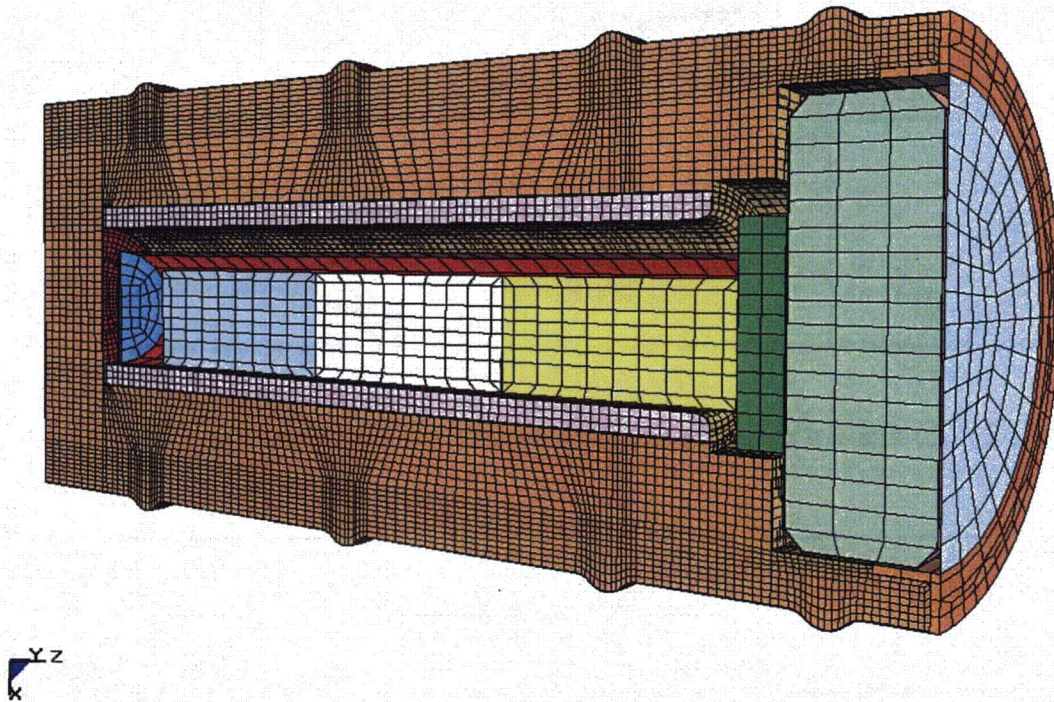3100 RUN-P000 APRIL 2004 KQH
Time =   0

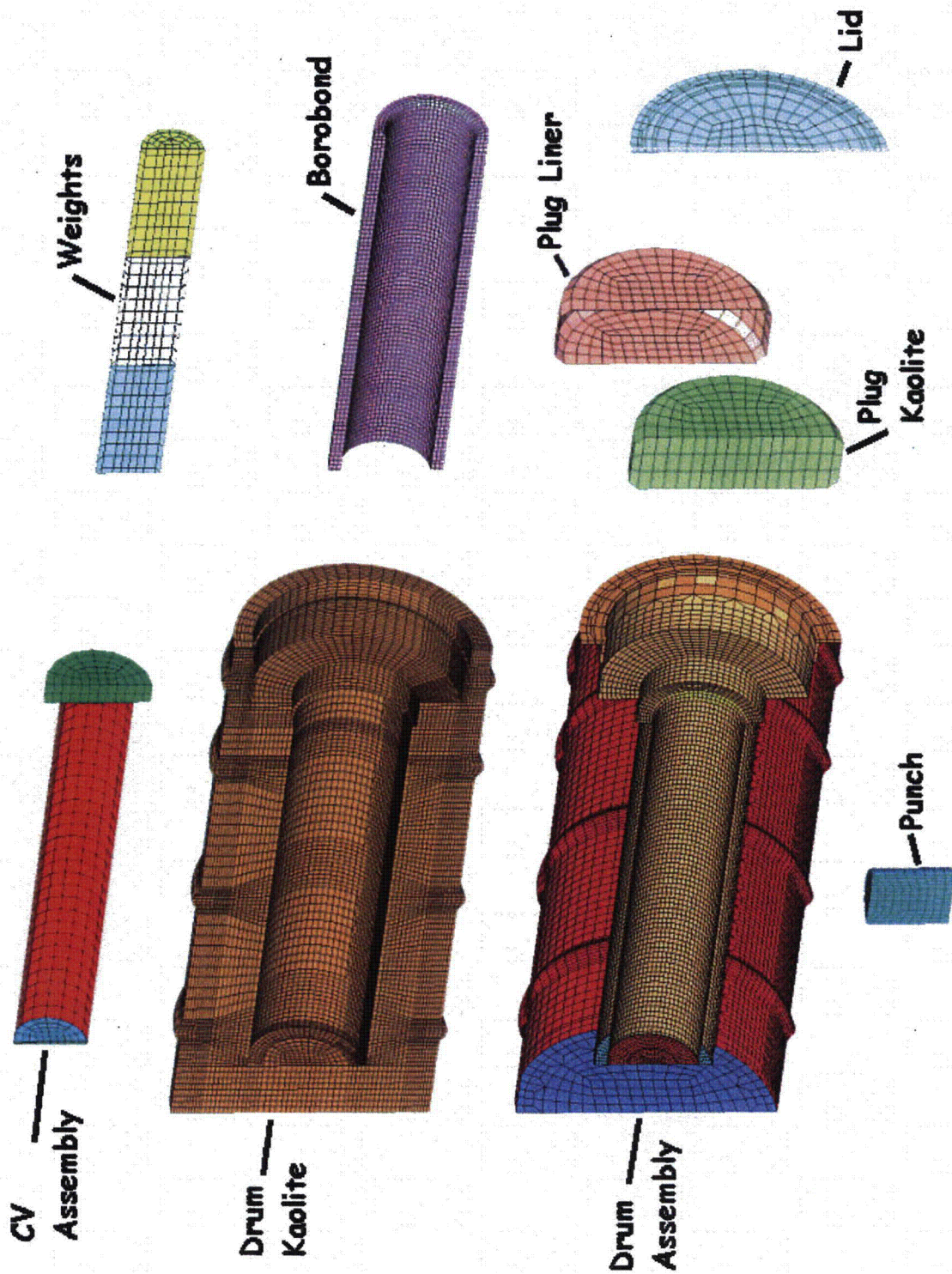Figure 2.2.3 - Simplified ES-3100 Shipping Package Model for the Series of Punch Impacts

Figure 2.2.4 - Exploded View of the ES-3100 Simple Model

Since the concern is the response of the drum skin to the punch, detail in the shipping container components remote from this concern is not warranted and only the mass/stiffness effects on the region of concern become important. In general, there is a simplification of the element mesh (coarser element mesh) away from the punch impact location. Items such as the CV, the plug and the drum lid retention details were greatly simplified in modeling detail (compare Figures 2.2.3 and 2.2.4 verses Figures 2.1.1 through 2.1.4). The CV was simplified to a simple cylinder (shell elements) with a simple solid lid. The drum lid attachment details were replaced by a simple flat lid whose nodes were allowed to merge with the angle nodes. The container plug was also simplified to a simple disk with chamfered corners. This simple model allowed a savings on computer run time and storage allotment without sacrificing the item of concern, the response of the drum liner due to the angled punch.

An effort was made in the geometrical/mesh simplification to maintain the mass distribution of the container as close as is reasonable to the detailed model. Table 2.2.2 shows the weights for all the punch impacts. The total weight for the simple model package assembly was 427.91 pounds with the 22.4 lb/ft^3 kaolite. The mass inertia about the global Y axis for the simple model is 89.64 in*lb*sec^2 and the CG is located at Z= 23.0 inches.

Table 2.2.2 - Analysis Weights for Punch Runs			
Material Number	Component Description	mass*	weight**
1	CV Body	2.6336E-02	20.33
2	CV Bottom Head	2.7398E-03	2.12
3	CV Flange/Lid	1.5492E-02	11.96
4	removed for punch runs	0.0000E+00	0.00
5	Angle	1.9249E-02	14.86
6	Drum	6.0236E-02	46.50
7	Drum Bottom	1.2318E-02	9.51
8	removed for punch runs	0.0000E+00	0.00
9	removed for punch runs	0.0000E+00	0.00
10	Liner	3.9641E-02	30.60
11	Liner Bottom	1.3361E-03	1.03
12	Lid	8.6358E-03	6.67
13	removed for punch runs	0.0000E+00	0.00
14	removed for punch runs	0.0000E+00	0.00
15	removed for punch runs	0.0000E+00	0.00
16	removed for punch runs	0.0000E+00	0.00
17	removed for punch runs	0.0000E+00	0.00
18	removed for punch runs	0.0000E+00	0.00
19	Plug Liner	1.2949E-02	10.00
20	Plug Kaolite	1.2573E-02	9.71
21	Drum Kaolite	1.4265E-01	110.13
22	Borobond	5.6607E-02	43.70
24	CV Lower Inner Weight	4.7530E-02	36.69
25	CV Middle Inner Weight	4.7530E-02	36.69
26	CV Upper Inner Weight	4.7530E-02	36.69
27	Liner Kaolite Cavity Bottom	9.3847E-04	0.72
28	removed for punch runs	0.0000E+00	0.00
29	removed for punch runs	0.0000E+00	0.00
30	removed for punch runs	0.0000E+00	0.00
31	Punch	8.2405E-02	63.62
32	removed for punch runs	0.0000E+00	0.00
pkg			427.91
punch			63.62
total		6.3670E-01	491.53

* - Mass is for the 1/2 model and is units of (pound * second^2) / inch
** - Weight is for the total package (2 x model weight) and is in units of pounds.

Y/LF-717/Rev 2/ES-3100 HEU SAR/Ch-2/rlw/3-06-08

2.3   Material Models

The LS-Dyna material models used in the ES-3100 analytical model are shown in the Table 2.3.1 index. Note that the designation 304L (capital L) is used for clarity.

Table 2.3.1 - Material Model Index for the ES-3100 LS-Dyna Model
LS-Dyna Part #	Part Description	Material Description	Described in DAC Section
1	CV Body	304L	2.3.1
2	CV Body Neck	304L	2.3.1
3	CV Lid	304L	2.3.1
4	CV Nut Ring	A-479 Nitronic-60	2.3.2
5	Angle	304	2.3.3
6	Drum	304	2.3.3
7	Bottom Head	304	2.3.3
8	Attachment Shell Elements	304	2.3.3
9	Attachment Shell Elements	304	2.3.3
10	Liner	304	2.3.3
11	Liner Bottom	304	2.3.3
12	Lid Shell Elements	304	2.3.3
13	Attachment Shell Elements	304	2.3.3
14	Lid Solid Elements	304	2.3.3
15	Lid Stiffener	304	2.3.3
16	Studs	304	2.3.3†
17	Stud Nuts	Bronze	2.3.4
18	Stud Washers	304	2.3.3
19	Plug Liner	304	2.3.3
20	Plug Kaolite	Kaolite 1600	2.3.5
21	Drum Kaolite	Kaolite 1600	2.3.5
22	Borobond	Borobond 4	2.3.6
23	Not Used	Not Used	Not Used
24	Lower Internal CV Mass	Mild Steel	2.3.7
25	Middle Internal CV Mass	Mild Steel	2.3.7
26	Upper Internal CV Mass	Mild Steel	2.3.7
27	Liner Bottom	304	2.3.3
28	Not Used	Not Used	Not Used
29	Visual Rigid Plane	Rigid	2.3.8
30	Crush Plate	Mild Steel	2.3.7
31	Punch	Mild Steel	2.3.7
32	Silicon Rubber Pads	Silicon Rubber	2.3.9

† - An elastic/plastic model with material failure is used for the studs as explained in the noted section.

Density values listed in Section 2.3 were used as initial values for the material weights. Once the model was completed and initial runs made, the initial density was then ratioed such that the preliminary weights obtained from the designer were matched by the analysis results. Table 2.1.2 shows the resulting component and assembly weights for the detailed model.

The material presented in this section is for room temperature (about 70°) unless otherwise stated. Section 2.3.5 presents Kaolite data at room temperature in section 2.3.5.1, 100°F in section 2.3.5.2 and -40°F in section 2.3.5.3.

2.3.1 304L Stainless Steel

The material 304L is used for the CV components except the nut ring. A software database obtained from Lawrence Livermore National Lab personnel is used to obtain the 304L material data which is reproduced below.

```
Material density . . . . . .        0.28600    lb/in**3
Young's Modulus. . . . . . .        2.800E+07  psi
Shear Modulus. . . . . . . .        1.085E+07  psi
Bulk Modulus . . . . . . . .        2.222E+07  psi
Poisson's ratio. . . . . . .        0.2900
Yield stress at offset . . .  32000.0          psi
Engineering ultimate stress.  85000.0          psi
Elongation at failure. . . .     57.00         %
Yield offset . . . . . . . .      0.20000      %
---------- Calculated values ----------------------
Strain Hardening equation      s  = s0 e**m
Equation constants             s0 = 160455     m  = 0.27916
Yield point                    sy =   21735    ey = 0.00078
Ultimate (Engineering)         Su =   85000    Nu = 0.32202
Ultimate (True)                sut= 112372     eut= 0.27916
Failure  (True)                sft= 168989     eft= 1.20397
Energy to ultimate                    24605 in-lb/in**3
```

The LS-Dyna power law plasticity model (*MAT_POWER_LAW_PLASTICITY) is used for 304L. The material model is:

$$\sigma = K\varepsilon^m$$

were, K = strength coefficient = 160455 (psi)
       m = hardening exponent = 0.27916

The density listed in the reference was an initial density (0.286 lb/in^3) and equates to an initial mass density of 7.4093e-4 lb*sec^2/in^4.

2.3.2 A-479 Nitronic-60

The CV nut ring is modeled with A-479 Nitronic-60 properties. The Reference 5.4 was used to obtain the following material data for the S21800 material.

> Tensile Strength   95 ksi
> Yield Strength   50 ksi
> Elongation   35%

The modulus of elasticity is assumed to be 26.2e6 psi.

From this data the following tangent modulus was calculated for the LS-Dyna, *MAT_PLASTIC_KINEMATIC material model.

$$\varepsilon = \frac{\sigma}{E} = \frac{50000psi}{26.2e6psi} = 0.00192 in/in$$

$$E_{tan} = \frac{95000psi - 50000psi}{0.35 - 0.00192} \approx 129000psi$$

A poisson's ratio of 0.298 was used. A density of 0.2754 lb/in^3 was initially used. This equates to an initial mass density of 7.1347 lb*sec^2/in^4.

2.3.3 304 Stainless Steel

The general shipping container components were modeled as 304 stainless steel. The LS-Dyna material model *MAT_POWER_LAW_PLASTICITY was used for the general container components. The 304 material data was obtained from a software database obtained from Lawrence Livermore National Lab personnel and is reproduced below.

```
Material density . . . . . .        0.29000   lb/in**3
Young's Modulus. . . . . . .        2.810E+07 psi
Shear Modulus. . . . . . . .        1.089E+07 psi
Bulk Modulus . . . . . . . .        2.230E+07 psi
Poisson's ratio. . . . . . .        0.2900
Yield stress at offset . . .  34000.0         psi
Engineering ultimate stress.  87000.0         psi
Elongation at failure. . . .     57.00        %
---------- Calculated values ----------------------
Strain Hardening equation     s  = s0 e**m
Equation constants            s0 = 162738     m  = 0.27208
Yield point                   sy =  23729     ey = 0.00084
Ultimate (Engineering)        Su =  87000     Nu = 0.31269
Ultimate (True)               sut= 114204     eut= 0.27208
Failure  (True)               sft= 167370     eft= 1.10866
```

Similar to section 2.3.1, the power law coefficients for the 304 model used for the general shipping container components were:

K = strength coefficient = 162738 (psi)
m = hardening exponent = 0.27208

The 0.290 lb/in³ density equates to 7.513 e-4 lb*sec²/in⁴ for the initial mass density.

The drum studs were modeled using the *MAT_PLASTIC_KINEMATIC material model in LS-Dyna using the following 304 material properties. This material model allowed material failure to be used for the studs. With material failure, LS-Dyna removes elements which reach the defined failure strain. The following elastic-plastic model was derived from the above material properties.

Modulus of Elasticity = 2.81e7 psi[†]
Poisson's Ratio = 0.29
Yield = 34000 psi
Plastic Modulus = 93180 psi
Failure Strain = 0.57 in/in

The modeling of the drum studs with engineering stress/strain data curve is conservative from a design standpoint. This approach has been used and accepted for NNSA-licensed shipping packages that were subject to independent review and verification analysis (i.e., DT-22 and DT-23).

† - Note: the value of 2.9e7 psi (vs 2.81e7 psi) was inadvertently used in the analysis for the modulus of elasticity. This is seen to cause minimal concern due to the minimal energy absorption in the elastic range.

2.3.4 Bronze

The drum lid nuts are made of bronze. A software database obtained from Lawrence Livermore National Lab personnel was used to obtain the material data which is reproduced below.

```
Material . . . .bronze commercial cu.9 zn.1 ½ hard
Material density . . . . . .     0.31800    lb/in**3
Young's Modulus. . . . . . .     1.700E+07  psi
Shear Modulus. . . . . . . .     6.391E+06  psi
Bulk Modulus . . . . . . . .     1.667E+07  psi
Poisson's ratio. . . . . . .     0.3300
Yield stress at offset . . .  45000.0          psi
Engineering ultimate stress.  52000.0          psi
Elongation at failure. . . .     15.00         %
---------- Calculated values -----------------------
Strain Hardening equation      s   = s0 e**m
Equation constants             s0  =   70989    m  = 0.09191
Yield point                    sy  =   40775    ey = 0.00240
Ultimate (Engineering)         Su  =   52000    Nu = 0.09626
Ultimate (True)                sut=    57006    eut= 0.09191
```

The LS-Dyna power law model was used for the bronze material. The coefficients used were:

K = strength coefficient = 70989(psi)
m = hardening exponent = 0.09191

The density of 0.318 lb/in^3, or 8.2371e-4 lb*sec^2/in^4 was the initial mass density.

2.3.5 Kaolite 1600

Kaolite 1600 properties were used to model the drum and plug kaolite. The LS-DYNA honeycomb material model (*MAT_HONEYCOMB) used for the ES-3100 has been shown to be a good representation of the Kaolite material and approved for NNSA-licensed shipping packages that were subject to independent review and verification analysis (i.e., DPP-2 and ES-2100). There have been several testing programs to determine the structural properties of Kaolite since 1995. Each time new data is obtained, it is compared to the old data to maintain enveloping upper and lower bound stiffness curves. The lower stress/strain portion of the curves presented in this section is shown in Figure 2.3.5.1 below. Each curve shown in Figure 2.3.5.1 is documented in the following sub-sections. The Kaolite test data was obtained from constrained test specimens. For the constrained Kaolite test data, the material data is the same for uniaxial and volumetric strain.
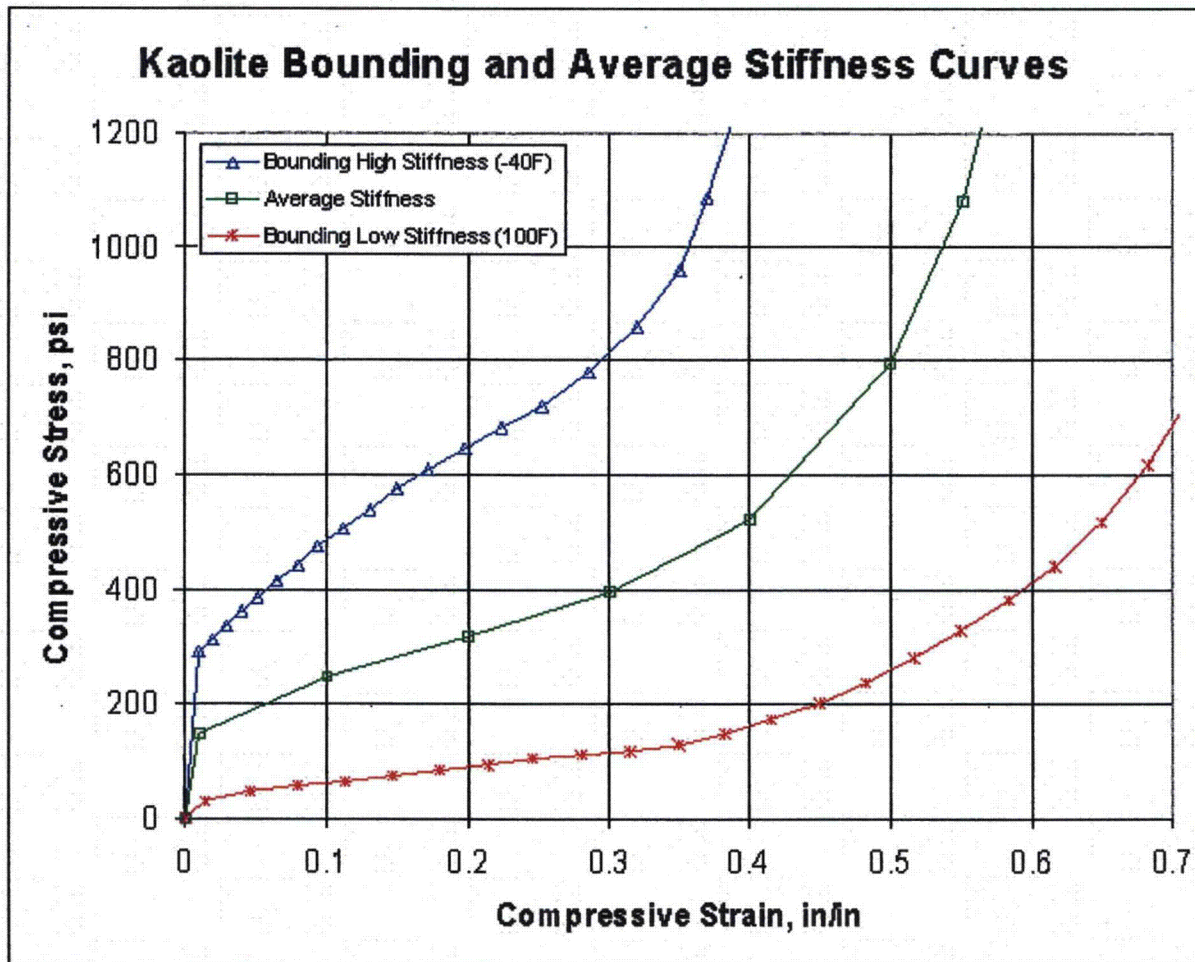
Figure 2.3.5.1 - Bounding Kaolite and Average Stiffness Curves

2.3.5.1   Kaolite 1600 - Averaged Stiffness

A Y12 report gives test data for constrained Kaolite 1600 material at 100°F and -40°F. The maximum peaks from the -40°F high density samples defined an upper bound load deflection curve. The minimum peaks to the 100°F low density samples defined a lower bound load deflection curve. The upper and lower curves were averaged to obtain the average stiffness results. The averaged results up to about 60% strain are then derived from test results for the LS-DYNA material model. The curve is extrapolated above 60% strain, to give a "lock-up" region (collapsing of voids). LS-Dyna does not extrapolate data curves, therefore, the curves must envelope all expected values and assumed values extend the curve well into the lock-up range. Figure 2.3.5.1 shows the lower portion of the averaged stiffness curve. The digital values for the points defined in the LS-DYNA material model are given below in Table 2.3.5.1.1.

Table 2.3.5.1.1 - Digital Load Curve for Kaolite 1600					
Strain, in/in	Stress, psi	Strain, in/in	Stress, psi	Strain, in/in	Stress, psi
0.00	0.0	0.40	523.	0.70	5000. [†]
0.01	148.	0.50	797.	0.75	10000. [†]
0.10	248.	0.55	1079.	0.775	20000. [†]
0.20	317.	0.60	1553.	0.79	30000. [†]
0.30	396.	0.65	2500. [†]	0.8	40000. [†]
[†] - Assumed values to obtain lockup					

The Young's Modulus for the compacted kaolite material is taken as the slope of the last two data points.

$$\frac{40000psi - 30000psi}{0.79\,in/in - 0.80\,in/in} = 1.0e6psi$$

The initial slope is taken as the uncompressed modulus of elasticity.

$$E_{uncompressed} = \frac{148.11psi - 0.0psi}{0.01 - 0.0} = 14811psi$$

Assuming a low poisson's ratio (0.01), the shear modulus is,

$$G = \frac{E}{2(1+v)} = \frac{14811psi}{2(1+0.01)} \approx \frac{14811psi}{2} = 7405\ psi$$

Full compaction is also assumed at a relative volume of 0.20 (this corresponds with the 80% strain assumed data point). The mass density used for the nominal kaolite runs in the analysis is 3.3583e-5 lb*sec²/in⁴, which equates to 22.4lb/ft³.

2.3.5.2   Kaolite 1600 - Lower Bound Stiffness

The kaolite lower bounding stiffness model shown in Figure 2.3.5.1, originated in the ES2LM shipping container calculation and is associated with 100°F. The digital values for the points which define in the LS-Dyna lower bound stiffness curve are given in Table 2.3.5.2.1.

Table 2.3.5.2.1 - Digital Load Curve for Kaolite 1600, Lower Bound		
Strain, in/in	Stress, psi	Origin
0.00	0.0	Test Data and ES2LM Shipping Container Calculation
0.0132	29.	
0.0456	48.	
0.0792	56.	
0.1128	64.	
0.1464	75.	
0.1800	83.	
0.2136	93.	
0.2460	105.	
0.2796	109.	
0.3144	117.	
0.3480	127.	
0.3816	148.	
0.4140	174.	
0.4488	202.	
0.4824	237.	
0.5160	281.	
0.5496	330.	
0.5832	381.	
0.6168	443.	
0.6492	520.	
0.6828	619.	
0.7140	744.	
0.7476	896.	
0.7800	1099.	
0.7944	1205.	
0.8200	3000.	Assumed[†]
0.8700	10000.	Assumed[†]
0.9000	40000.	Assumed[†]
[†] - Assumed to provide "lock-up"		

The Young's Modulus for the compacted kaolite material is taken as the slope of the last two data points.

$$\frac{40000psi - 10000psi}{0.90\,in/in - 0.87\,in/in} = 1.0e6psi$$

The initial slope is taken as the uncompressed modulus of elasticity.

$$E_{uncompressed} = \frac{29.psi - 0.0psi}{0.0132 - 0.0} = 2197psi$$

Assuming a low poisson's ratio, the shear modulus is,

$$G \approx \frac{E}{2} = 1099\ psi$$

A low poisson's ratio is assumed, 0.01. Full compaction is also assumed at a relative volume of 0.10. The density used is 27 lb/ft^3, or 4.0479e-5 lb*sec^2/in^4.

2.3.5.3   Kaolite 1600 Upper Bound Stiffness

The upper bound stiffness of the kaolite 1600 material is an enveloping curve obtained from two sets of material test data. Table 2.3.5.3.1 shows the digital values of the curve.

The Young's Modulus for the compacted kaolite material is taken as the slope of the last two data points.

$$\frac{40000psi - 22000psi}{0.88\,in/in - 0.85\,in/in} = 6.0e5\ psi$$

The initial slope is taken as the uncompressed modulus of elasticity.

$$E_{uncompressed} = \frac{292.1psi - 0.0psi}{0.01 - 0.0} = 29210psi$$

Assuming a low poisson's ratio, the shear modulus is,

$$G \approx \frac{E}{2} = 14605\ psi$$

A density of 27 lb/ft^3 is used as in the low stiffness run. A low poisson's ratio is assumed, 0.01. Full compaction is also assumed at a relative volume of 0.12.

Table 2.3.5.3.1 - Upper Bounding Kaolite Curve		
Strain, in/in	Stress, psi	Origin
0	292.1	Summer 2004 Material Testing
0.01	292.1	
0.019	313.3	
0.029	336.1	
0.04	360.5	
0.051	386.6	
0.064	414.3	
0.079	443.6	
0.094	474.5	
0.111	506.9	
0.13	540.7	
0.15	575.7	
0.172	611.6	
0.197	647.9	
0.224	684.1	
0.253	719.6	
0.285	780	assumed for smooth transition[†]
0.32	860	
0.3504	958	DPP2 Shipping Container Calculation
0.3696	1086	
0.3888	1231	
0.45	2000	assumed for lock-up [†]
0.5	3000	
0.6	6000	
0.7	10000	
0.8	16000	
0.85	22000	
0.88	40000	
† - Assumed values for transition and lock-up		

2.3.6 Borobond 4 Casting Material

The following soil and foam model is used for the borobond 4 casting material. The model is obtained from work done on the Y12, HEU storage pallet and the subsequent physical testing.
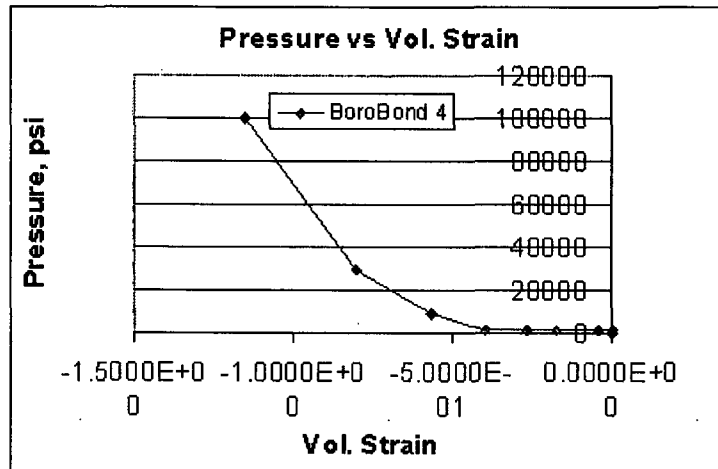
Figure 2.2.3 - Pressure vs Volumetric Strain

The following material data was used for the model of the Borobond 4 casting material.

LS-Dyna Material Model	*MAT_SOIL_AND_FOAM
Density	$1.7991e-4$ lb-sec^2/in^4 (120 lb/ft^3)
Shear Modulus	$1.019e6$ psi
Bulk Modulus	$2.491e6$ psi
A_0	$1.008e7$ (psi)^2
A_1	0
A_2	0
Tensile Cutoff	309.3 psi

Pressure vs Volumetric Strain Data:

Pressure, psi	Volumetric Strain, in^3/in^3
0	0
1833.3	-7.387e-4
1850	-4.2363e-2
1866	-1.7334e-1
1883	-2.6993e-1
1900	-3.9631e-1
10000	-5.6503e-1
30000	-7.9972e-1
100000	-1.1536

2.3.7 Mild Steel

AISI 1020 carbon steel was used to obtain properties for a typical or nominal low carbon steel. A software database obtained from Lawrence Livermore National Lab personnel was used to obtain the material data for AISI 1020 and is reproduced below.

```
Material . . . .steel carbon AISI 1020 plate bar sheet strip to 18 in.
Young's Modulus. . . . . . .           3.000E+07 psi
Shear Modulus. . . . . . . .           1.163E+07 psi
Bulk Modulus . . . . . . . .           2.381E+07 psi
Poisson's ratio. . . . . . .             0.2900
Yield stress at offset . . .   30000.0         psi
Engineering ultimate stress.   55000.0         psi
Elongation at failure. . . .     25.00         %
```

A modulus of elasticity of 2.9e7 (vs 3.0e7 psi) was inadvertently used in the analysis for this material. This material model was used for the inner CV weights, the crush plate and the punch. This is seen to be of minimal concern due to the fact that the components which use this modulus are not of concern themselves, it is their effect on the package/CV that is of concern.

A density of about 490 lb/ft^3 is also initially assumed, which equates to a mass density of 7.35 lb-sec^2/in^4. This initial mass value was then adjusted based on the expected component weight.

Using the ultimate (55000 psi) and yield (30000 psi); the failure strain of 0.25 and assuming a 2% offset, a simple bi-linear tangent modulus of 1.0e5 is assumed.

$$E_{tan} = \frac{55000 psi - 30000 psi}{0.25 - 0.002} \approx 1.0e5 psi$$

2.3.8 Rigid Plane

The following properties were assigned to the rigid plane (for contact surface concerns):

Modulus of Elasticity = 28e6 psi
Poisson's Ratio = 0.29

A relatively low value of density was also specified for the rigid plane, 1e-6 lb*sec^2/in^4. Each node of the rigid plane was restrained from rotation and translation in the material definition.

2.3.9 Silicon Rubber

The pads outboard of the CV bottom and top are used to isolate the CV with regards to a transportation vibration concern. The following properties were assumed for the silicon rubber pads:

$$E \approx 150000 \text{ psi}$$
$$\text{Density} = 0.0446 \text{ lb/in}^3 = 1.1554 \text{ e-4 lb*sec}^2/\text{in}^4$$

A modulus of elasticity for the silicon rubber of about 150 psi can be obtained from Figure 35.13 of reference 5.6 (relative magnitude can be mimicked by various sources on the internet). However, this low E value will not allow a stable solution of LS-Dyna. The value of E = 150000 psi results in a stable solution. The silicon rubber piece at the CV lid/flange and the piece at the base of the CV offer only bearing to the CV. A stiffer silicon material would tend to minimize the bearing footprint on the CV, hence force higher stresses/strains in the CV. Initial runs show this to be the case, up to the point that the softer (E = 150 psi) solution fails. Therefore, the value of E = 150000 psi is used due to the fact that it tends to be conservative with respect to the CV and it allows a stable solution of LS-Dyna.

The density shown above is assumed and was found by averaging several nominal silicon rubber values obtained from the internet.

The shear modulus was calculated as:

$$G = \frac{E}{2(1+v)} = \frac{150000 psi}{2(1+0.463)} = 51260 psi$$

The LS-Dyna *MAT_BLATZ-KO_RUBBER was used to model the silicon rubber components. The model defines the poisson's ratio as 0.463.

3.0   Solution Results

In this section, the results of the different analyses are presented. A voluminous amount of data can be obtained for each and every run presented in this DAC. An attempt is made to present the response story of each impact, yet not to overburden the reader, nor the expense of this report with similar images/data. Components of relatively low strain, or whose strain contour patterns are similar to other impacts which have been presented, may be presented digitally in a table (maximum) and not visually in an image. In the bounding kaolite runs, an effort was made to present the same images for comparison purposes.

Results from run1g are presented in detail as are results from the crush impact of run1ga. An effort is made to abbreviate the results of the other runs due to repetition. Only configuration and strain results of note, or uniqueness due to the configuration are included in the other runs. For ease of reading, the plots in sub-sections of Section 3.0 will be shown after the discussion in each section. Time is generally given in seconds, displacements in inches and velocity in inches/seconds.

The kinetic energy and velocity time history plots are nodal averages for the set of nodes that make up the body of concern (e.g., the shipping package for 4-foot impacts or the crush plate for crush impacts). Therefore, the plots are an averaged value to represent the body of concern.

The element mesh is generally not included on package assembly views such as Figure 3.0.1. The element mesh is generally quite small and its inclusion would make it more difficult to observe the components. In close up images, the element mesh is generally included.

The effective plastic strain level contour plots in the shell elements are surface strains (bending/peak strains) unless otherwise noted. Maximum, or in effect, bending strain is the default in LS-Post fringe plotting of shell elements. The maximum value for the plotted elements is given in the title block in the upper left corner of each fringe plot. The maximum fringe value (shown in the upper right hand corner of each fringe plot) may be redefined by the analyst and may or may not reflect the maximum value shown in the left, title block corner. In some fringe plots, the range may be adjusted to show regions in excess of a specific level. Note that shell elements are modeled at the centerline of the thickness. Therefore, in time history plots, one-half the shell thickness needs to be added/subtracted to obtain the desired metal surface for each node.

The nodes on the plane of symmetry and near the rigid plane are termed at "0°". The nodes initially on the Y plane are termed at "90°". And the nodes on the plane of symmetry

and typically nearer the crush plate are termed "180°". This terminology is typically used only in the side and slapdown impacts and denotes the circumferential positions.

The global coordinate system is the default system in LS-Dyna and is the coordinate system of default in this calculation. The global system is centered on the package centerline, at the bottom of the package as shown in Figure 3.0.1 (if the package were sitting on a flat floor, the surface of the floor would define Z = 0.0). The global XZ axes define the plane of symmetry. The global coordinate system triad icon is shown on most images in this section; offset by default in LS-Post for visual purposes. A local coordinate system was defined for the CV assembly due to lid/body flange separation concerns. The local system used is shown in Figure 3.0.2 and moves with the three defining nodes on the CV body and lid. The local X direction is in the direction of CV lid separation at the O-ring location in the flange. The local CV coordinate system is used in the lid separation time history plots in the results sections.
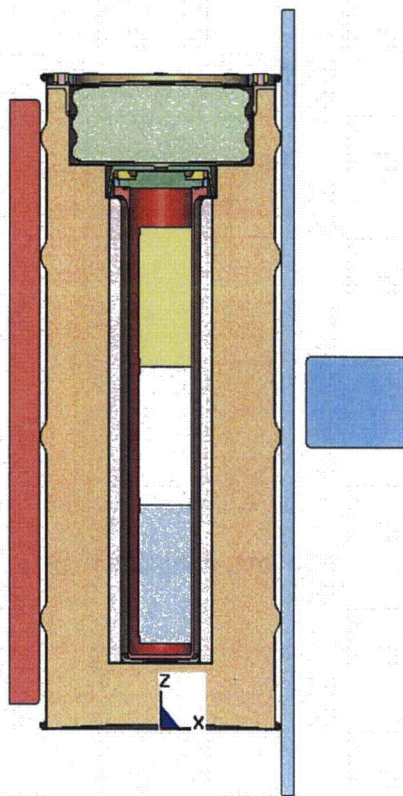
Figure 3.0.1 - Global
Coordinate System
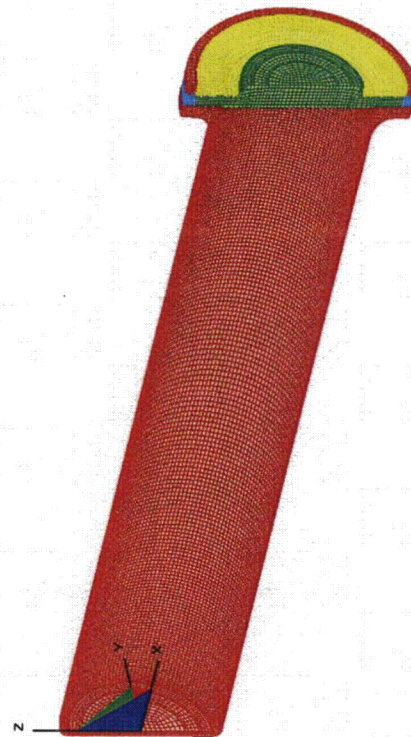
Figure 3.02 - CV Local
Coordinate System

A study of the slapdown angle was performed using a computer code obtained from Los Alamos National Lab. The code considers a simplified, deformable body whose slapdown angle can be varied through multiple runs. The response of interest was the velocity of the secondary impacting end as it strikes the rigid surface.

To obtain all the input constants needed by the slapdown code, trial runs of the ES-3100 model were made. From the trial run, the load on the rigid surface and the deflection of the ES-3100 package ends were used to obtain the simple spring constants. The overall body dimensions, center of gravity location, mass moment of inertia and container mass were also input to the slapdown code.   Figure 2.1.7 shows the results of the slapdown study. The friction factor between the rigid surface and the container was varied between 0.0 and 0.3. An angle of 12° was found to maximize the secondary impact and was chosen for the slapdown angle for the ES-3100.
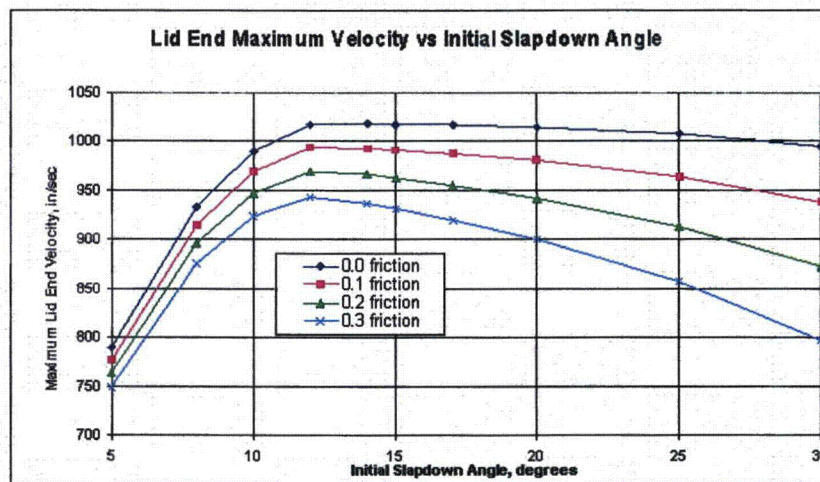
Figure 2.1.7 - Secondary Velocity Maximum from the Slapdown Study

3.1   Run1g - Side

Run1g is a design run with a 30-foot side impact (run time from 0 to about 0.0085 seconds) followed by a 30-foot, centered crush impact (from about 0.0085 to 0.025 seconds). Figure 3.1.1 shows the initial configuration of the model. Note that the punch was in the model, but a punch impact was not included in this run. Figure 3.1.2 shows the configuration of the model after the 30-foot impact. Figure 3.1.3 shows the lid region of the model after the 30-foot impact. Figure 3.1.4 shows the final configuration in the bottom region of the drum nearest the 30-foot impact with the rigid plane.

The effective plastic strain in the CV body at the end of the 30-foot impact is shown in Figure 3.1.5 to be a maximum of 0.0346 in/in. The maximum effective plastic strain occurs near the bottom head as shown in one of the enlarged views in the figure. Figure 3.1.6 shows the maximum effective plastic strain in the CV lid to be 0.0002 in/in for the 30-foot impact. The nut ring remained elastic during the 30-foot impact and is not shown in an image.

The effective plastic strain in the drum angle for the 30-foot impact is shown in Figure 3.1.7. The maximum strain is found to be 0.0682 in/in nearest the rigid plane. Figure 3.1.8 shows the maximum effective plastic strain in the drum to be 0.2218 in/in near the location of the angle and rigid plane. Figure 3.1.9 shows the effective plastic strain in the drum bottom head to be a maximum of 0.2444 in/in. The maximum effective plastic strain in the liner is 0.1189 in/in as given in Figure 3.1.10. The maximum is localized at the junction of the borobond/kaolite liner, near the CV flange, opposite the impact (180°). Figure 3.1.11 shows the maximum effective plastic strain in the drum lid to be 0.3580 in/in and occurs near the stud nearest the impact (0°). The maximum effective plastic strain in the lid stiffener is 0.0060 in/in and is not shown in a Figure. The maximum effective plastic strain in the drum studs is shown in Figure 3.1.12 to be 0.1171 in/in. The maximum effective plastic strain in the drum stud nuts is 0.0005 in/in and in the washers is 0.1628 in/in. The maximum effective plastic strain in the plug liner is 0.08260 in/in. Figures for the nuts, washers and plug liner are not shown.

The time history for the kinetic energy of the package assembly in the 30-foot impact is shown in Figure 3.1.13. Figure 3.1.14 shows the assembly X velocity time history. A constant rebound velocity was obtained at 0.0085 seconds, so the solution was halted at that point. The abrupt response near 0.0085 seconds in both figures is a precipitate of the successive impact restarts (redefining the velocities for the successive impact).

A restart of the LS-Dyna solution is used to create the crush impact. The state of the shipping package at time = 0.0085 seconds was written to a restart file at the end of the 30-foot impact. A second file, the restart input file (user defined) was used to extend the solution to 0.025 seconds, redefine the shipping container nodal velocity to 0.0 in/sec, and

redefine the crush plate nodal velocity to 528 in/sec. With the restart file and the restart input file, the crush impact solution was initiated on the 30-foot damaged container.

The initial configuration of the crush impact was the final configuration of the 30-foot impact as shown in Figure 3.1.2. The final configuration for the crush impact is shown in Figure 3.1.15. Figure 3.1.16 shows a view of the lid region near the rigid plane after the crush impact (0°). Figure 3.1.17 shows the upper lid region (180°). Figure 3.1.18 shows the lower bottom region (0°) and Figure 3.1.19 shows the upper bottom region after the crush impact (180°).

Figure 3.1 20 shows the maximum effective plastic strain in the CV body after the crush impact to be 0.0348 in/in. This is approximately the value after the 30-foot impact. The internal weights bare on the CV side wall forcing the local elevated strain region. Figure 3.1.21 shows the effective plastic strain in the CV lid to be a maximum of 0.0002 in/in. The CV nut ring remains elastic during the crush impact.

Figure 3.1.22 shows the maximum effective plastic strain in the drum angle due to the crush impact to be 0.0945 in/in. The maximum effective plastic strain in the drum is 0.3028 in/in as shown in Figure 3.1.23. Elevated regions of plastic strain occur in localized crimped regions at each end of the crush plate and at the attachment of the angle to the drum near the rigid surface (0°). Figure 3.1.24 shows the effective plastic strain in the drum bottom head. The maximum in the bottom head is 0.2945 in/in. The maximum effective plastic strain in the liner is 0.2063 in/in as shown in Figure 3.1.25. The maximum value occurs at the borobond/kaolite liner junction at 180°, as in the initial 30-foot impact.

The maximum effective plastic strain in the lid due to the crush impact occurs at the base of the hole for the upper stud (180°), near the crush plate. The maximum is 0.6430 in/in as shown in Figure 3.1.26. The membrane strain maximum is 0.4475 in/in and is very localized to the upper stud hole (similar to the bending shown in Figure 3.1.26). If failure were to occur it would be very localized to the lower region of the upper stud hole (near the crush plate - possible surface cracking). There is a lack of a general region of high strain in the lid which would promote an extended tear, or ripping of the lid.

Figure 3.1.27 shows the drum studs with a maximum effective plastic strain of 0.1937 in/in due to the crush impact. Not shown in figures: the maximum effective plastic strain in the lid stiffener is 0.0303 in/in; the maximum effective plastic strain in the drum stud nuts is 0.0005 in/in; the maximum effective plastic strain in the drum stud washers is 0.1628 in/in and the maximum effective plastic strain in the plug liner is 0.1212 in/in.

Figure 3.1.28 shows the kinetic energy time history for the crush plate. Figure 3.1.29

shows the X velocity time history for the plate.

The location of the nodes chosen to investigate the separation of the CV lid and the body flange at the O-rings are shown in Figure 3.1.30. The nodes are at 45° positions around the half model. The nodes are at the inside radius of the inner O-ring groove on the body and are at comparable positions on the opposite, lid surface. Figure 3.1.31 shows the separation time history for the node pairs. A positive value in the plot indicates separation (gap). The plot is quite noisy with ringing (contact chatter) of the node pair separations, but its purpose is to show relative magnitudes of separation in the model. From the figure, it can be seen that a gap spike of almost 0.004 in is obtained in the 30-foot impact just before 0.005 seconds. In the crush impact, spikes of almost 0.005 in in gap separation are seen. When the solution was halted, spikes on the order of 0.004 in are evident (there is no damping in the model other than friction). The ringing maximum is approximately 0.004 in and its minimum is about 0.00 in at the end of the solution (sinusoidal in nature). The ringing would then be about a mid-point value of 0.002 in. An implicit solution, or relaxed state is not obtained. In a relaxed state, if a permanent set were obtained in the flange region, then the average gap would be about 0.002 in, or less would be expected.

Figure 3.1.32 shows the kaolite nodes on the plane of symmetry chosen to obtain the kaolite thickness response to the impacts. Figure 3.1.33 shows the time history thickness at the nodal pairs shown. The thickness is obtained by subtracting one node X-coordinate time history from another nodes. The time in Figure 3.1.33 is in seconds and the X coordinate is the relative value in inches. For example, curve "A" represents the kaolite thickness on the plane of symmetry between the angle and the drum, nearest the crush plate. From Figure 3.1.33 it can be seen that the curve "A" thickness initially is about 1.75 inches and remains at that value for the 30-foot impact. The crush impact is seen to reduce the kaolite thickness to just under 1.0 inches for curve "A". The correlation of nodes, Figure 3.1.33 curve letter and a description of the location is given in Table 3.1.1.

Table 3.1.1 - Location of Kaolite Thickness Measurements
Model Direction	Description	Figure 3.1.33 Curve	Figure 3.1.32 Nodes
-X	Liner at Base of Angle / Drum	A	191112 / 206004
	Liner at Base of Plug Cavity / Drum	B	188411 / 200529
	Liner at Top of CV Cavity / Drum	C	224181 / 200522
	Liner at Second Drum Roll from the Lid / Drum Roll Extreme	D	222721 / 361713
	Liner at Second Drum Roll from the Bottom / Drum Roll Extreme	E	218049 / 350033
	Liner at First Drum Roll from the Bottom / Drum Roll Extreme	F	213377 / 338353
	Liner at Base of CV Cavity / Drum	G	210749 / 334338
+X	Liner at Base of CV Cavity / Drum	H	333258 / 209669
	Liner at First Drum Roll from the Bottom / Drum Roll Extreme	I	338281 / 213305
	Liner at Second Drum Roll from the Bottom / Drum Roll Extreme	J	349961 / 217977
	Liner at Second Drum Roll from the Lid / Drum Roll Extreme	K	361641 / 222649
	Liner at Top of CV Cavity / Drum	L	199946 / 223677
	Liner at Base of Plug Cavity / Drum	M	199953 / 187835
	Liner at Base of Angle / Drum	N	205932 / 191040

Figure 3.1.34 shows nodes in the drum, drum bottom and drum lid which will be used to define the diameter changes in the outer surfaces of the shipping package. Figure 3.1.35 gives the relative X coordinate values (diameter changes) for the nodes on the plane of symmetry. From the plot it is seen that the minimum diameter reaches approximately 14.5 inches and then rebounds slightly. This minimum is at the lower barrel roll in the drum. From Figure 3.1.35 it is seen that the barrel roll diameters decrease from top to bottom. The greater deflection of the crush plate nearer the bottom of the package is evident in the Figure 3.1.15 final configuration plot. Figure 3.1.36 gives the Y coordinate time history response of the nodes at the Y extreme of the shipping package (see Figure 3.1.34). The values in Figure 3.1.36 are relative to the plane of symmetry and therefore need to be doubled to obtain the diameter changes. The correlation of nodes, curve numbers and a description of the location are given in Table 3.1.2. The ovalization of the package is also evident in comparing Figures 3.1.35 and 3.1.36.

Table 3.1.2 - Nodal Locations for Drum Diameter Time Histories				
Description	Diameter (X Direction)		Radius (Y Direction)	
	Figure 3.1.35 Curve	Figure 3.1.34 Nodes	Figure 3.1.36 Curve	Figure 3.1.34 Nodes
Lid Roll	A	133634 / 133778	A	133706
First Drum Roll Below Lid	B	98158 / 98230	B	98194
Second Drum Roll Below Lid	C	100202 / 100274	C	100238
Second Drum Roll Above Bottom	D	102976 / 103048	D	103012
First Drum Roll Above Bottom	E	105750 / 105822	E	105786
Bottom Attachment Roll to Drum	F	108889 / 108961	F	108925

Figure 3.1.37 shows nodes chosen to obtain liner diameter time histories. Figure 3.1.38 shows the diameter time histories for the node pairs. Table 3.1.3 shows the location of the nodal pairs along the length of the liner.

Table 3.1.3 - Nodal Locations for Liner Diameter Time Histories		
Curve	Node Pairs	Distance Above Base of Liner (in)
A	122522 / 122666	0.0
B	123259 / 129667	5.0
C	123276 / 129684	10.3
D	123292 / 129700	15.3
E	123309 / 129717	20.6
F	123324 / 129732	25.2
G	123340 / 129748	30.2

3100 RUN1G SIDE NOV 2003 KQH
Time =   0
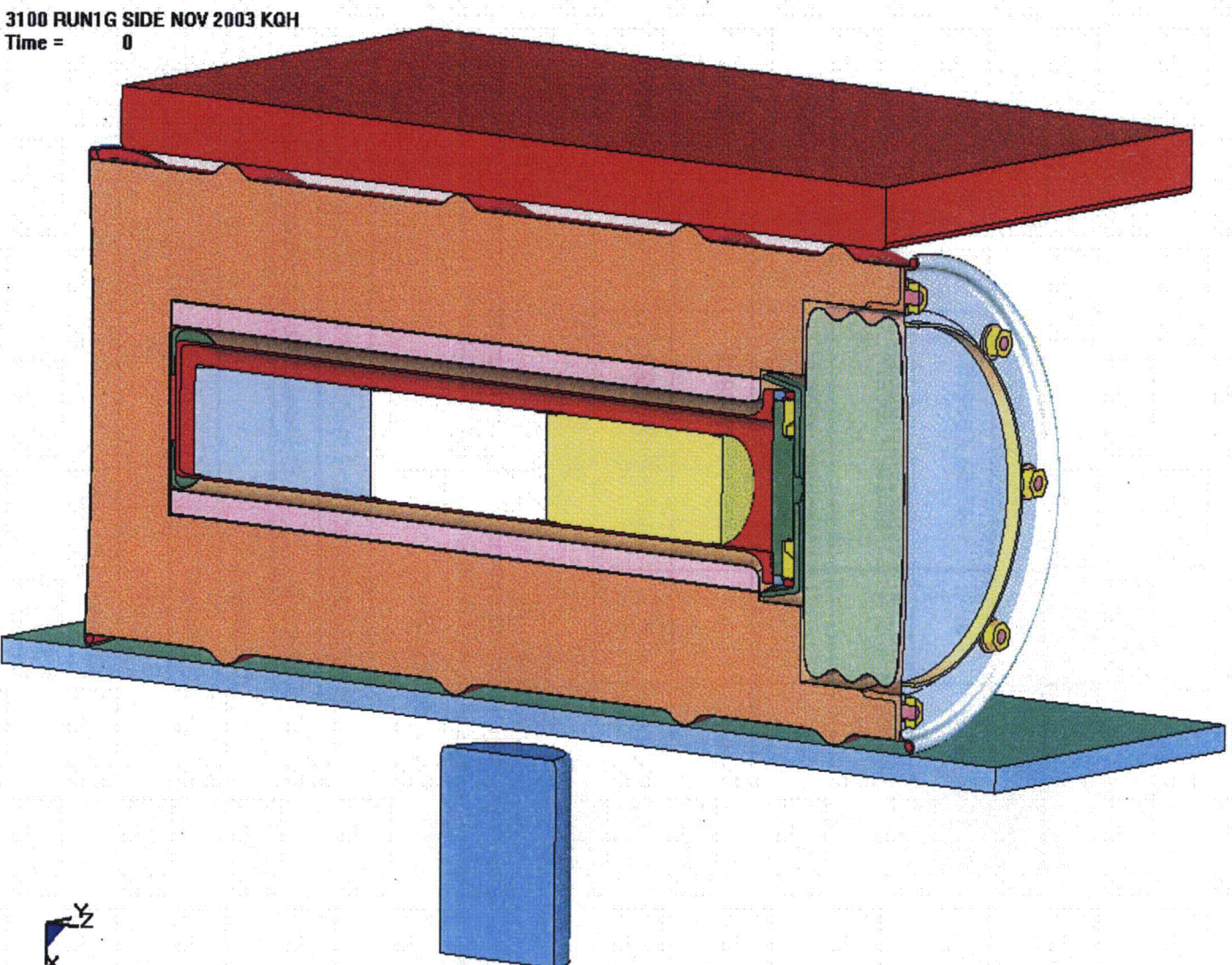
Figure 3.1.1 - Run1g, Initial Configuration

3100 RUN1G SIDE NOV 2003 KQH
Time = 0.0085001
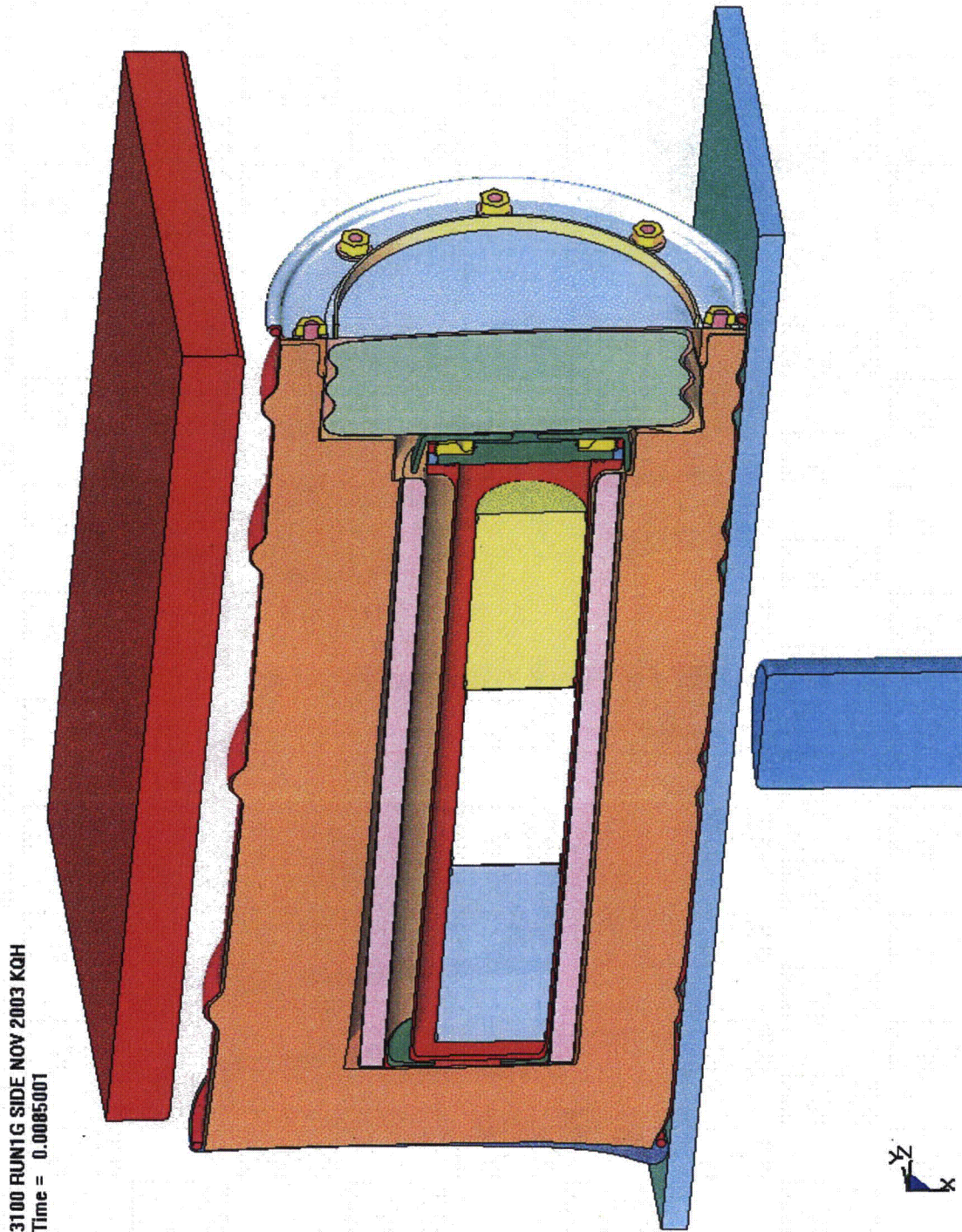
Figure 3.1.2 - Run1g, 30-Foot Impact, Final Configuration
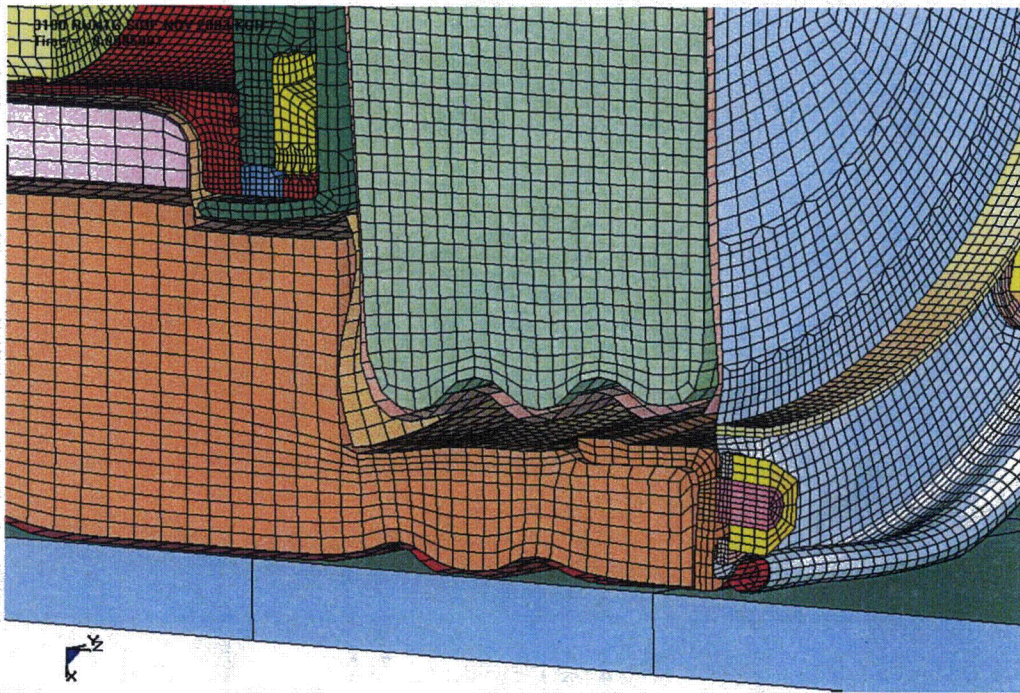
Figure 3.1.3 - Run1g, 30-Foot Impact, Configuration of the Drum Bolted Region
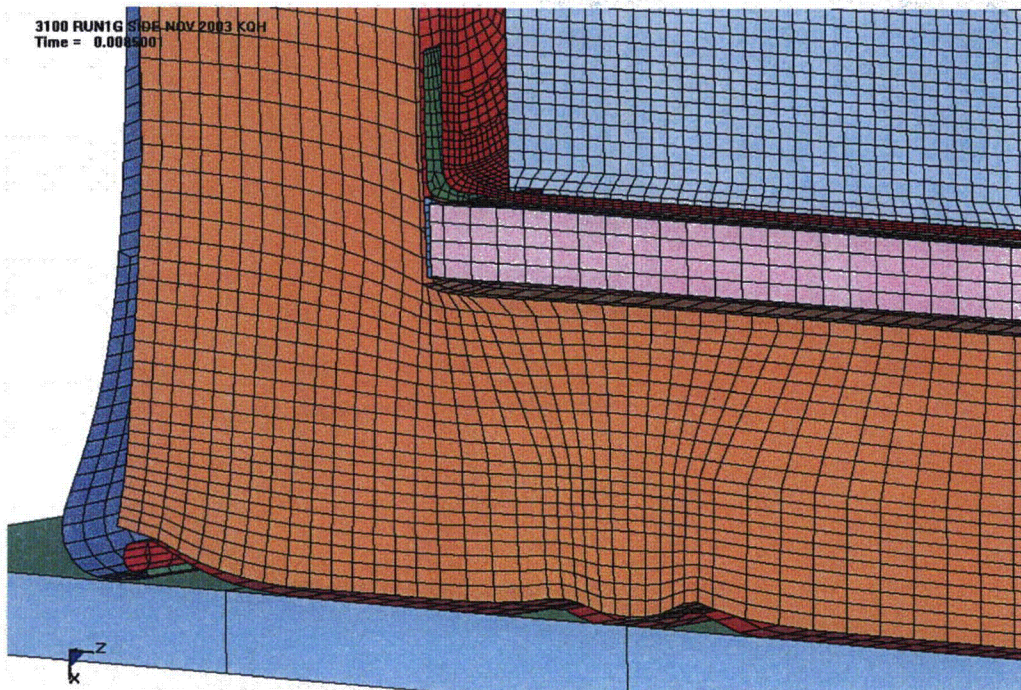
Figure 3.1.4 - Run1g, 30-Foot Impact, Configuration of the Bottom Drum Corner
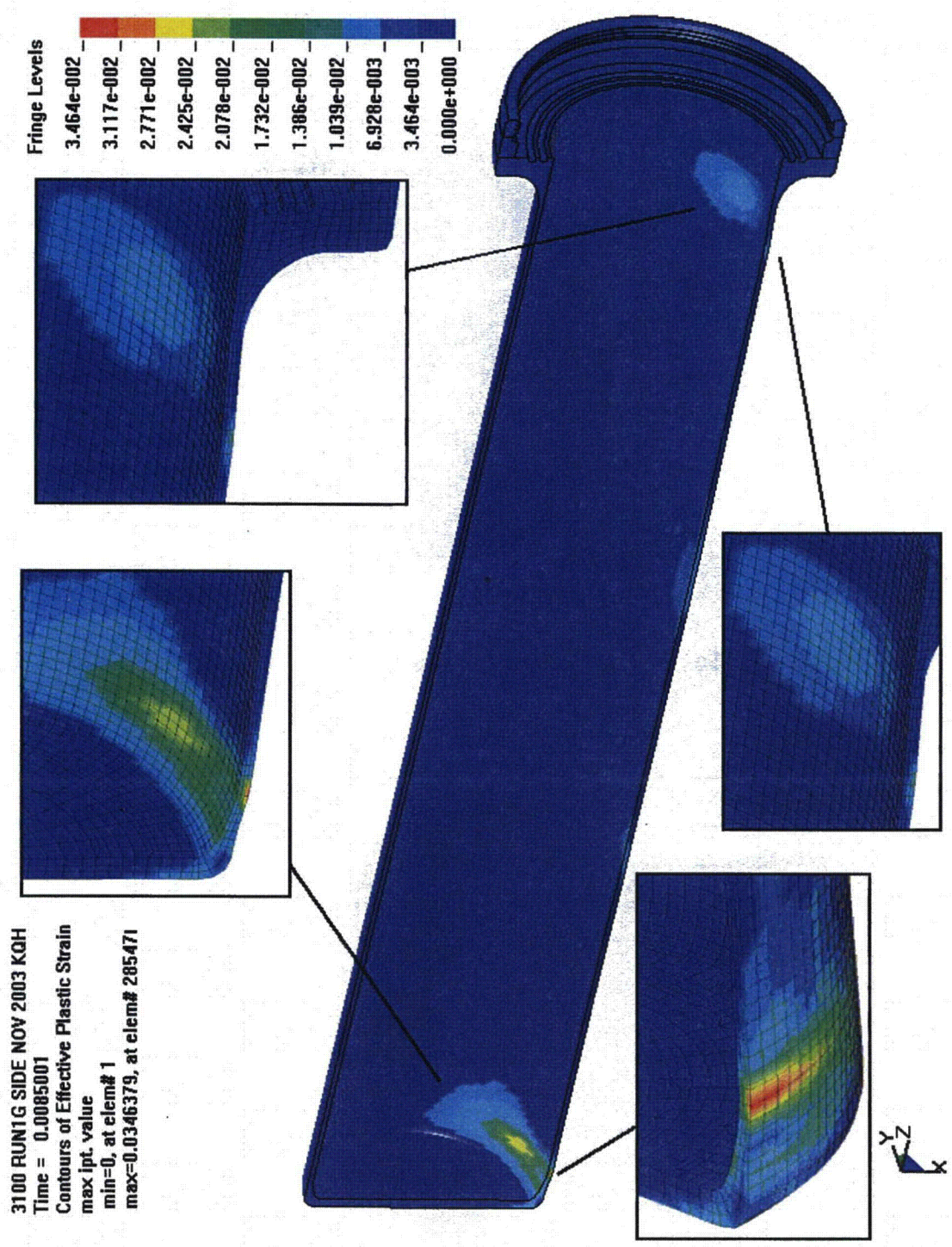
Figure 3.1.5 - Run1g, 30-Foot Impact, Effective Plastic Strain in the CV Body

3100 RUN1G SIDE NOV 2003 KQH
Time = 0.0085001
Contours of Effective Plastic Strain
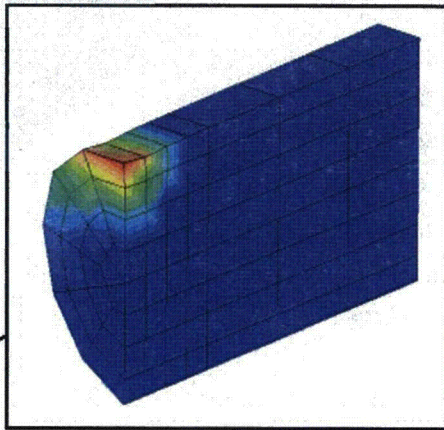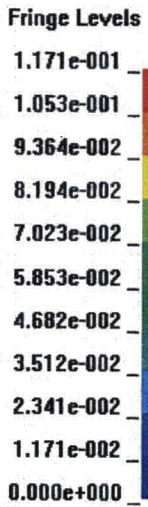max ipt. value
 min=0, at elem# 51809
 max=0.000174097, at elem# 565471

Fringe Levels

1.741e-004
1.567e-004
1.393e-004
1.219e-004
1.045e-004
8.705e-005
6.964e-005
5.223e-005
3.482e-005
1.741e-005
0.000e+000
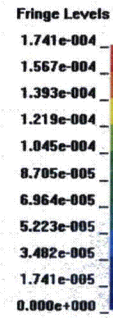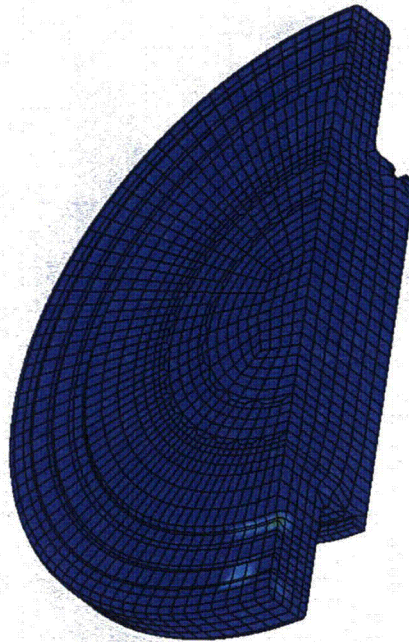
Figure 3.1.6 - Run1g, 30-Foot Impact, Effective Plastic Strain in the CV Lid

3100 RUN1G SIDE NOV 2003 KQH
Time = 0.0085001
Contours of Effective Plastic Strain
max ipt. value
 min=0, at elem# 60885
 max=0.0682127, at elem# 632111

Fringe Levels

6.821e-002
6.139e-002
5.457e-002
4.775e-002
4.093e-002
3.411e-002
2.729e-002
2.046e-002
1.364e-002
6.821e-003
0.000e+000
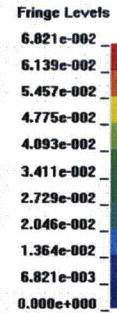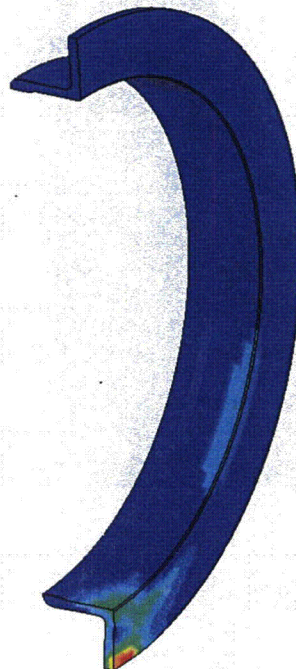
Figure 3.1.7 - Run1g, 30-Foot Impact, Effective Plastic Strain in the Drum Angle

Y/LF-717/Rev 2/ES-3100 HEU SAR/Ch-2/rlw/3-06-08

3100 RUN1G SIDE NOV 2003 KQH
Time = 0.0085001
Contours of Effective Plastic Strain
max ipt. value
 min=0, at elem# 90
 max=0.221774, at elem# 4331

Fringe Levels

2.218e-001

1.996e-001

1.774e-001

1.552e-001

1.331e-001

1.109e-001

8.871e-002

6.653e-002

4.435e-002

2.210e-002
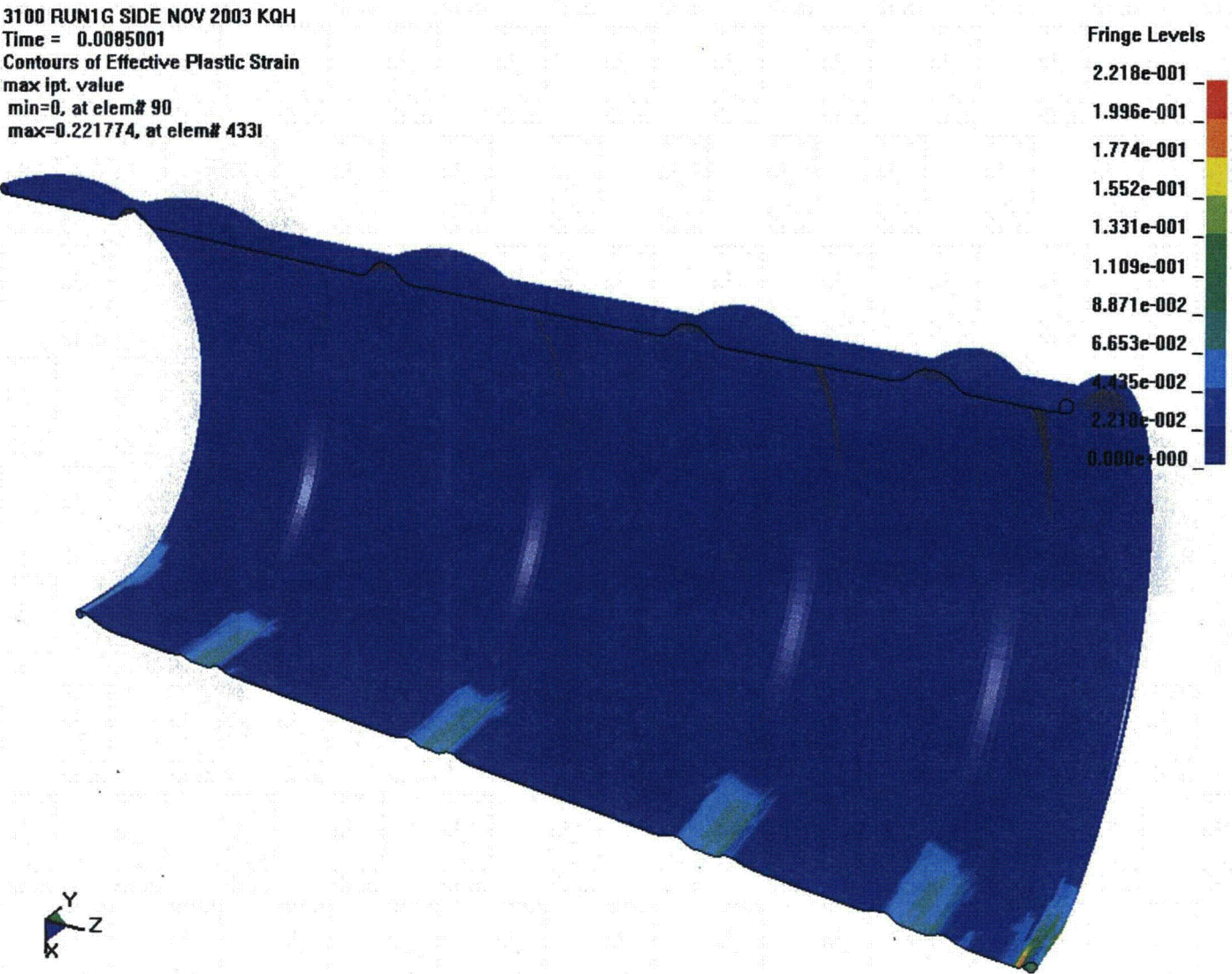
0.000e+000

Figure 3.1.8 – Run1g, 30-Foot Impact, Effective Plastic Strain in the Drum Outer Liner

3100 RUN1G SIDE NOV 2003 KQH
Time = 0.0085001
Contours of Effective Plastic Strain
max ipt. value
 min=0, at elem# 15012
 max=0.24441, at elem# 151951

Fringe Levels

2.444e-001
2.200e-001
1.955e-001
1.711e-001
1.466e-001
1.222e-001
9.776e-002
7.332e-002
4.888e-002
2.444e-002
0.000e+000

Figure 3.1.9 - Run1g, 30-Foot Impact, Effective Plastic Strain in the Drum Bottom Head

3100 RUN1G SIDE NOV 2003 KQH
Time = 0.0085001
Contours of Effective Plastic Strain
max ipt. value
 min=0, at elem# 17724
 max=0.118866, at elem# 218681

Fringe Levels

1.189e-001
1.070e-001
9.509e-002
8.321e-002
7.132e-002
5.943e-002
4.755e-002
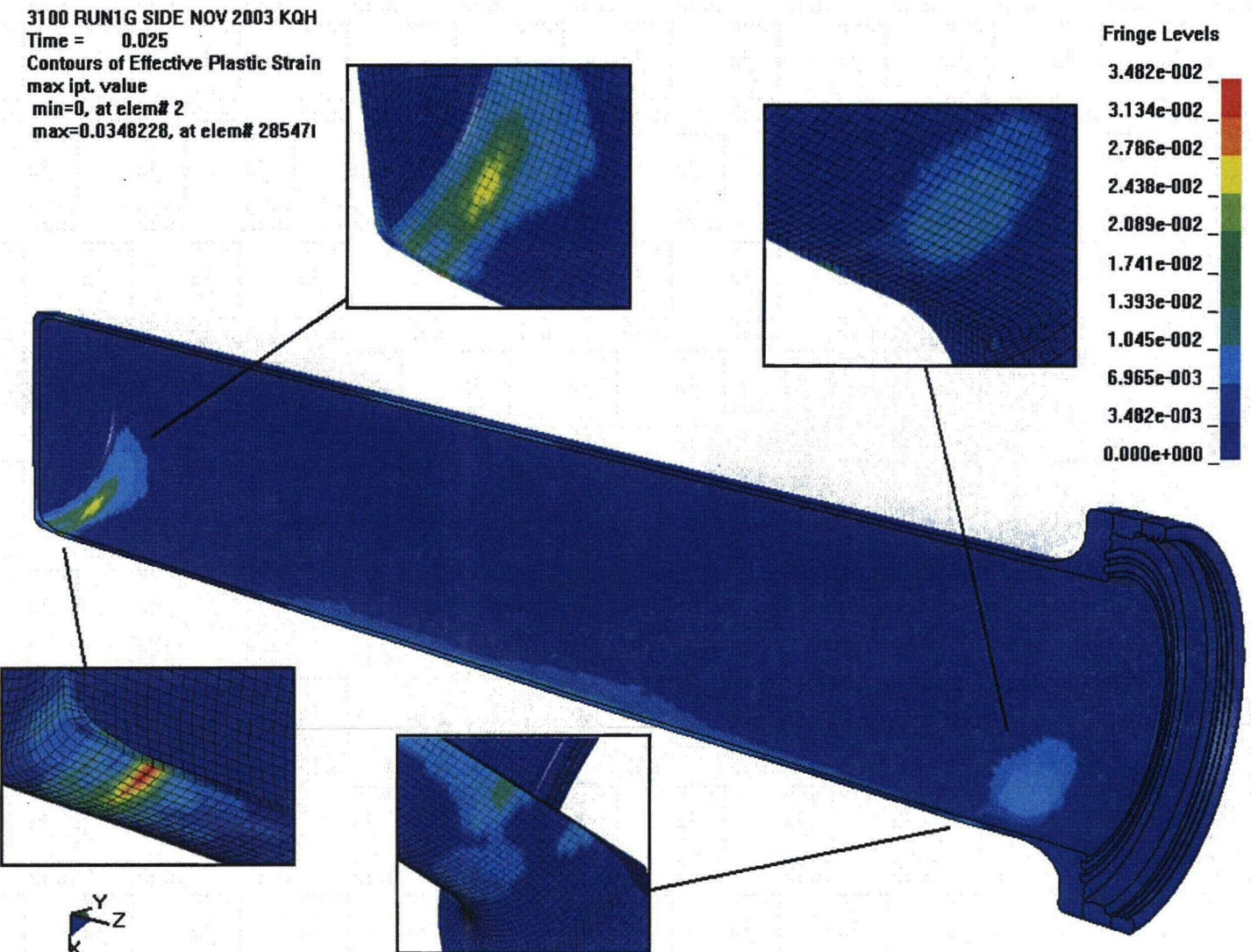3.566e-002
2.377e-002
1.189e-002
0.000e+000
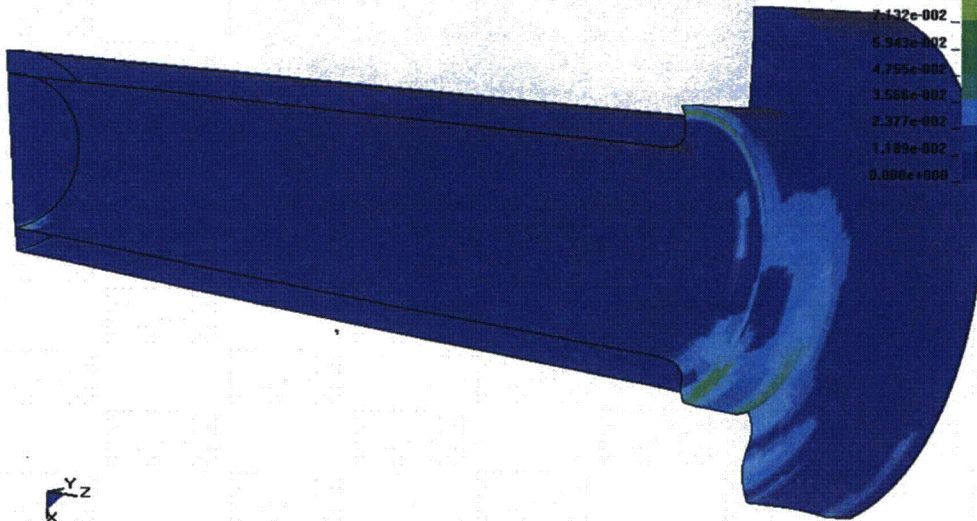
Figure 3.1.10 - Run1g, 30-Foot Impact, Effective Plastic Strain in the Liner

3100 RUN1G SIDE NOV 2003 KQH
Time = 0.0085001
Contours of Effective Plastic Strain
max ipt. value
 min=0, at elem# 37788
 max=0.357987, at elem# 41128l

Fringe Levels

3.580e-001 _
3.222e-001 _
2.864e-001 _
2.506e-001 _
2.148e-001 _
1.790e-001 _
1.432e-001 _
1.074e-001 _
7.160e-002 _
3.580e-002 _
0.000e+000 _
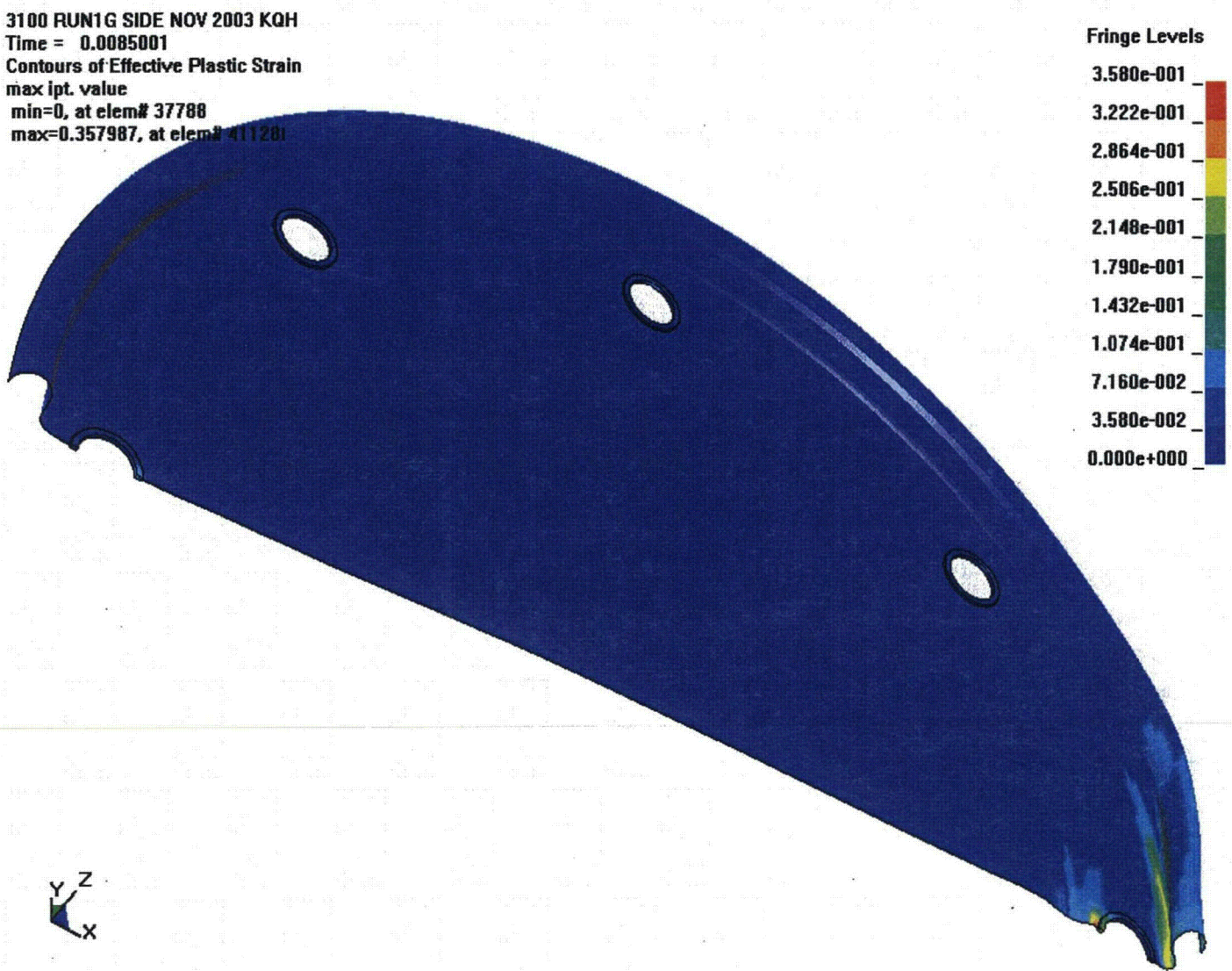
Figure 3.1.11 - Run1g, 30-Foot Impact, Effective Plastic Strain in the Drum Lid

3100 RUN1G SIDE NOV 2003 KQH
Time =   0.0085001
Contours of Effective Plastic Strain
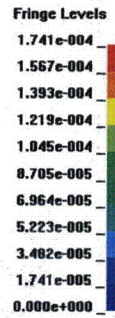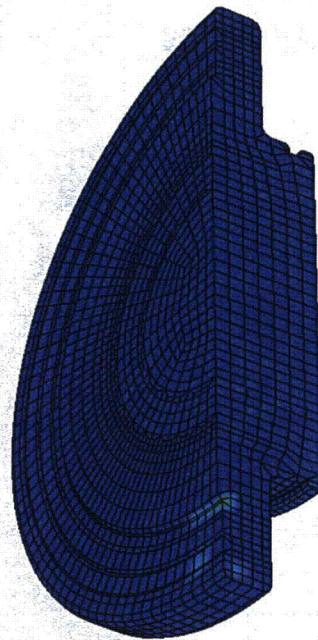max ipt. value
 min=0, at elem# 71875
 max=0.117053, at elem# 71992I

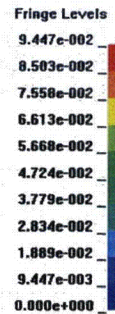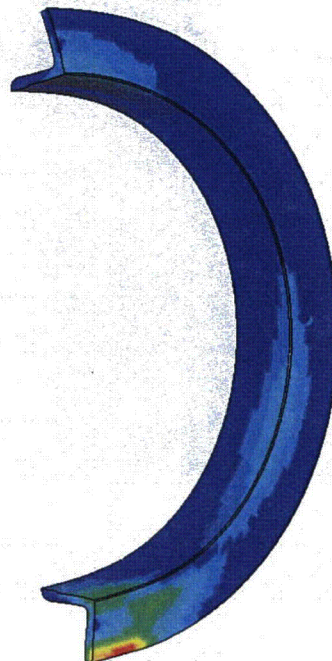Fringe Levels

1.171e-001 _

1.053e-001 _

9.364e-002 _

8.194e-002 _

7.023e-002 _

5.853e-002 _

4.682e-002 _

3.512e-002 _

2.341e-002 _

1.171e-002 _

0.000e+000 _

Figure 3.1.12 - Run1g, 30-Foot Impact, Effective Plastic Strain in the Drum Studs

3100 RUN1G SIDE NOV 2003 KQH

Material No:

A_sum-1
2,3,4,5,6,7,8,9,10,11,12,13
14,15,16,17,18,19,20,21,22
24,25,26,27,32

min=39.802
max=77295
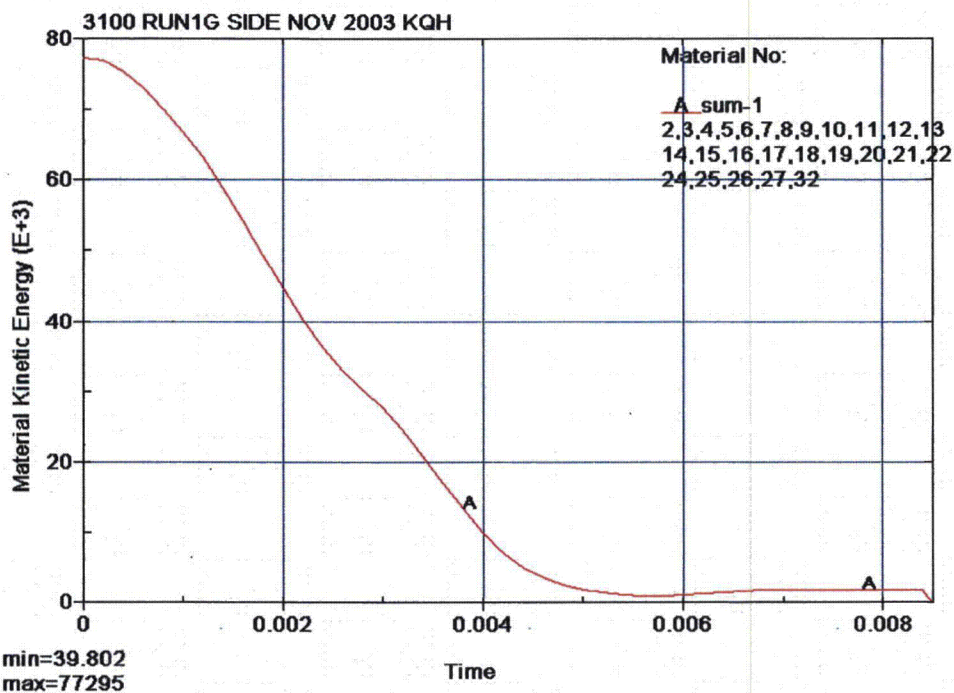
Figure 3.1.13 - Run1g, 30-Foot Impact, Kinetic Energy Time History

3100 RUN1G SIDE NOV 2003 KQH

Material No:

A_avg-1
2,3,4,5,6,7,8,9,10,11,12,13
14,15,16,17,18,19,20,21,22
24,25,26,27,32

min=-69.633
max=528.07
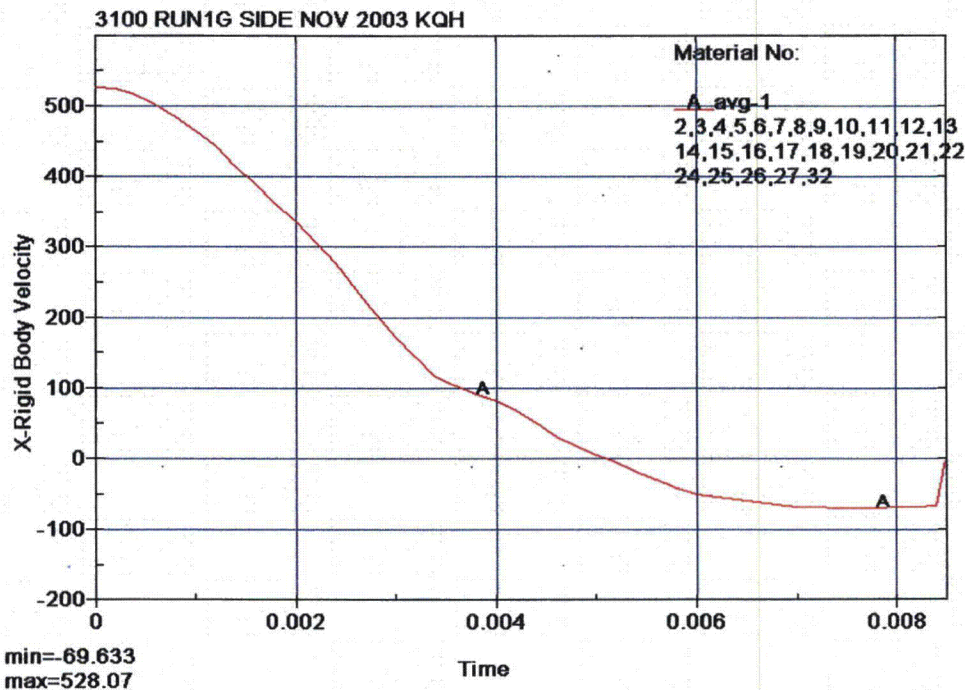
Figure 3.1.14 - Run1g, 30-Foot Impact, X Velocity Time History

3100 RUN1G SIDE NOV 2003 KQH
Time =   0.025
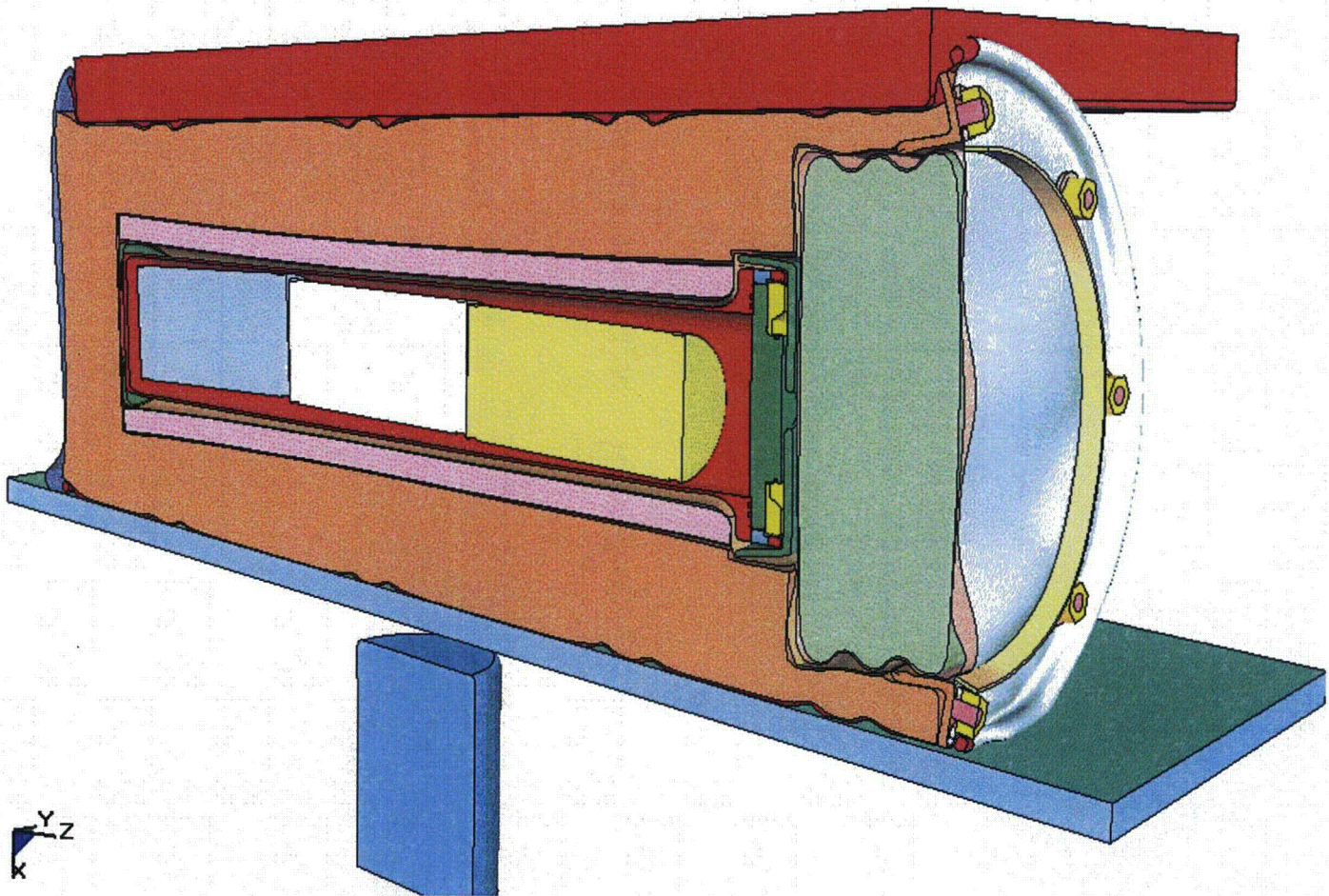
Figure 3.1.15 - Run1g, Crush Impact, Final Configuration
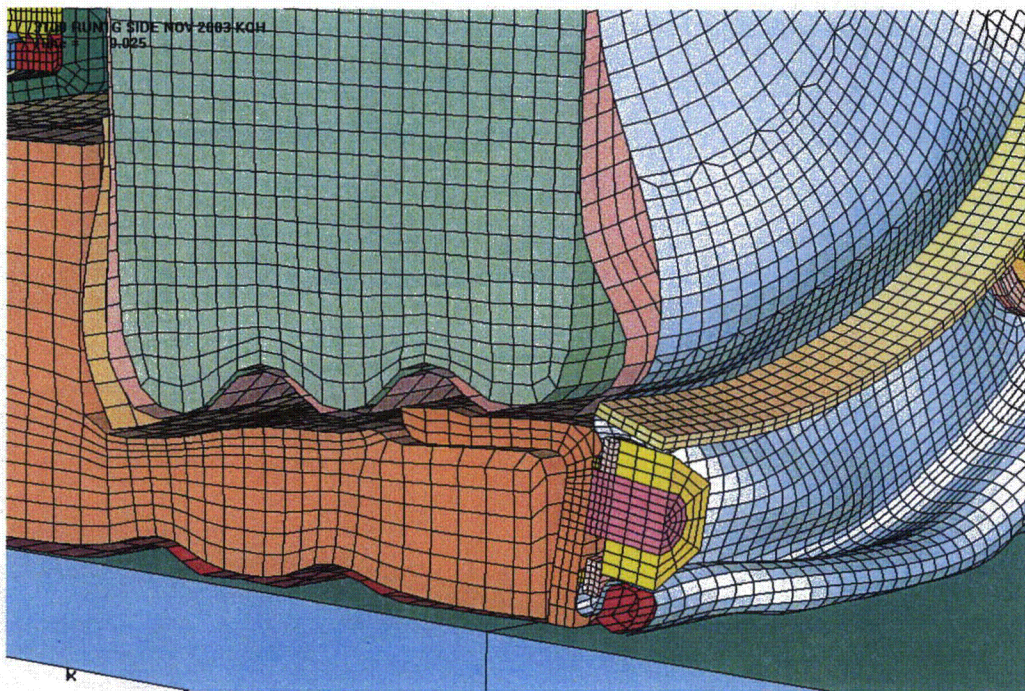
Figure 3.1.16 - Run1g, Crush Impact, Configuration of the Lower Lid Region
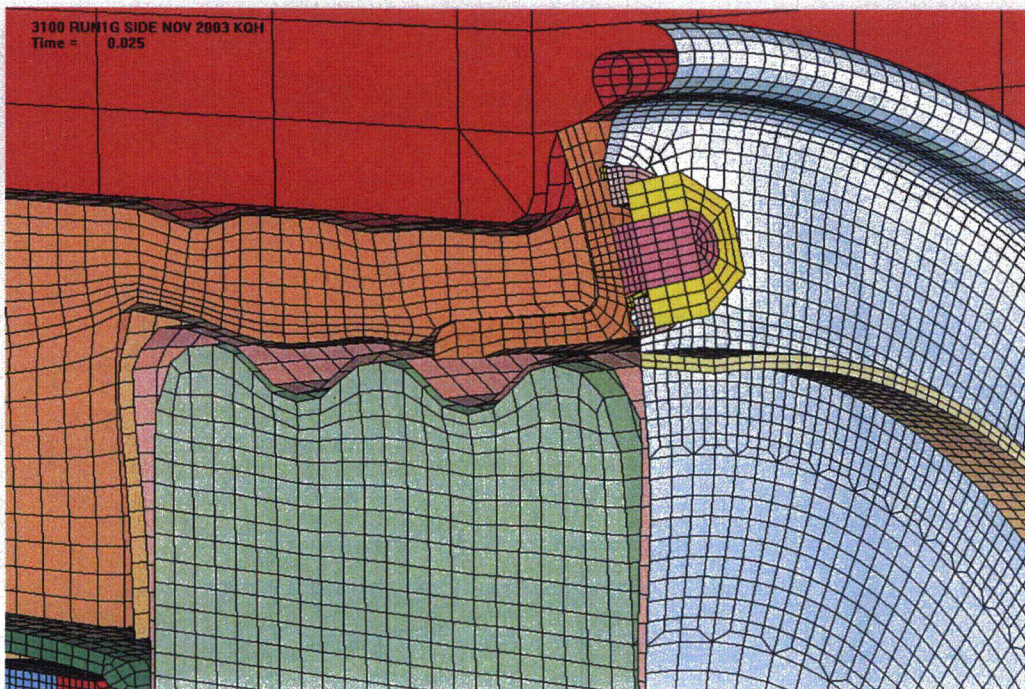
Figure 3.1.17 - Run1g, Crush Impact, Configuration of the Upper Lid Region
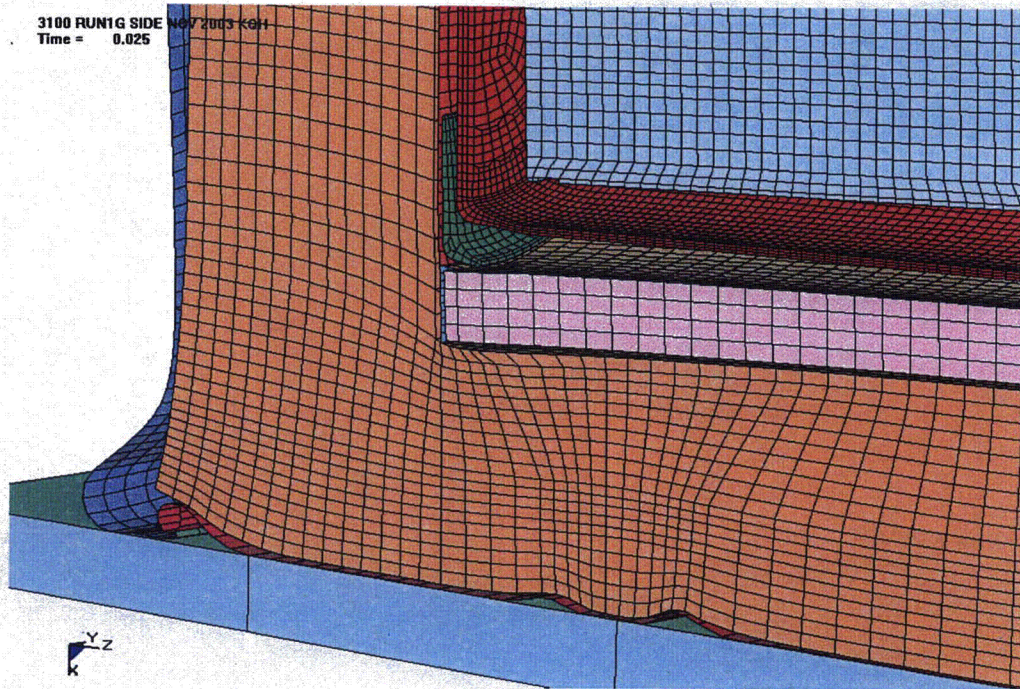
Figure 3.1.18 - Run1g, Crush Impact, Configuration of the Lower Bottom Region
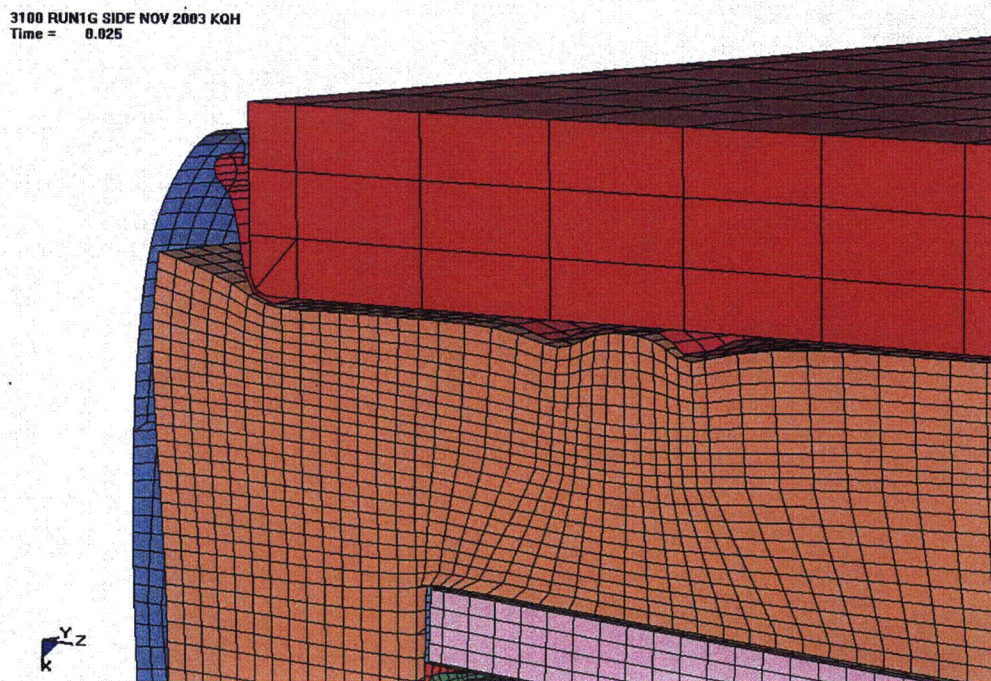
Figure 3.1.19 - Run1g, Crush Impact, Configuration of the Upper Bottom Region

3100 RUN1G SIDE NOV 2003 KQH
Time =   0.025
Contours of Effective Plastic Strain
max ipt. value
 min=0, at elem# 2
 max=0.0348228, at elem# 285471

Fringe Levels

3.482e-002
3.134e-002
2.786e-002
2.438e-002
2.089e-002
1.741e-002
1.393e-002
1.045e-002
6.965e-003
3.482e-003
0.000e+000
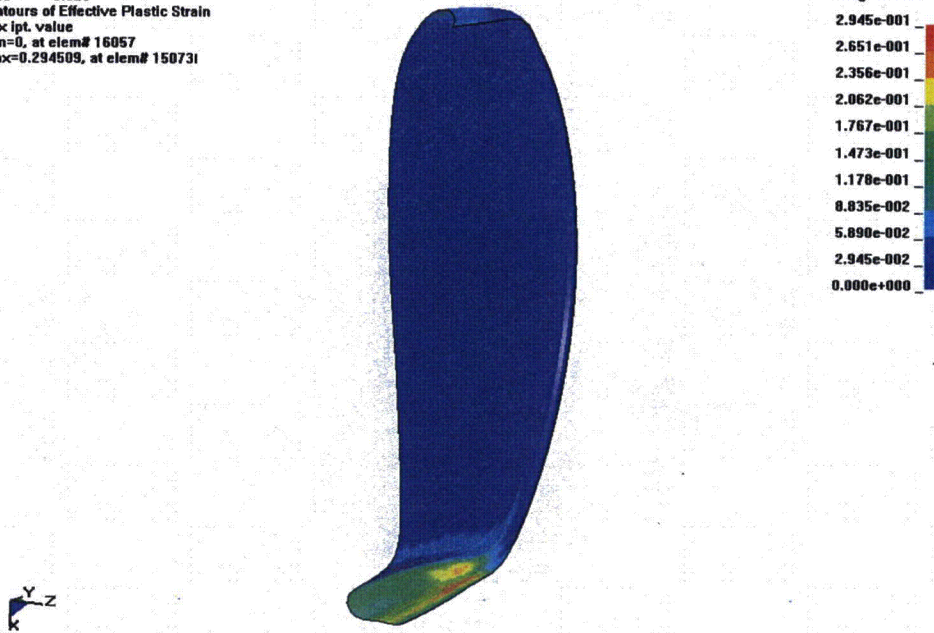
Figure 3.1.20 - Run1g, Crush Impact, Effective Plastic Strain in the CV Body

3100 RUN1G SIDE NOV 2003 KQH
Time =   0.025
Contours of Effective Plastic Strain
max ipt. value
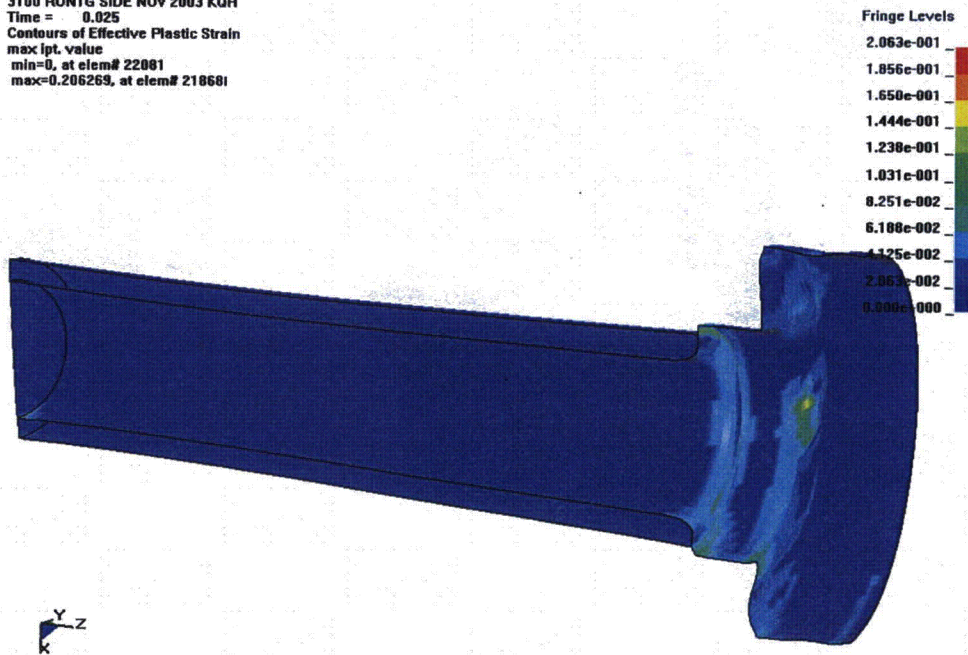 min=0, at elem# 51809
  max=0.000174097, at elem# 56547l

Fringe Levels
1.741e-004
1.567e-004
1.393e-004
1.219e-004
1.045e-004
8.705e-005
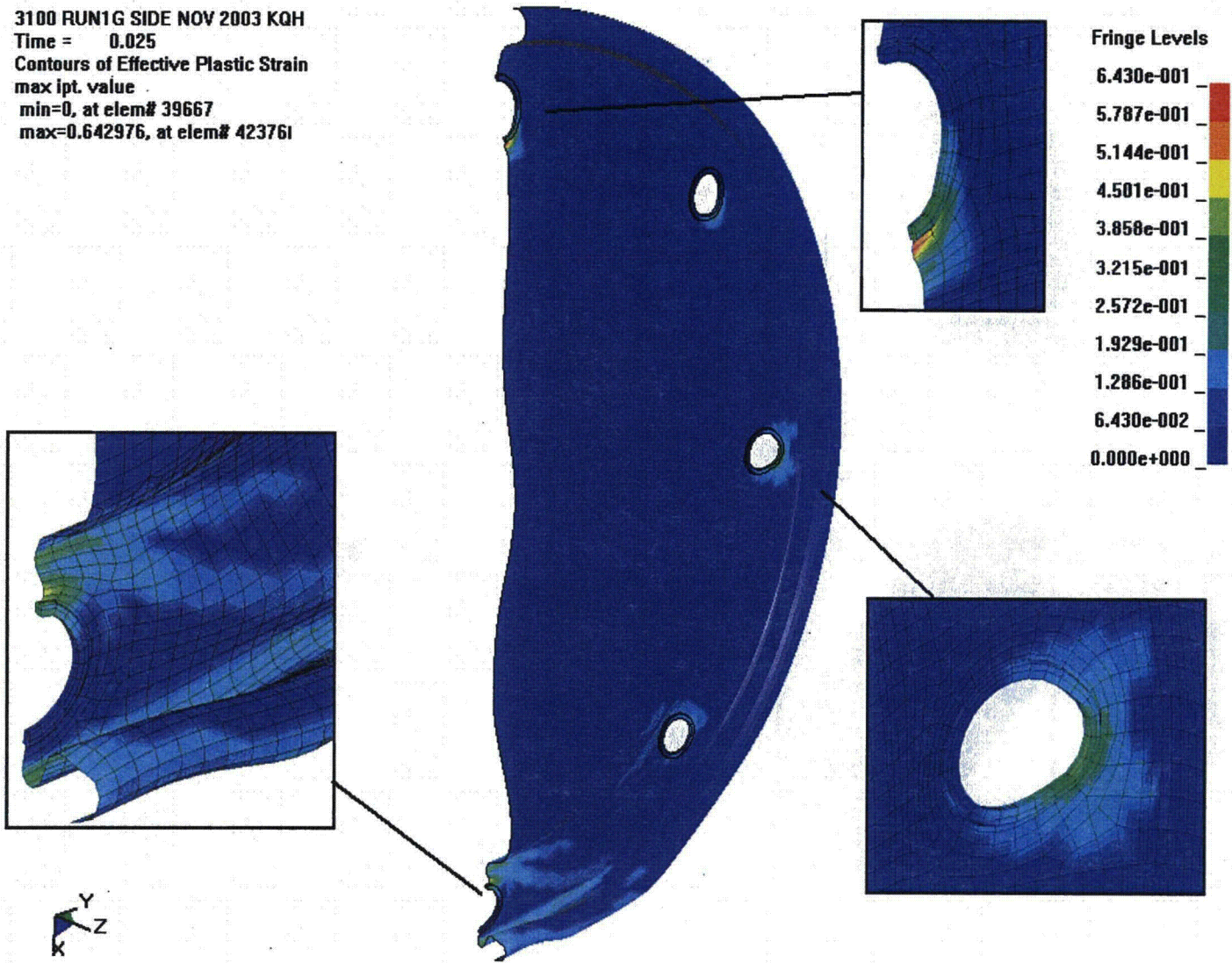6.964e-005
5.223e-005
3.482e-005
1.741e-005
0.000e+000

Figure 3.1.21 - Run1g, Crush Impact, Effective Plastic Strain in the CV Lid

3100 RUN1G SIDE NOV 2003 KQH
Time =   0.025
Contours of Effective Plastic Strain
max ipt. value
 min=0, at elem# 61134
  max=0.0944739, at elem# 63263l

Fringe Levels
9.447e-002
8.503e-002
7.558e-002
6.613e-002
5.668e-002
4.724e-002
3.779e-002
2.834e-002
1.889e-002
9.447e-003
0.000e+000

Figure 3.1.22 - Run1g, Crush Impact, Effective Plastic Strain in the Drum Angle

3100 RUN1G SIDE NOV 2003 KQH
Time = 0.025
Contours of Effective Plastic Strain
max ipt. value
 min=0, at elem# 1823
 max=0.302838, at elem# 35761

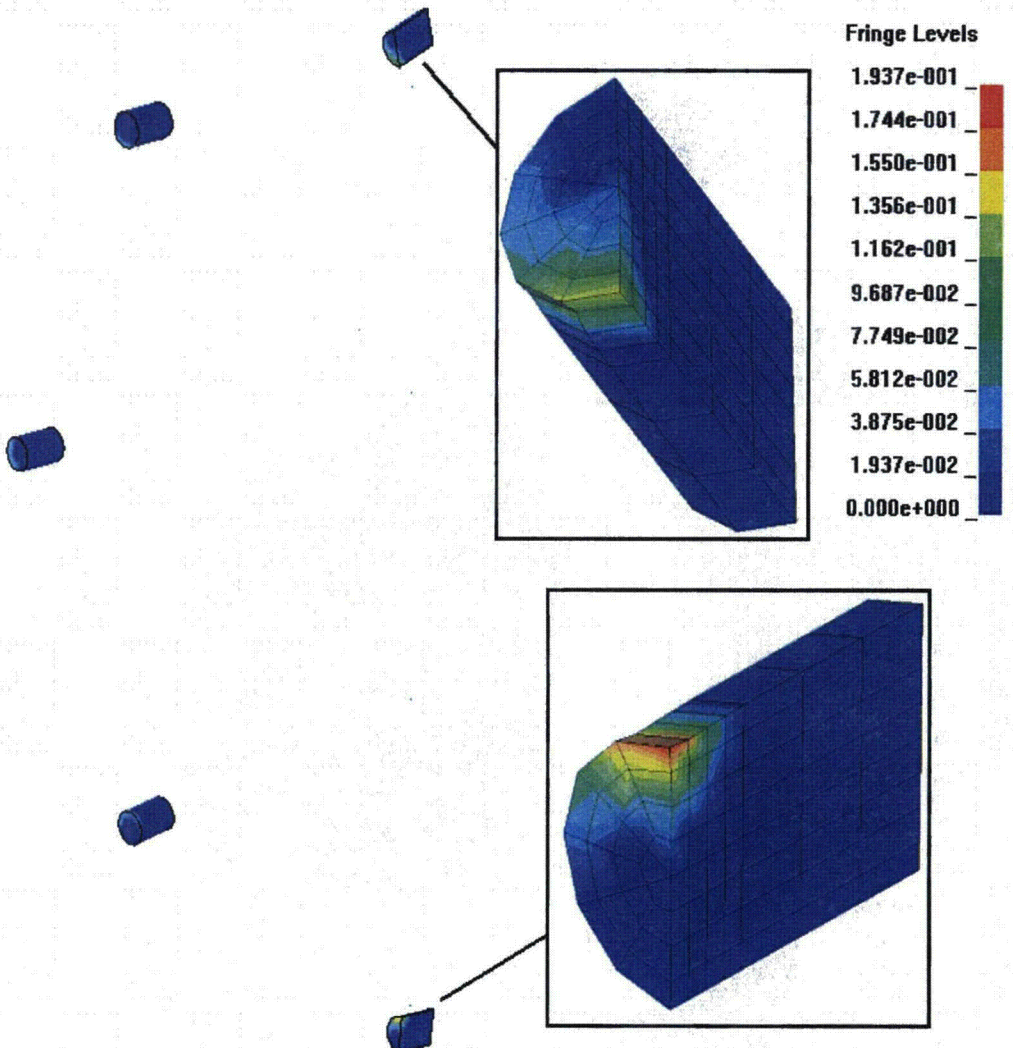Fringe Levels

3.028e-001
2.726e-001
2.423e-001
2.120e-001
1.817e-001
1.514e-001
1.211e-001
9.085e-002
6.057e-002
3.028e-002
0.000e+000
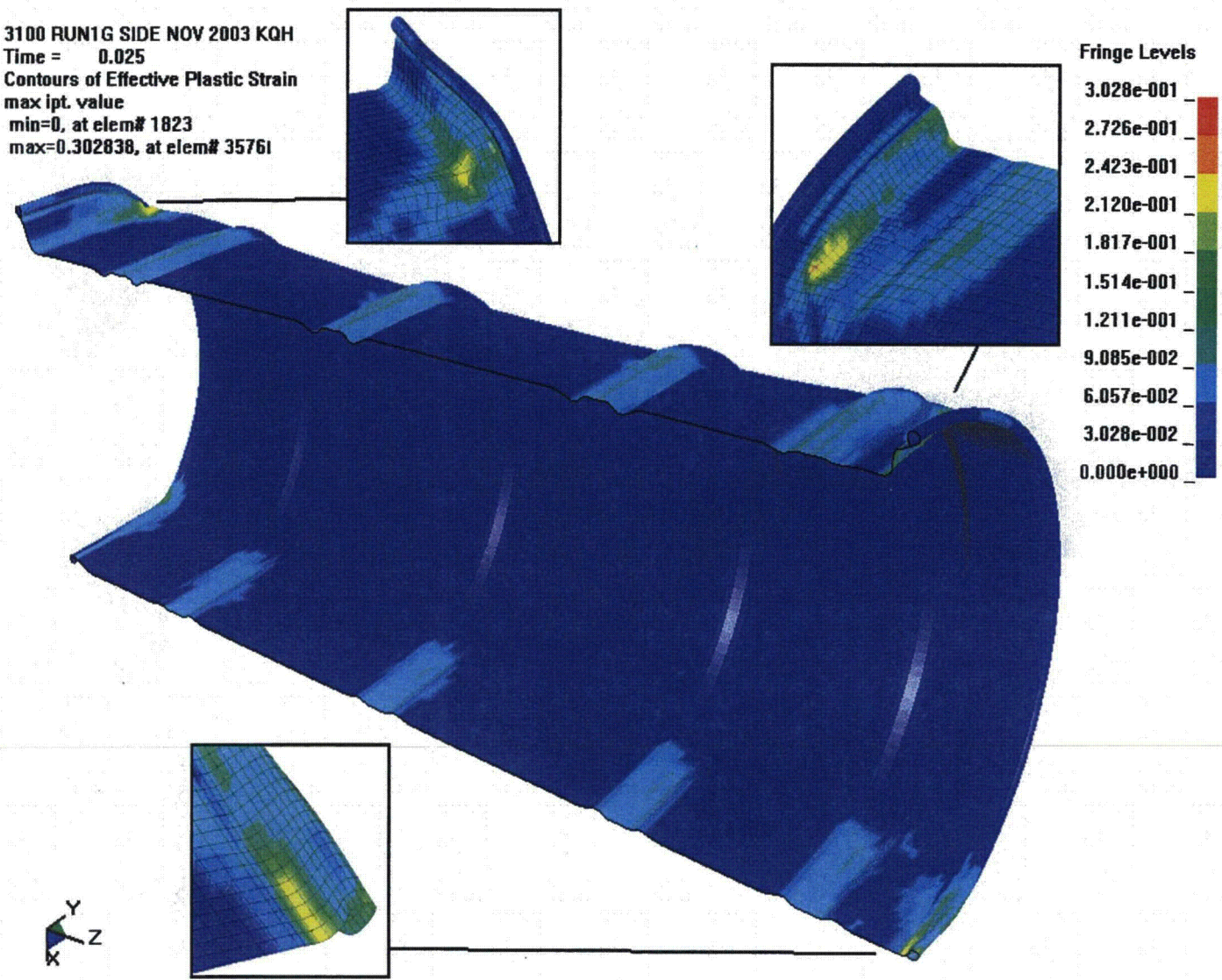
Figure 3.1.23 - Run1g, Crush Impact, Effective Plastic Strain in the Drum

3100 RUN1G SIDE NOV 2003 KQH
Time = 0.025
Contours of Effective Plastic Strain
max ipt. value
 min=0, at elem# 16057
 max=0.294509, at elem# 15073I

Fringe Levels

2.945e-001
2.651e-001
2.356e-001
2.062e-001
1.767e-001
1.473e-001
1.178e-001
8.835e-002
5.890e-002
2.945e-002
0.000e+000

Figure 3.1.24 - Run1g, Crush Impact, Effective Plastic Strain in the Drum Bottom Head

3100 RUN1G SIDE NOV 2003 KQH
Time = 0.025
Contours of Effective Plastic Strain
max ipt. value
 min=0, at elem# 22081
 max=0.206269, at elem# 21868I

Fringe Levels

2.063e-001
1.856e-001
1.650e-001
1.444e-001
1.238e-001
1.031e-001
8.251e-002
6.188e-002
4.125e-002
2.063e-002
0.000e+000

Figure 3.1.25 - Run1g, Crush Impact, Effective Plastic Strain in the Drum Inner Liner

3100 RUN1G SIDE NOV 2003 KQH
Time = 0.025
Contours of Effective Plastic Strain
max ipt. value
 min=0, at elem# 39667
 max=0.642976, at elem# 423761

Fringe Levels

6.430e-001
5.787e-001
5.144e-001
4.501e-001
3.858e-001
3.215e-001
2.572e-001
1.929e-001
1.286e-001
6.430e-002
0.000e+000

Figure 3.1.26 - Run1g, Crush Impact, Effective Plastic Strain in the Drum Lid

63

3100 RUN1G SIDE NOV 2003 KQH
Time =   0.025
Contours of Effective Plastic Strain
max ipt. value
 min=0, at elem# 71875
 max=0.193733, at elem# 71992I

Fringe Levels

1.937e-001 _
1.744e-001 _
1.550e-001 _
1.356e-001 _
1.162e-001 _
9.687e-002 _
7.749e-002 _
5.812e-002 _
3.875e-002 _
1.937e-002 _
0.000e+000 _

Figure 3.1.27 - Run1g, Crush Impact, Effective Plastic Strain in the Drum Studs

64
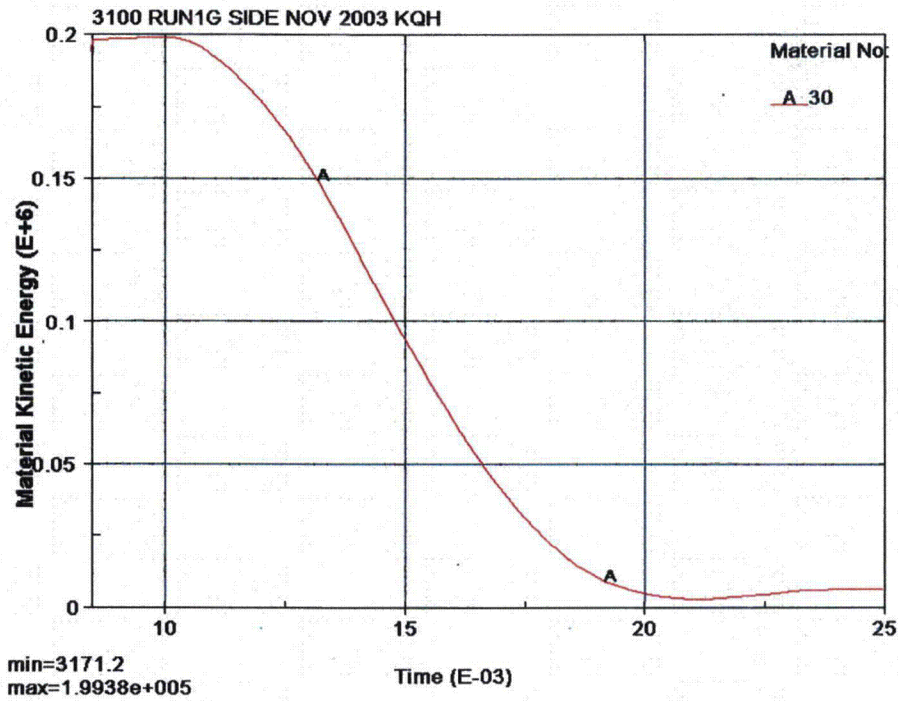
Figure 3.1.28 - Run1g, Crush Impact, Kinetic Energy Time History of the Crush Plate
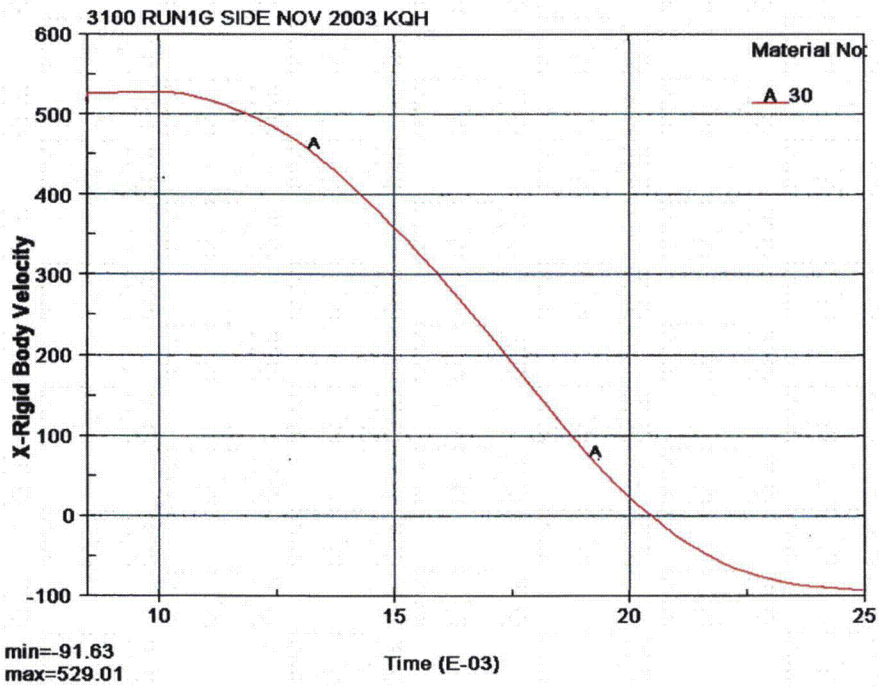
Figure 3.1.29 - Run1g, Crush Impact, X Velocity Time History of the Crush Plate
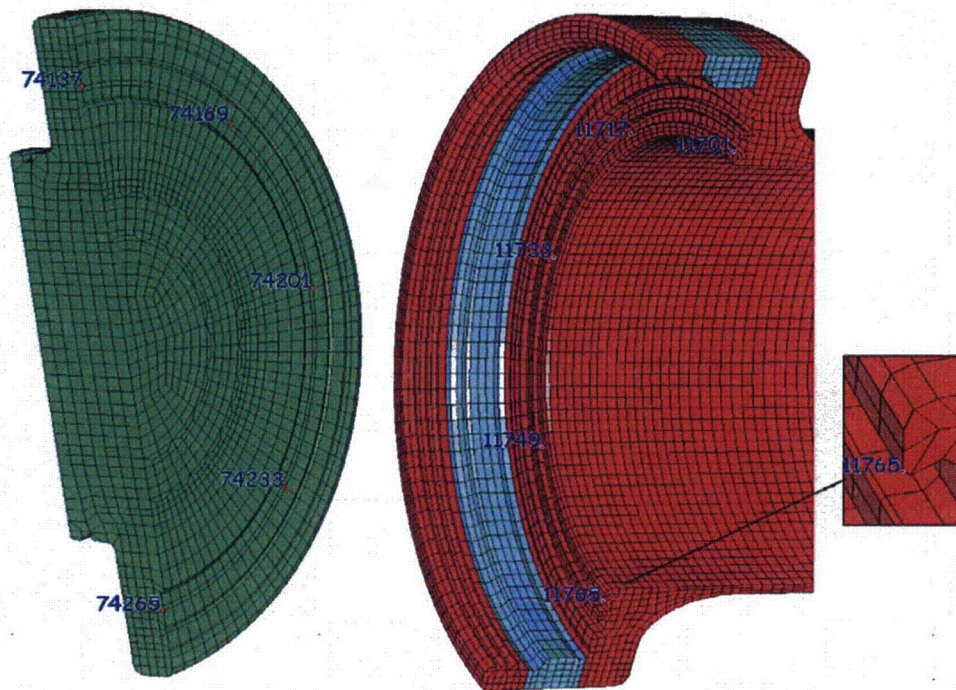
Figure 3.1.30 - Run1g, Nodes on CV Lid and Body Flange for Separation Time History
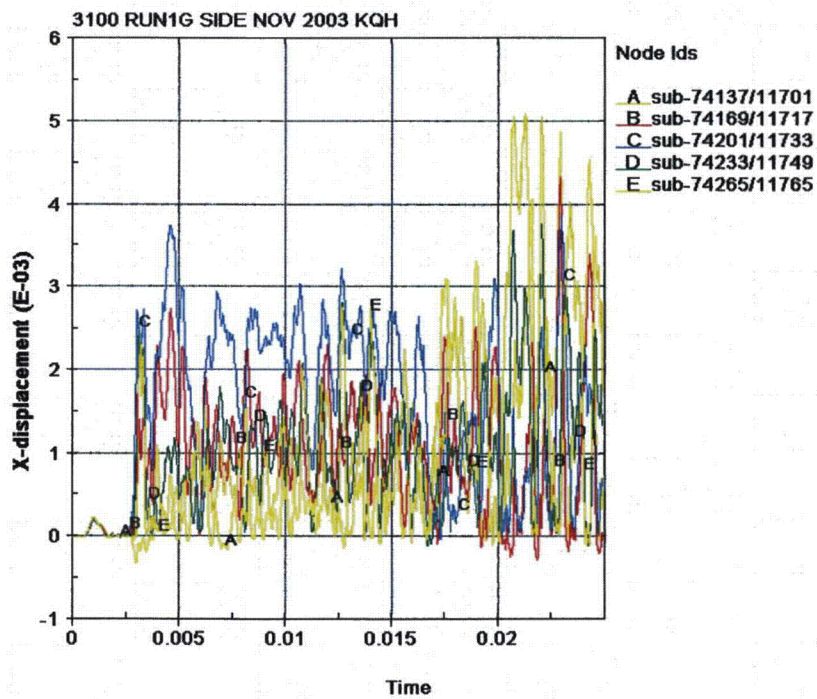
Figure 3.1.31 - Run1g, CV Flange Separation Time History
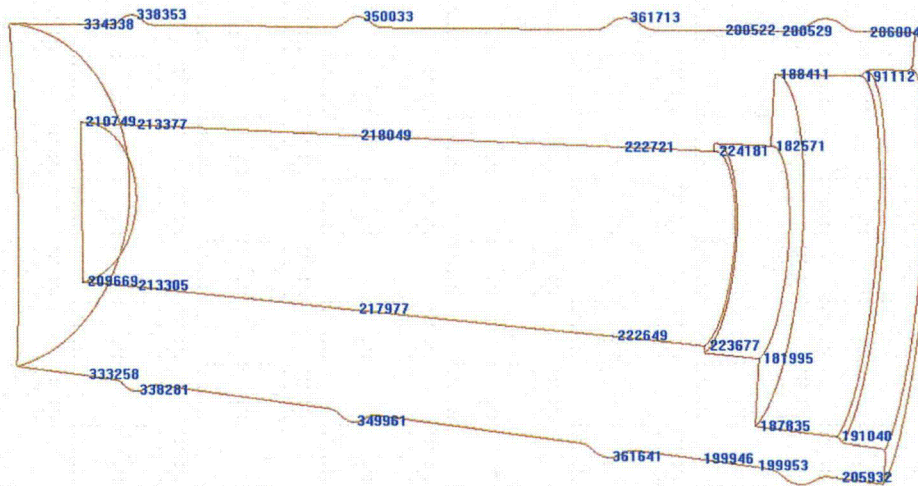
Figure 3.1.32 - Run1g, Drum Kaolite Nodes Used for Thickness Time Histories
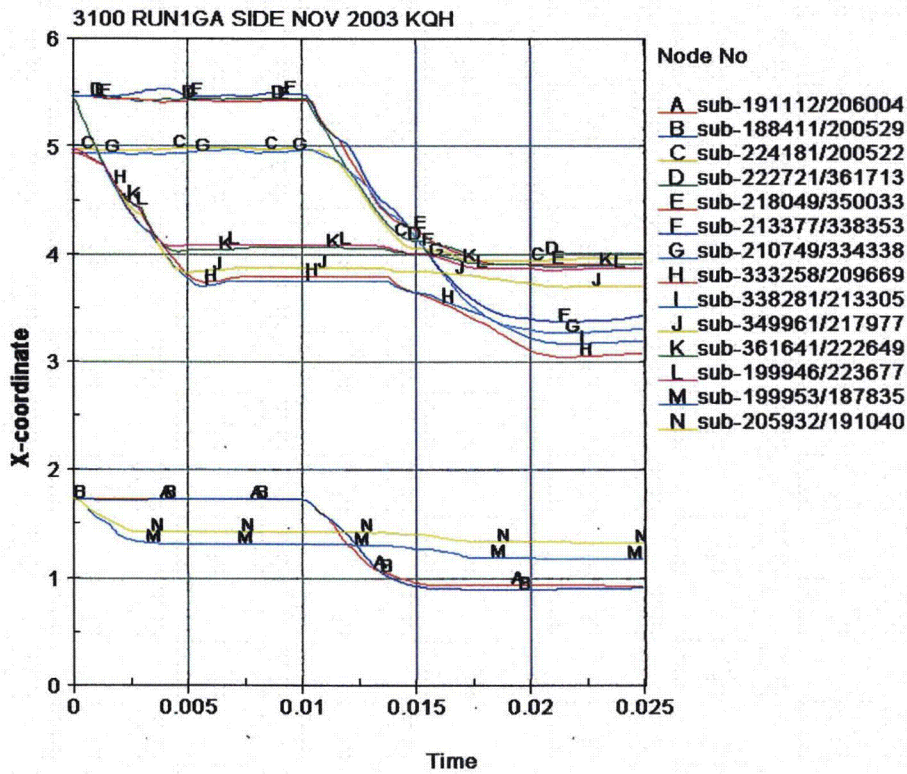
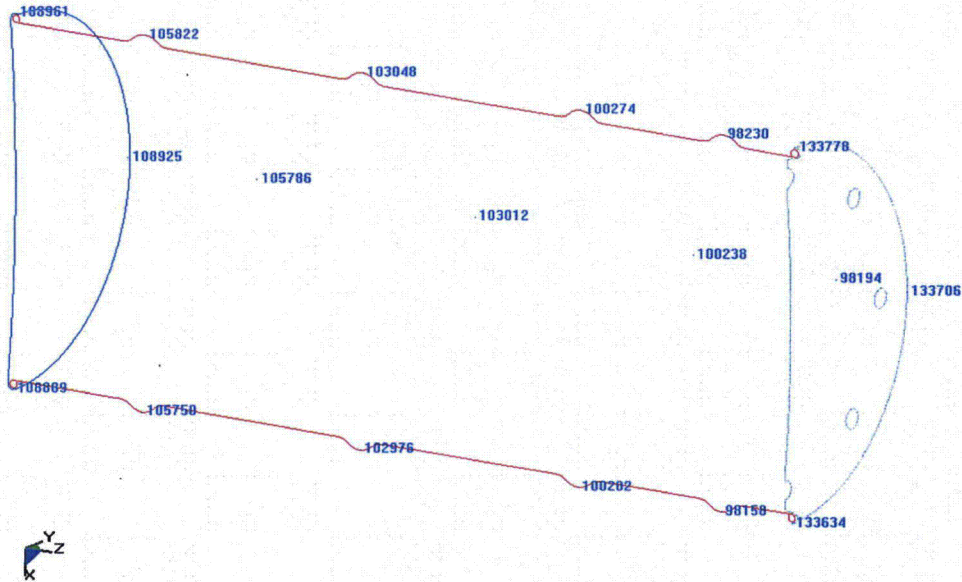Figure 3.1.33 - Run1g, Drum Kaolite Thickness Time History

3100 RUN1G SIDE NOV 2003 KQH
Time =   0

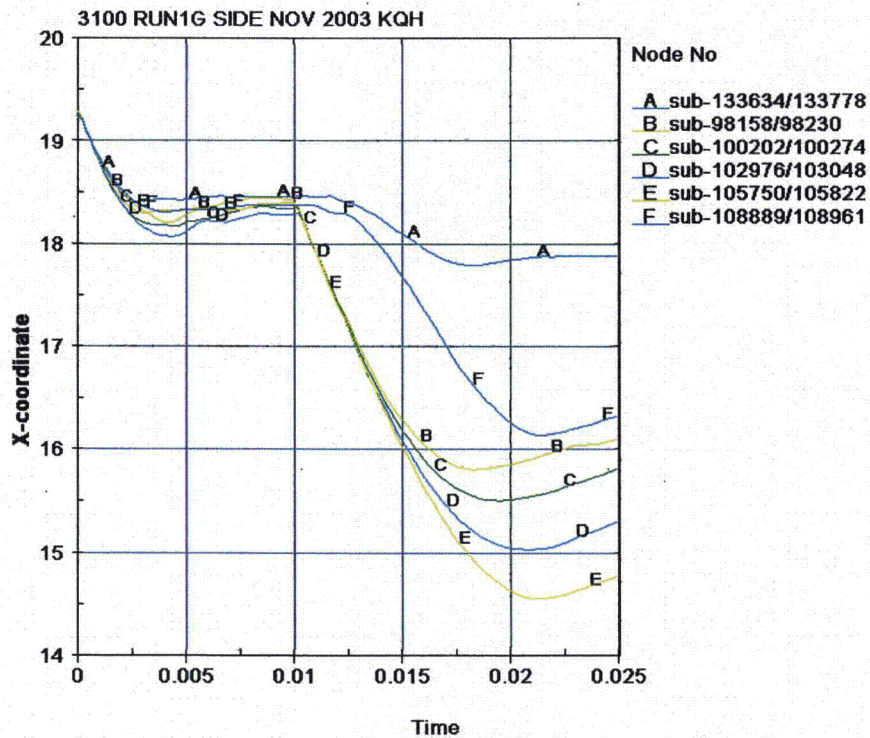Figure 3.1.34 - Run1g, Drum Nodes Used to Measure Deformation Time Histories

3100 RUN1G SIDE NOV 2003 KQH

Node No

A sub-133634/133778
B sub-98158/98230
C sub-100202/100274
D sub-102976/103048
E sub-105750/105822
F sub-108889/108961

X-coordinate

Time

Figure 3.1.35 - Run1g, Drum Measurement Time History in the X-Direction
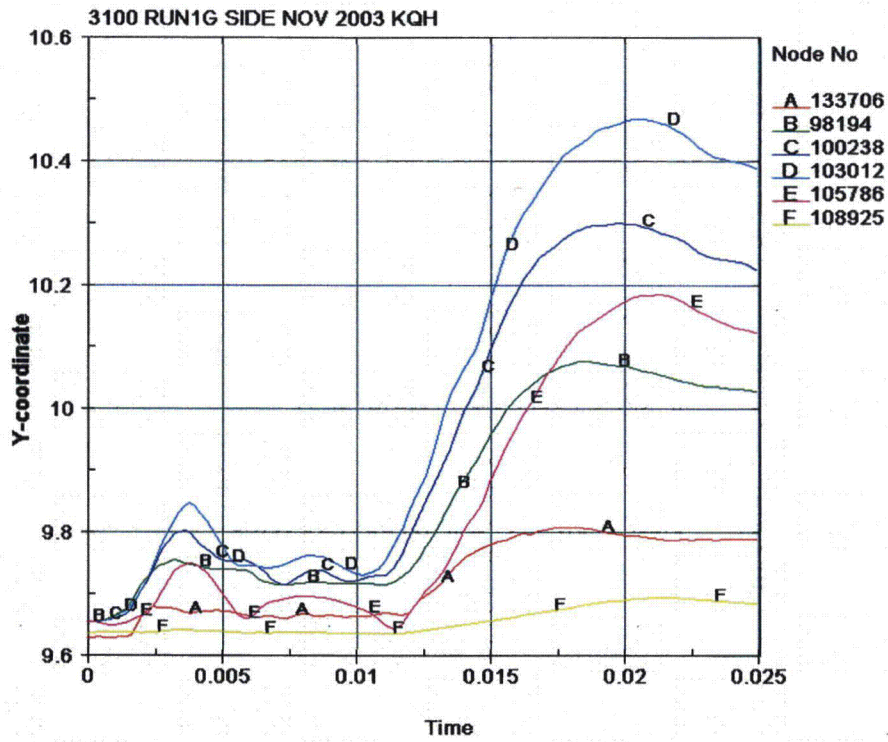
Figure 3.1.36 - Run1g, Drum Measurement Time History in the Y-Direction
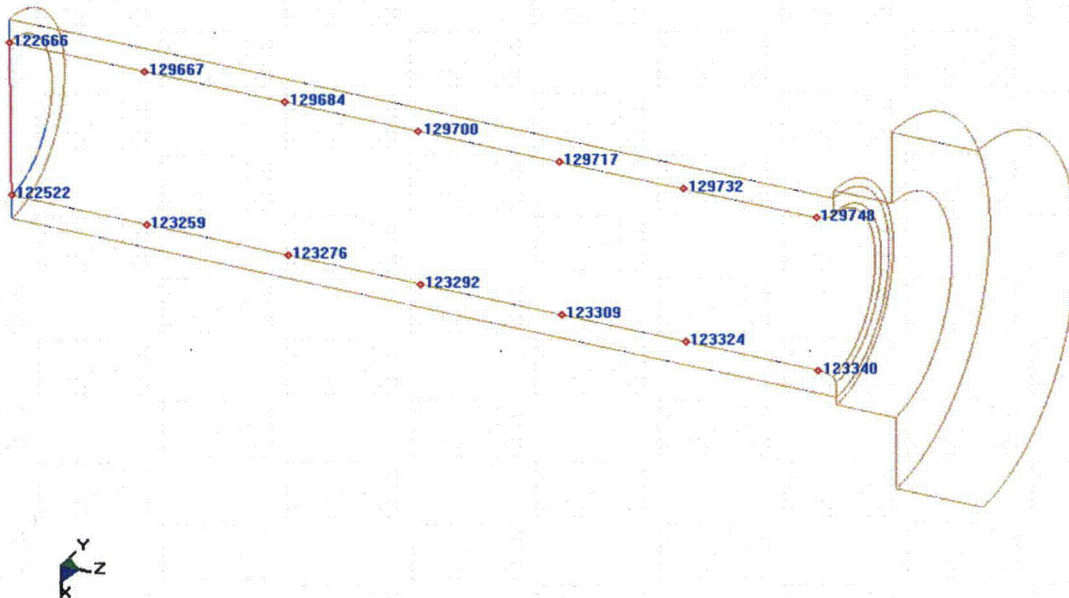

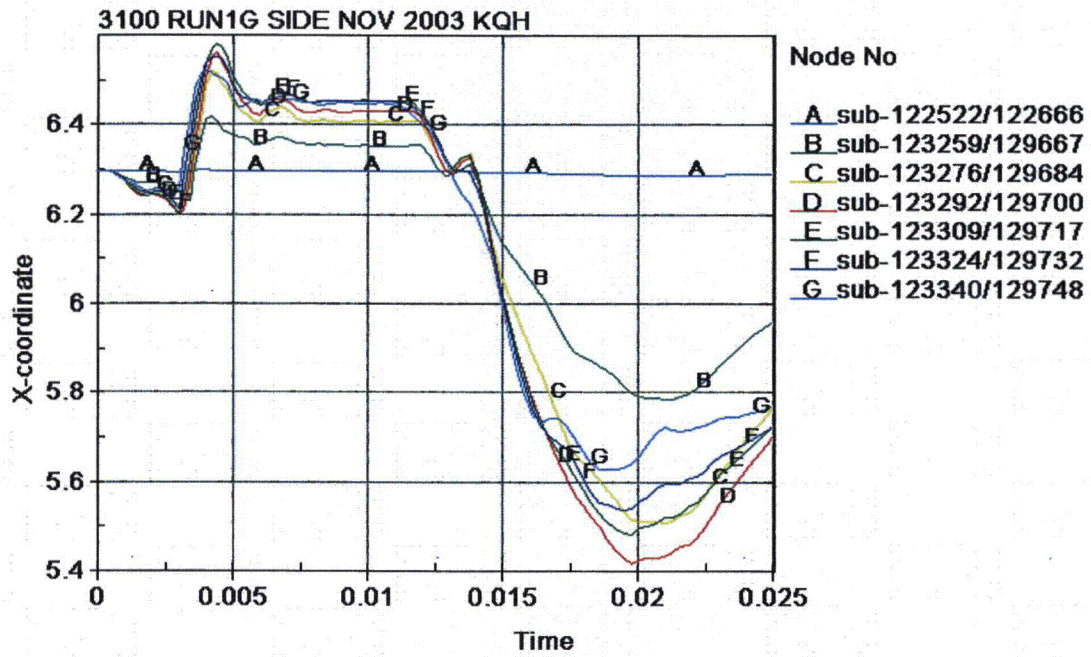Figure 3.1.37 - Run1g, Position of Inner Liner Nodes Used for Diameter Time History

Figure 3.1.38 - Run1g, Inner Liner Diameter Time History